SINTERING AND GRAIN GROWTH OF NANOSIZED POWDER

by

Hongtao Wang

A dissertation submitted to the faculty of
The University of Utah
in partial fulfillment of the requirements for the degree of

Doctor of Philosophy

Department of Metallurgical Engineering

The University of Utah

December 2010

The University of Utah Graduate School

STATEMENT OF DISSERTATION APPROVAL

The dissertation of   **Hongtao Wang**

has been approved by the following supervisory committee members:

Zhigang Zak Fang	, Chair	**10/26/2010** Date Approved
Hong Yong Sohn	, Member	**10/26/2010** Date Approved
Sivaraman Guruswamy	, Member	**10/26/2010** Date Approved
Ravi Chandran	, Member	**10/26/2010** Date Approved
Dinesh Shetty	, Member	**10/26/2010** Date Approved

and by   **Jan D. Miller**   , Chair of

the Department of   **Metallurgical Engineering**

and by Charles A. Wight, Dean of The Graduate School.

ABSTRACT

The sintering of nanosized particles (or nanosintering) is an approach to the manufacture of bulk nanocrystalline materials. The goal of nanosintering is to achieve fully densified parts with grain size less than 100 nm. However, in practice, it is very difficult to reach. Due to the extremely small size and the high surface to volume ratio of nanosized powders, nanosintering exhibits a number of different phenomena compared to the sintering of coarse powders. For example, it is generally found that the sintering temperatures of nanosized particles are drastically lower than those of their micron or submicron sized counterparts, and grain growth during heating up is considerably rapider for nanosized powders in comparison with micronsized powders. In order to obtain a comprehensive understanding about these different phenomena during nanosintering, this study, by using tungsten as the example material, aims to examine size dependence of the sintering behavior and further explore the characteristics of densification and grain growth of nanosized powders, especially during initial and intermediate stages of sintering. The nanosized tungsten powder was produced by high energy mechanical milling. It is demonstrated that the sinterability of nanosized tungsten powder, compared with that of coarser powder, is significantly enhanced at lower sintering temperatures, and the enhancement of sintering at low temperatures for nanosized powders can be rationalized by Herring scaling law. The characteristics of densification and grain growth during nanosintering are examined by both nonisothermal heating up and isothermal

holding experiments. The experimental results show linear densification behavior during the initial stage of sintering at low temperatures when density is less than ~50% relative density. Grain growth also exhibits a linear behavior during initial and intermediate stages of sintering. The mechanisms for linear densification and linear grain growth during early stage of sintering of nanosized tungsten powder are discussed based on kinetic analysis of experimental data. The evaluation results show surface diffusion is the mass transport mechanism for linear densification and linear grain growth. On the basis of the understanding of the densification and grain growth mechanisms, the general principles for inhibiting grain growth during nanosintering are proposed.

TABLE OF CONTENTS

LIST OF TABLES

LIST OF FIGURES

x

ACKNOWLEDGEMENTS

Foremost, I would like to express my sincere gratitude to my advisor, Professor Zhigang Zak Fang, for his expert guidance in my research work. This dissertation would not have been possible without his direction.

I would like to thank Professor Hong Yong Sohn, Prof. Guruswamy, Prof. Chandran, and Prof. Shetty for being my committee members. Their comments and suggestions on my thesis are of great value in this study.

I am grateful to Kyu Sup Hwang for his help with my experiments and to other colleagues for their cooperation during my study at University of Utah.

I owe my special gratitude to my farther and my brother, who have been always inspired and supported me for my entire student life. Without their love, I would not be able to finish my PhD.

Last but not least, I would like to extend my appreciation to all of my relatives and my friends for their encouragement and help in my life.

CHAPTER 1

INTRODUCTION

Nanomaterials are defined as those which have structured components with at least one dimension less than 100 nm. Nanomaterials can be categorized into four groups with respect to dimensions: 0 dimension (e.g., nanoparticle), 1 dimension (e.g., nanowire), 2 dimension (e.g., nanofilm), and 3 dimension (bulk nanocrystalline materials). Bulk nanocrystalline materials are solids composed of crystallites (grains) with a characteristic size of a few nanometers [1]. The sintering of nanosized powders is a viable approach to the manufacture bulk nanocrystalline materials. Therefore, since the emergence of nanoscaled science and technology, nanosintering has been a topic of both scientific and technological importance.

In the context of engineering processes, sintering implies the bonding of solid particles to each other. The sintering process can be regarded as consisting of two intertwined processes: densification and grain growth. Although the sintering of nanoparticles shares the same principles as that of the sintering of coarser particles, a number of issues and challenges are unique to nanosintering. For example, the driving force for nanosintering is extremely large, calling into question the use of conventional sintering doctrines based on linear diffusion theories. A nonlinear diffusion behavior leads to different kinetics of diffusion, which in turn would result in different rates of sintering. Another unique issue of nanosintering is that nanoparticles almost always

experience extremely rapid grain growth during sintering, rendering the loss of nanocrystalline characteristics at fully sintered state. With respect to the manufacture of bulk nanocrystalline materials from nanoscale particles, the objective of nanosintering is to achieve maximum densification while retaining nanoscale grain sizes. This goal, however, has been very difficult to reach. In fact, it is a glaring technological challenge for many materials.

In order to find solutions to control and optimize densification and grain growth, this study will focus on understanding the characteristic behaviors of nanoparticles, particularly the size dependent properties and their effects on nanosintering. Based on literature research and experiments, the differences in sintering of nanoparticles versus that of coarser particles will be highlighted from the perspectives of grain growth and densification. The characteristics and mechanisms of densification and grain growth during nanosintering will also be discussed.

1.1 References

[1]   Gleiter H. Nanostruct Mater 1995;6:3.

CHAPTER 2

LITERATURE REVIEW

Bulk nanocrystalline materials, characterized by the grain size which is less than 100 nm, have unique properties due to the small grain size and high surface/interface volume fraction, e.g., transition from brittle materials to ductile materials, transition from opaque materials to transparent materials, etc. Manufacture of bulk nanocrystalline materials can be divided into two categories: top-down approach and bottom-up approach. Top-down approach includes severe plastic deformation such as equal channel angle pressing (ECAP) and controlling crystallization from amorphous phase. Bottom-up approach indicates consolidation of nanosized powder into bulk nanocrystalline materials. Therefore, since the emergence of nanoscience and nanotechnology, the sintering of nanosized powder has been a hot research topic.

Owing to the importance of the sintering of nanoparticles, a large body of literature on nanosintering has been accumulated and published over the past 20 years. The literature on nanosintering can be classified into two groups: those focused on the densification and grain growth behavior during sintering at the nanoscale and those on innovative sintering technologies and processes. Fundamental studies included molecular dynamics (MD) simulations at the atomic scale, the kinetic studies of sintering using nonlinear diffusion theories, and the modeling of kinetic behavior based on generalized parabolic model of grain growth. In addition, a number of efforts have been directed

toward the grain growth of nanosized particles. This literature review will examine and summarize the characteristics of nanosintering from the perspectives of densification and grain growth.

2.1 Densification During Nanosintering

In general, the sintering of nanosized or nanocrystalline powders follows the same path as larger grain powders. However, compared to conventional micron sized or submicron sized particles, densification behavior of nanoparticles during sintering exhibits notably different behavior with respect to the rate of densification and the temperature range at which densification occurs. The densification of nanoparticles is strongly affected by agglomeration of particles, pores, and other processing variables. Although many of those factors also impact the sintering of conventional micron sized particles, those effects are more dramatic and magnified in the case of nanosized particles. The densification behavior of nanosintering can be analyzed from both the perspectives of the thermodynamics and kinetics of the process.

2.1.1 Thermodynamic Driving Force of Nanosintering

The thermodynamic driving force for sintering particles of any size is the reduction of surface energy. Based on conventional sintering theories, the driving force of sintering can be given by [1]

$$\sigma = \gamma \kappa = \gamma (\frac{1}{R_1} + \frac{1}{R_2}) \tag{2.1}$$

where γ is the surface energy of the material, κ is the curvature of a surface, which is

defined by $\kappa = \dfrac{1}{R_1} + \dfrac{1}{R_2}$ (for a convex surface, it is taken to be positive; for a concave

surface, it is taken to be negative), R_1 and R_2 are the principal radii of the curvature. The

driving force for the sintering of nanosized particles is, therefore, inversely proportional

to the sizes of the particles. This relationship would lead to a much higher driving force

for the sintering of nanosized particles compared to micron sized particles. For example,

based on equation (2.1), the driving force for a 10 nm particle is two magnitudes higher

than that for a one micron particle.

The driving force of nanosintering is also affected by surface energy - γ. The value of

γ may change as a function of the particle size. Campbell et al. [2] studied the effect of

size dependent nanoparticle energetics on catalyst sintering. By using microcalorimetric

measuring the heat of adsorption of Pb onto MgO (100), they showed that the surface

energy increases substantially as the radius decrease below ~3 nm. Separately, Nanda et

al. [3] also showed that the surface energy of nanoparticles is significantly higher,

compared to that of the bulk by studying size dependent evaporation of Ag nanoparticles.

2.1.2 Kinetic Behavior of Nanosintering

2.1.2.1 Sintering Temperature

Notably the sintering of nanosized particles occurs at lower temperatures than that for

the sintering of conventional micron sized or submicron sized powders, as shown

schematically in Fig. 2.1. Sintering temperature is, in general, a loose concept, referring

to the entire temperature range of densification. In order to be specific and quantitative,

the starting temperature is often used for comparison. However, because sintering and

The onset temperature of sintering of nano-sized particles

The onset temperature of sintering of micron-sized particles

Relative Density
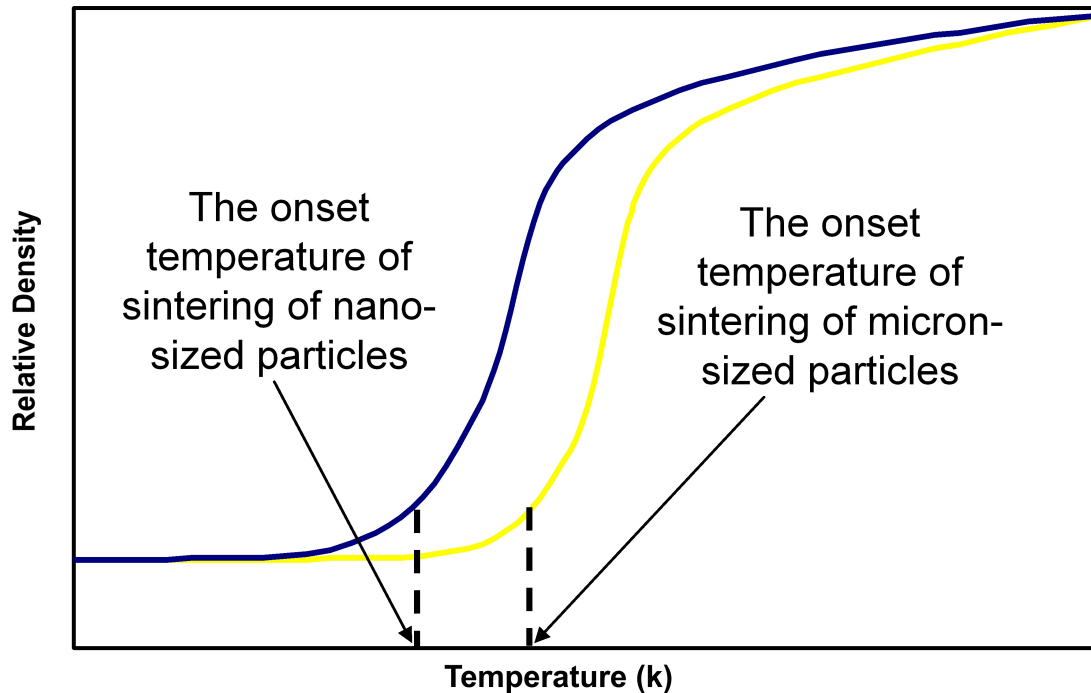
Temperature (k)

Fig. 2. 1 Schematic diagram illustrating different onset temperatures of sintering of nano- and micron-sized particles

densification is a continuous kinetic process, rigorously speaking, a single point demarcation for the starting temperature of sintering does not exist. Based on typical experimental behavior, the starting temperature can be defined as the temperature at which the rapid densification stage initiates, as marked on Fig. 2.1. In general, the densification versus temperature plot shifts to the left (lower temperature) when nanosized powders are used rather than micron sized powders. For example, several studies on the sintering of nano yitrium stabilized zirconia (YSZ) have shown that the sintering temperature of nanocrystalline ZrO_2 initiates at a temperature 200 degrees lower than that of the microcrystalline powders [4-6]. An even greater temperature difference of sintering—400 ^{o}C--was reported by Mayo [7] for nanosized titania compared to

commercial TiO$_2$ powders. Similar results were observed for sintering nanosized ceria[8] and nano titanium nitride powders [9].

Relatively speaking, fewer systematic studies exist on the densification behavior of nanosized metal powders than on nanosized ceramic powders [10-12]. A direct and systematic study of the sintering of nanocrystalline Fe and Cu powder was reported by Dominguez et al. in 1998 [13]. Compared to micrometric powder, the rapid densification of nanosized Fe and Cu powders started at approximately 200°C lower temperatures. The reduction of the sintering temperatures was also reported for nanotungsten [14, 15]. The reported sintering temperature of nanosized tungsten powders produced by high energy mechanical milling was dramatically decreased from conventional temperature of 2500 $^{\circ}$C to 1700 $^{\circ}$C. More surprisingly, Oda et al. [15] showed that the nanosized tungsten powders could be sintered even at 1000 $^{\circ}$C by using spark plasma sintering.

General sintering theories hold that a material's sintering temperature is often correlated with the material's melting. It has long been known that the melting temperature of very fine particles decreases with the size of particles [16-31]. For nanosintering, the decreasing onset temperature of sintering can be understood, therefore, on the basis of the lowered melting temperature of nanoparticles. Troitskii et al. [32] studied the initial sintering temperature of different sized TiN powders and found the relationship between initial sintering temperature T_{is} and particle size r is:

$$T_{is}(r) = T(\infty)\exp\left[-c \cdot (r'-r)/r\right] \qquad (2.2)$$

where $T(\infty)$ is the initial sintering temperature of coarse particles; c is a constant determined by the properties of the material and the energetic state of the surface layer; r' is arbitrary size.

Jiang [33] ascribed size dependent initial sintering temperature of nanosized particles to the decreased melting temperature of nanosized particles based on the relationship:

$$T_{is}(r) = 0.3 T_m(r) = 0.3 \cdot T_m(\infty) \exp\left[-\frac{2S_m(\infty)}{3k} \frac{1}{(r/r_0)-1}\right] \qquad (2.3)$$

where $T_m(\infty)$ is melting temperature of the bulk material, $S_{vib}(\infty)$ is bulk melting entropy, r is particle radius, $r_0=3h$ (h is atomic diameter) for nanoparticles, k is Boltzman constant. Fig. 2.2 shows the predicted size dependent initial sintering temperature of some metallic powders by using equation (2.3) [33]. Note that the significant changes of the initial sintering temperature do not occur until the particle size is less than approximately 20 nm.

2.1.2.2 Scaling Law

In conventional sintering theories, the dependence of densification behavior on the size of particles is described by the scaling law. In 1950, Herring [34] first introduced the scaling law as follows:

$$\Delta t_2 = \lambda^n \Delta t_1 \qquad (2.4)$$

where $\lambda = R_2/R_1$, R_1 and R_2 are particle radius, n depends on specific diffusion mechanisms of the densification. Specifically, n = 1 for viscous flow, 2 for evaporation and condensation, 3 for volume diffusion, and 4 for surface diffusion or grain boundary
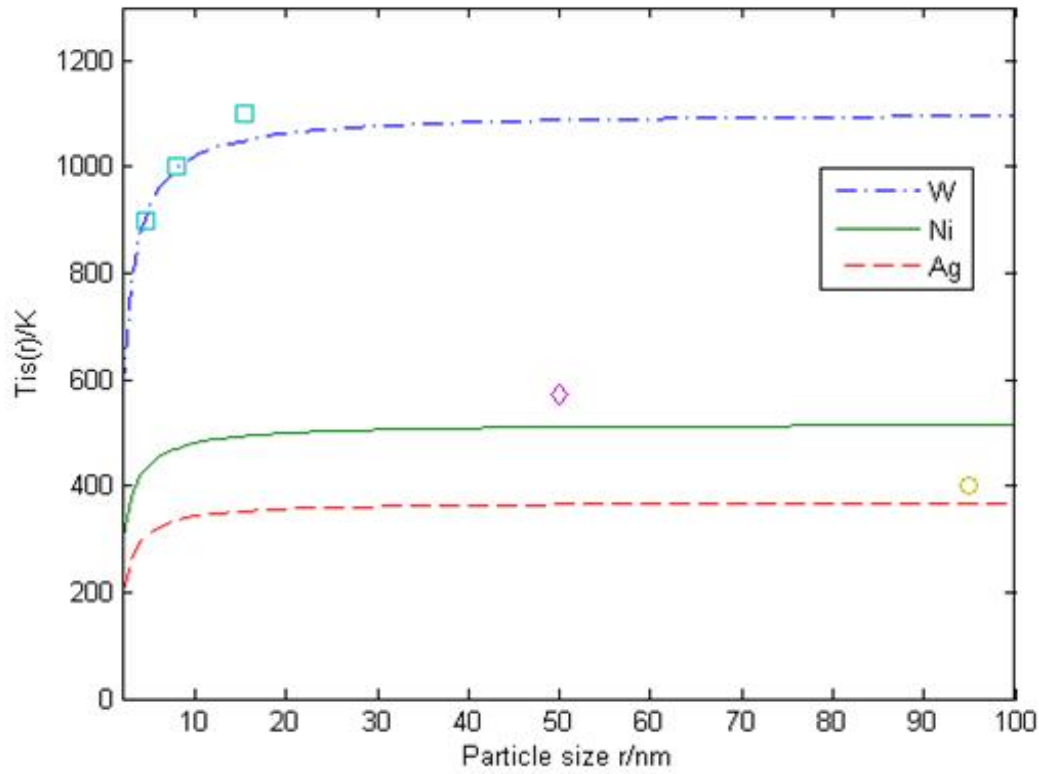
Fig. 2. 2 Theoretical prediction of initial sintering temperature - Tis(r) - for selected metals in terms of equation (2.3). The experimental initial sintering temperature of W, Ni, and Ag are also plotted in the figure for comparison. (After Ref. 33)

diffusion. The scaling law states that the time required to sinter powders with particle radii of R_1 and R_2 is proportional to the ratio of the particle radius. Although the densification behavior of nanosized powders can be qualitatively understood on the basis of the scaling law, few direct analyses of experimental data exist in the literature. The few studies that applied the scaling law used the following expression to analyze the activation energies of the sintering of nanosized powders [35, 36]:

$$n \ln\left(\frac{d_1}{d_2}\right) = \frac{Q}{R}\left[\frac{1}{T_2} - \frac{1}{T_1}\right] \tag{2.5}$$

where d_1, d_2 are particle sizes, T_1 and T_2 are corresponding sintering temperatures, R is the gas constant, and Q is the activation energy. By using the above equation, some reported studies obtained activation energy values that are closer to grain boundary diffusion, while others obtained values closer to volume diffusion, which is believed to be unlikely at low temperatures for small particles. The discrepancies in the values of activation energies obtained using this method, therefore, raise questions on the validity of the scaling law for sintering of nanoscale particles.

The derivation of scaling law is based on an assumption that the particle size of two different powder systems used for comparison does not change during sintering and microstructural changes remain geometrically similar for the two systems. This assumption leads to key limitations to the use of the scaling law because it is difficult to maintain the conditions in the assumption in real powder systems [37]. During nanosintering, particle size changes rapidly and some characteristics of nanoparticles, such as agglomeration and the nonuniformity of green density, increase the difficulty of maintaining similar microstrutural evolutions during sintering. In addition, because the classic scaling law was derived from linear equations, the validty of the scaling law during nanosintering is called into question. The nonlinear diffusion behavior of nanosintering [38] and the size dependent diffusion activation energies [39] will change the expression for calculating the diffusion flux. Furthermore, the scaling law considers different mechanisms separately. In practice, multiple mechanisms of sintering may occur simultaneously, especially in nanosintering.

2.1.2.3 Effect of Green Density, Agglomeration on Nanosintering

In the practice of nanosintering, the densification behavior of nanoparticles is affected by not only the intrinsic nature of the nanoscale size of the particles, but also by the processing conditions and related difficulties, such as green density, agglomeration.

First, similar to powder compacts of micron sized powders, the densification of a powder compact depends significantly on the green density of the compact. The green density must be sufficiently high in order to achieve adequate densification under similar sintering conditions. On the other hand, the finer the particle sizes, the lower the green density of powder compacts assuming the compaction pressure is the same. Therefore, it is generally observed that the sintering of nanosized powders is affected by the compaction pressure [40-42].

It has been widely recognized that agglomeration of nanoparticles has a critical impact on the sintering of nanoparticles. Due to the extremely fine size and the strong interactive force between particles, nanoparticles tend to form agglomerate. The size and the strength of the agglomerated particles affect the densification rate. The most direct investigation of the agglomeration of densification was summarized by Mayo [43] whose data were based on numerous published experimental results as shown in Fig 2.3.

In essence, a powder compact can be viewed as consisting of a bilevel hierarchical structure: the compact is made of agglomerates which are made of nanosized particles. There is, therefore, a bimodel pore size distribution. The pores existing within agglomerates are finer than the pores between agglomerates. The densification of individual agglomerate is relatively easy, while the elimination the interagglomerate pores is more difficult.
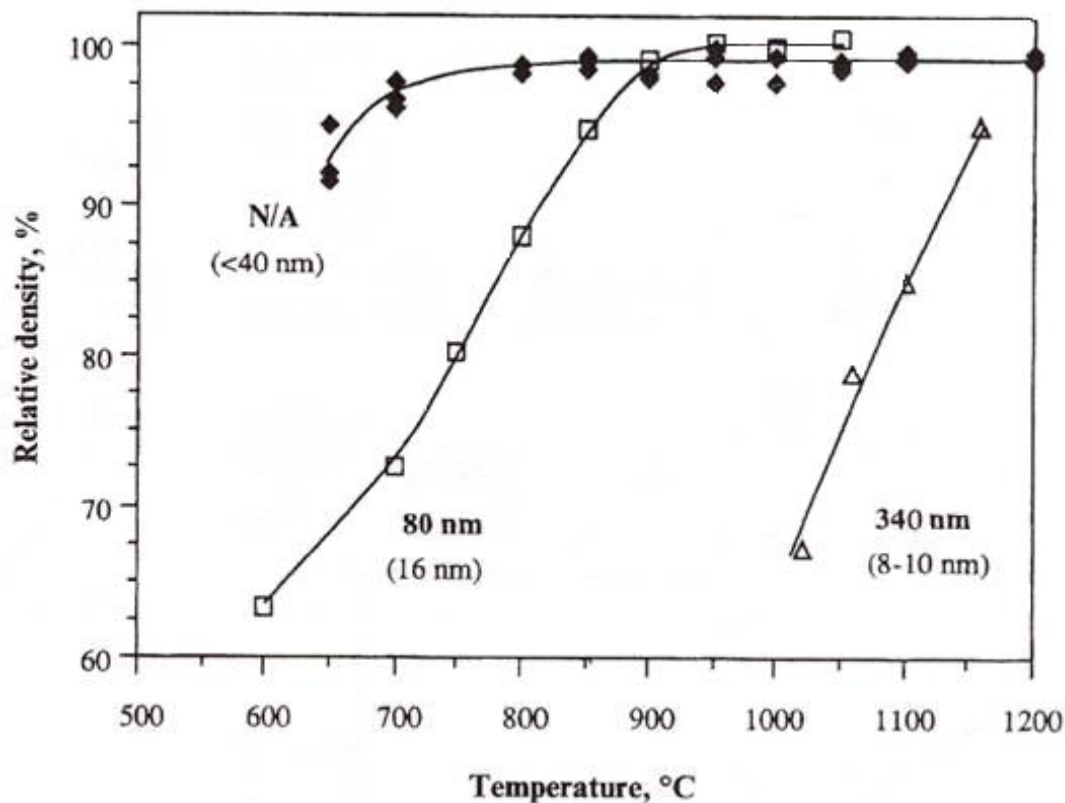
Fig. 2.3 Densification behavior of nanocrystalline TiO₂ with three different agglomerate sizes: note that the larger the agglomerate size, the higher the sintering temperature (agglomerate size in bold, crystallite size in light). For the nonagglomerated (N/A) powder, sintering time is 120 min; for the 80 and 340 nm agglomerate powders, sintering time is 30 min. (After Ref. 43)

By tracking the evolution of pore size distributions, Peterson et al. [44] studied the sintering of fine grain cemented tungsten carbide and cobalt system (WC-Co). They showed that during the intermediate stage of sintering, the considerable densification obtained is primarily connected to removal of small pores rather than shrinkage of larger ones.

To sinter nanoparticles for fabrication of bulk engineering components, a colloidal solution must be dried; agglomerates will inevitably form. Ideally, the agglomerates are

soft and the interagglomerate pores are small. Lange provided a more extensive discussion on ceramic powder processing techniques for avoiding agglomeration and achieving uniform pore distributions within a powder compact [45].

2.1.2.3 Effect of Pores on Nanosintering

A common thread for the effect of green density and agglomeration on sintering is the effect of pores on densification [46].

A compact consists of particles and pores, and each pore has a volume, shape and coordination number. The pore coordination number is defined as the number of touching particles surrounding and defining each void space. A pore's surface morphology is determined by the dihedral angle and the pore's coordination number. In general, for a given dihedral angle, a critical coordination number, n_c, exists that defines the transition of the pore surface morphology from convex ($n>n_c$) to concave ($n<n_c$). Kingery and Francois [47] first recognized that only those pores with $n<n_c$ are able to shrink during sintering because the concave surface morphology with negative chemical potential is thermodynamically unstable. As a result, atoms will diffuse to the pore surface and fill the void space. The stability of pores is dependent on the dihedral angles and the coordination number. For a given dihedral angle, which is dictated by the material, there is a critical coordination number below which the pores will shrink and above which the pores will grow.

The effects of green density and agglomeration on densification can be explained by the pore coordination number theory. Higher green density and less agglomeration result in fine and uniform pores that shift the pore coordination number distribution from high values to low values, i.e., more pores fall into the category below the critical pore

coordination number. These pores are easily removed during sintering and, thus, lead to denser products. As for the large pores that are thermodynamically stable and have coordination numbers higher than the critical value, a process by which the coordination number can be reduced during sintering is essential, since the pores will again become unstable and the densification will then continue. Particle rearrangement and grain growth are the two processes that can play this role, creating a dilemma, of course, and difficulty for any attempt to achieve maximum densification without grain growth.

2.1.3 Densification Mechanisms During Nanosintering

2.1.3.1 Calculation of Activation Energy

In order to understand the mechanisms of sintering, activation energy is commonly used as an indicator of the internal mechanistic process. In most cases, activation energy can be calculated from isothermal experimental data. A derivation by Johnson et al. [48] resulted in a densification equation based on two sphere models and both volume and grain boundary diffusion mechanisms. The initial stage sintering of a powder compact is described by Theunissen et al. [49]

$$[\frac{(\Delta l / l_0)}{T}] = const \exp(\frac{-mE_a}{RT}) \tag{2.6}$$

where m is a constant characteristic for the sintering mechanism, i.e., 1/2 for volume diffusion and 1/3 for grain boundary diffusion, E_a is the apparent activation energy for densification, $\Delta l/l_0$ is the relative shrinkage during continuous heat up and R and T are the gas constant and absolute temperature, respectively. Linearization of the equation results in [49]

$$\ln[\frac{(\Delta l / l_0)}{T}] = \frac{-mE_a}{RT} + const \tag{2.7}$$

On plotting $(-\ln[(\Delta l/l_0)/T]$) vs $1/T$, a straight line with slope mE_a/R is obtained when only one single mechanism is operative.

Obviously, isothermal relationships of densification as a function of time at several temperatures are required to obtain relatively reliable data of activation energy. An inherent assumption of this approach is that the mechanisms of densification, or any other process of interest, should not change within the temperature range of the experiments. Otherwise, the calculated value does not represent a single mechanism; rather, it is an effective activation energy that results from multiple mechanisms.

As stated earlier, densification and grain growth during sintering of nanosized powders take place rapidly during the heating up process. In order to capture the changes during continuous heating, Dorn method [50] can be used to calculate activation energy. To determine the activation energy of creep, Dorn allowed a sample to deform under a constant tensile stress at a temperature T_1 and then rapidly raised or lowered the temperature to a new value T_2 where the sample was allowed to deform further. Then the deformation rates corresponding to the temperatures are determined for the time in which the temperature is changed. According to this method, the activation energy of the responsible mass transport phenomenon can be determined using the relationship

$$Q = \frac{RT_1T_2}{T_1 - T_2} \ln\{\frac{T_1(de_1 / dt)}{T_2(de_2 / dt)}\} \tag{2.8}$$

where T_1 and T_2 and are the temperatures of the sample before and after rapid heating, (de_1/dt) and (de_2/dt) are the respective shrinkage rates immediately before and after the temperature rise, R is the universal gas constant, and Q is the activation energy. The temperature difference between T_1 and T_2 should not exceed 50°C.

To evaluate activation energies of kinetic processes during continuous heating, a number of other methods can be found in literature [51-53].

2.1.3.2 Analysis of the Mechanism of Densification

Using the various methods described above, activation energies for sintering a variety of nanosized powders were reported. For example, a very low activation energy for densification is observed in initial sintering--about 234 kJmol^{-1} for nanocrystalline Al_2O_3 and 96.2 kJmol^{-1} for nanocrystalline TiO_2 [54], 268 kJmol^{-1} for nanocrystalline ZnO [55], 66.2 kJmol^{-1} for nanocrystalline nickel [56], 82 kJmol^{-1} for nanocrystalline α titanium and 49 kJmol^{-1} for nanocrystalline β titanium [57].

Using these activation energy values to deduce sintering mechanisms has inherent shortcomings with respect to accuracy, because in almost all cases, multiple mechanisms may be operating simultaneously. Especially during the early stages of sintering, when no one clearly dominant mechanism can be identified, the activation energy values calculated using the kinetic data give an effective activation energy value that is the combined effect of multiple mechanisms.

It can be seen from the data, however, that the majority of studies point toward lower activation energies for early stages of sintering. This is reasonable for the obvious reason of the huge surface areas and expected high activity of nanoparticles. Surface diffusion is one of the most cited mechanisms that contribute to the sintering of nanosized particles.

However, in conventional sintering theories, surface diffusion is believed to induce initial neck formation between particles, but not densification. In principle it is correct that surface diffusion will only cause the bonding of particles to each other, but not the dimensional shrinkage, i.e., the densification, of a multiparticle compact. This seemingly conflicting thought on the effects of surface diffusion on sintering of nanoparticles can be understood from a perspective of indirect roles of surface diffusion to densification.

The indirect role of surface diffusion on densification can be understood based on theories of the relationship between coarsening and sintering of particles [58-61]. As discussed earlier, effects of pores on nanosintering, according to theories first proposed by Kingery and Francois and further elaborated by Lange et al. [46, 47], a pore will shrink during sintering only if the coordination number of the pore is smaller than a critical value $n<n_c$ because only then is the surface of the pore concave. Thermodynamic driving force dictates that mass will diffuse from convex surfaces to concave surfaces. Initial sintering of a compact will develop an equilibrium configuration at which the driving force for further sintering is zero. Grain growth, or coarsening, will perturb the equilibrium configuration to reinitiate neck growth (sintering) and densification. In other words, at a critical value of coordination number, a pore is at equilibrium. The shrinkage of the pore, i.e., sintering will no longer progress until the equilibrium condition can be tipped in favor of sintering again by grain growth. With respect to the mechanisms of densification of nanosized particles, surface diffusion can cause the coarsening of nanoparticles which, in turn, contributes to the process of densification. Therefore, it can be stated that the surface diffusion contributes indirectly to densification by inducing

coarsening. Further discussion on the relationship between grain growth and densification will be given later.

Surface premelting is another mechanism that could lead to rapid densification at low temperature during nanosintering. As a result of large surface to volume ratio in nanoparticles, surface premelting can happen at low temperature, and under this condition, particle rearrangement is facilitated by sliding, rotation, or viscous flow. Alymov et al. [10] calculated the dependence of the melting point of a particle as a function of its size using the following equation:

$$T_m / T_0 = 1 - 2Q^{-1}\rho_s^{-1}\left[\sigma_{sl} /(r - \delta) + \sigma_{lg} r^{-1}\left(1 - \rho_s / \rho_l\right)\right] \tag{2.9}$$

where T_0 is the bulk melting point of the solid, Q is its latent heat of fusion. σ_{sl} and σ_{lg} are the interfacial surface tensions between the solid and the liquid and between the liquid and its vapor respectively, and ρ_s and ρ_l are the densities of the solid and liquid respectively, r is the radius of particle, and δ is the thickness of melted layer on a particle surface.

Based on the relation that sintering temperature is proportional to the melting point, it was suggested that as the melting point decreases, the sintering temperature decreases. It was stated that the melting of a particle with diameter d will result in its coagulation with its neighbors and will become the center of a new big particle. In an independent study of the sintering of nanometric Fe and Cu, Dominguez et al. [13] attributed the initial densification to surface melting mechanisms because the activation energies that were obtained from either constant heating or isothermal experiments were too small to ascertain lattice diffusion mechanisms. In fact, Dominguez et al. claimed that the

activation energy measured in the course of their experiments is very small, compared to the values published for the self-diffusion of the metal in the liquid state. Therefore, it was reasoned that the presence of a liquid-like layer on the surface of the nanometric particles during sintering could simultaneously explain such phenomena as high diffusivity, enhanced grain growth at a narrow temperature range.

Although surface melting is a reasonable mechanism for sintering nanosized particles, no direct experimental evidence supporting the formation of liquid phase has been published to date. In fact, because the formation of any liquid at temperatures below equilibrium melting point will be thermodynamically unstable, there could be only transient liquid which makes experimental verification of the presence of liquid phase even more difficult.

A more generally applicable theory that explains the rapid densification of nanosized particles is based on the hypothesis of nonequilibrium high concentration of vacancies at the interparticle grain boundaries. In 1974, Vergnon et al. studied the "initial stage for the sintering of ultrafine particles TiO_2 and Al_2O_3" [54]. Using flash sintering and isothermal experimental techniques, it was shown that during the first 20 seconds, a fraction up to 95% of the total observed shrinkage was registered [54]. There was an initial loss of surface area, before the shrinkage starts during the heating of the compact to the desired temperature, a process which requires only a few seconds. It was reasoned that this almost instantaneous loss of the surface area corresponds to the formation of junction zones between particles of the compact. The fast formation of the junctions between particles, before the shrinkage onset, involves the creation of a high concentration of vacancies inside these junctions. The shrinkage of the compact results then from a

decrease of the distance between the centers of particles due to annihilation of the trapped vacancies in the junction zone. Because the concentration of trapped vacancies inside the junction zone largely exceeds the thermodynamic equilibrium concentration, the diffusion can be considered as independent of time and controlled only by the probability of jumping of ions, as long as the concentration of vacancies exceed the equilibrium content. Any further sintering, after the initial nonequilibrated concentration of vacancies is exhausted, corresponds with the diffusion of equilibrated vacancies.

Also based on the theory that there is excessive concentration of vacancies ($c>10^{-4}$), Trusov et al. [12] stipulated that there appears the possibility of liquid like merging (coalescence) of particles into large ones. Liquid-like coalescence as well as slippage causes the ultrafine particles' compact shrinkage.

In another study focusing on size dependent grain growth kinetics observed in nanocrystalline Fe, Krill et al. [62] also established their model on the basis of existence of excess volume at the grain boundaries. The "excess" volume is in the form of vacancies, which leads to a nonequilibrium vacancy concentration. The issues of grain growth of nanoparticle during sintering will be further discussed in later sections of this review.

Finally, the rapid densification mechanisms of nanosized particles are also related to the preferential crystalline orientations. In loose nanocrystalline powders, it has been observed that the first neck formation occurs not randomly between particles, but by the orderly mating of parallel, crystallographically aligned facets on the particle surfaces [63, 64]. Some nanocrystalline powder compacts also appear to reflect a kind of ordered

structure resulting from less than random type matings of particles during the initial stage of sintering [65].

2.1.3.3 Kinetic Theories, Modeling and Simulations of Nanosintering

Given the unique physics when sintering nanosized particles, considerable work has also been reported on theoretical modeling of thermodynamics and kinetics of sintering of nanosized particles. In one of the more significant studies, Pan recognized that the rapid kinetic rate of sintering is a direct result of the large driving force for sintering of nanosized particles, and revised the two-sphere sintering model by using nonlinear diffusion law [38]. Because the diffusion is the result of jumping atoms, the flux of diffusion as a function of the frequency of jumping (f), volume atomic concentration (C_{solid}), and the atomic spacing (a) can be given by

$$ J = \frac{2D}{a\Omega} \sinh\left(\frac{aF}{2kT}\right) \qquad (2.10) $$

where D is the diffusion coefficient; Ω is the atomic volume; a is the atomic spacing; F is the driving force for diffusion; k and T are the Boltzmann constant and absolute temperature, respectively. Pan pointed out that this equation reduces to linear diffusion law, when aF≤kT, then sinh(aF/2kT)≈aF/2kT. However, when particle sizes are in the range of nanometers, the linear approximation is no longer reasonable. Then, the diffusion equation becomes a nonlinear equation that can only be solved via numerical methods. Applying this approach to the case of sintering two particles, the ratio of the neck to particle radius as a function of the time at a given temperature was calculated and the rate predicted by nonlinear solutions is larger than that predicted by linear solutions

during initial stage of sintering. But the differences between the two diminish as sintering time increases. The distinction between linear and nonlinear solutions also diminishes as particle size increases.

The rapid rate of sintering based on the rapid rate of diffusion is also supported by recent studies that indicate that the coefficient of diffusion, D, is size dependent as shown in equation 2.11 [39]:

$$D(r,T) = D_0 \exp\left[\frac{-E(\infty)}{RT} \exp\left[\frac{-2S_{vib}(\infty)}{3R} \frac{1}{r/r_0 - 1}\right]\right] \quad\quad (2.11)$$

where D_0 is preexponential constant, $E(\infty)$ is bulk activation energy, $S_{vib}(\infty)$ is bulk melting entropy, r is particle radius, $r_0=3h$ (h is atomic diameter) for nanoparticles, R is ideal gas constant, T is absolute temperature.

The dependence of the coefficient of diffusion on particle size is attributed to the fact that, as the size of the nanocrystals decreases, the activation energy of diffusion decreases and the corresponding coefficient of diffusion increases based on the Arrhenius relationship between them. Together these theories, based on nonlinear diffusion law and the increase of the coefficient of diffusion with decreasing particle size, convincingly argue for the rapid formation of necks bonding neighboring particles together.

With the development of modern tools of computational materials science, considerable effort has been made toward numerical simulation of the sintering of nanoparticles. One of the most notable works was published by Zhu and Averback [66, 67] in 1995, who simulated the sintering of YSZ using molecular dynamics (MD) approach. MD simulations of sintering have been conducted on numerous other materials

as well [68-73] The basic approach toward simulating sintering using MD method involves tracking the motion of atoms under the stress that is caused by surface or interfacial energy. The kinetics of sintering is given as the rate of decreasing distance between two atoms in the middle of two particles in contact. It was shown that the sintering of nanosized particles at the atomic level can be accomplished by dislocation motion and grain boundary rotation, as well as other mechanisms. It was further predicted that the sintering time of nanoparticles would be in the range of a few hundred picoseconds. Although the predicted sintering time is far from engineering reality, the results of the simulation can be used as a basis for understanding the initial bonding or formation of the necks between nanoparticles.

Due to the limitations of studying sintering by using atomic scale simulation, multiscale simulation is considered a promising approach. Pan [74] categorized the simulations of sintering in three levels: atomic level, particle level, and component level. The primary method of atomic level simulation is MD, as mentioned earlier. In particle level simulation, which is also classified as mesoscale simulation [75], classic sintering models [1, 48, 49, 76-88] based on mass transport between two or multiple particles provide the basis of simulation. The kinetics of sintering densification depends on the kinetics of specific diffusion mechanisms that control the rate at this stage of the process. In Pan's review, the typical numerical methods used in particle level simulations include finite difference method, variational calculus, and finite element method. To model the evolution of the microstructure during sintering, however, Monte Carlo method is often a popular choice [89-93]. The finite element method is the primary method for simulation

at the component level, which is chiefly concerned with macro scale shrinkage, distortion, and dimensional accuracy control.

Overall, most published studies of simulations of sintering were not nanoscale specific, except for the MD simulations described above. Although these methods are arguably applicable to sintering of nanosized particles, especially during the later stages of sintering, further details on simulation of sintering is beyond the scope of this review, which focuses on the size dependent characteristics of sintering of nanoparticles.

2.2 Grain Growth During Nanosintering

2.2.1 The Issues of Grain Growth During Nanosintering

A primary motivate for studying sintering of nanosized particles is rooted in the issue of rapid grain growth during sintering. In many cases, particularly when the goal is to produce nanocrystalline bulk materials, the objective of nanosintering is to not only achieve full densification but also retain nanoscaled grain structure in the sintered material. Research has generally shown that after sintering, nanosized particles lose nanoscale characteristics because grain size grows to greater than 100 nm. Therefore, understanding and controlling grain growth is a critical scientific and technical issue of nanosintering.

In a systematic study of the stabilities of nanosized metal powders, Malow and Koch [94-96] reported that the rate of grain growth of nanocrystalline iron (Fe) powders made by ball milling is initially very rapid (<5 min) when annealed at various temperatures (Fig. 2.4). Grain growth then stabilizes during the extended isothermal holding (up to 142
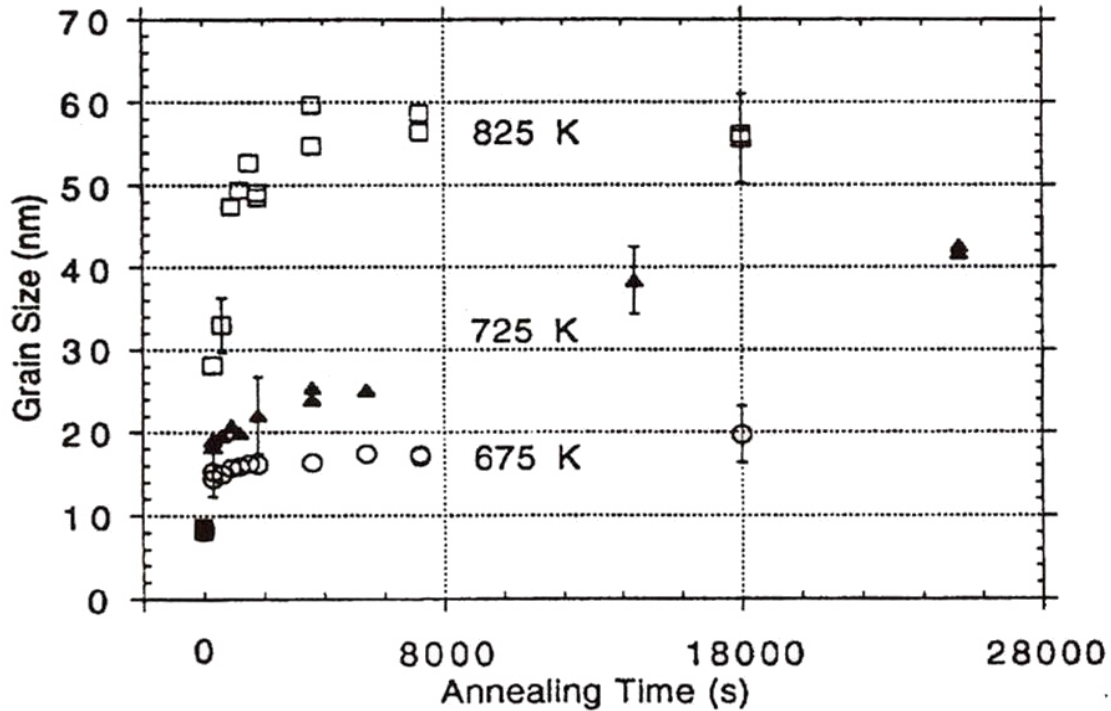
Fig. 2. 4 Evolution of the grain size as a function of the annealing time at three annealing temperatures for nanocrystalline iron. The grain size was determined by the Scherrer equation. (Reprinted with permission from The Minerals, Metals & Materials Society)

hours). During the isothermal holding, grain growth follows a generalized parabolic grain growth law and is similar to that found in bulk materials. It is noted, based on Fig. 2.4, that at the first data point of the isothermal annealing curves at higher annealing temperatures (825 and 875 K), the grain sizes are already several times (3-6x) greater than the original as milled grain size (~8 nm). In other words, grains grow rapidly during heat up, prior to reaching the preselected isothermal holding temperature.

In another study of the grain growth of nanocrystalline Fe using in situ synchrotron X-ray diffraction techniques, Krill et al. [62] further demonstrated that grain growth of nano Fe particles is comprised of three steps: the "initial growth spurt," a linear growth stage, and then the normal parabolic stage, as shown in Fig. 2.5. Once again, the normal parabolic stage can be modeled using the classic grain growth parabolic law. However the "initial growth spurt" of nanocrystalline Fe during annealing was not captured by isothermal studies.
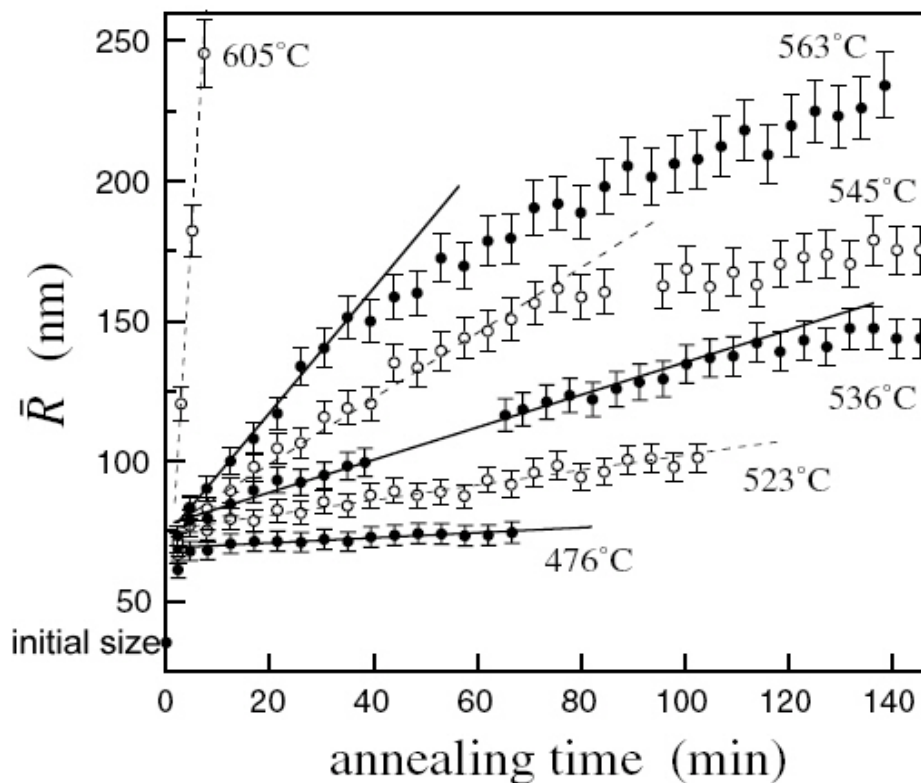
Fig. 2.5 Size-dependent grain growth kinetics observed in nanocrystalline Fe (Reprinted with permission from American Physical Society)

Grain growth during nanosintering is also a strong function of temperature. Fig. 2.6 [97] shows the relationship between grain size and temperature during heat treatment of nanocrystalline cobalt powder. It is obvious that the grain growth is initially slow at very low temperatures and it accelerates dramatically when the temperature is above an apparent critical temperature range. Similar behavior has also been reported for sintering of other nanocrystalline ceramic, as well as for metallic powders [98-104]. It appears that a critical temperature exists, above which the grain growth accelerates dramatically as a function of temperature.
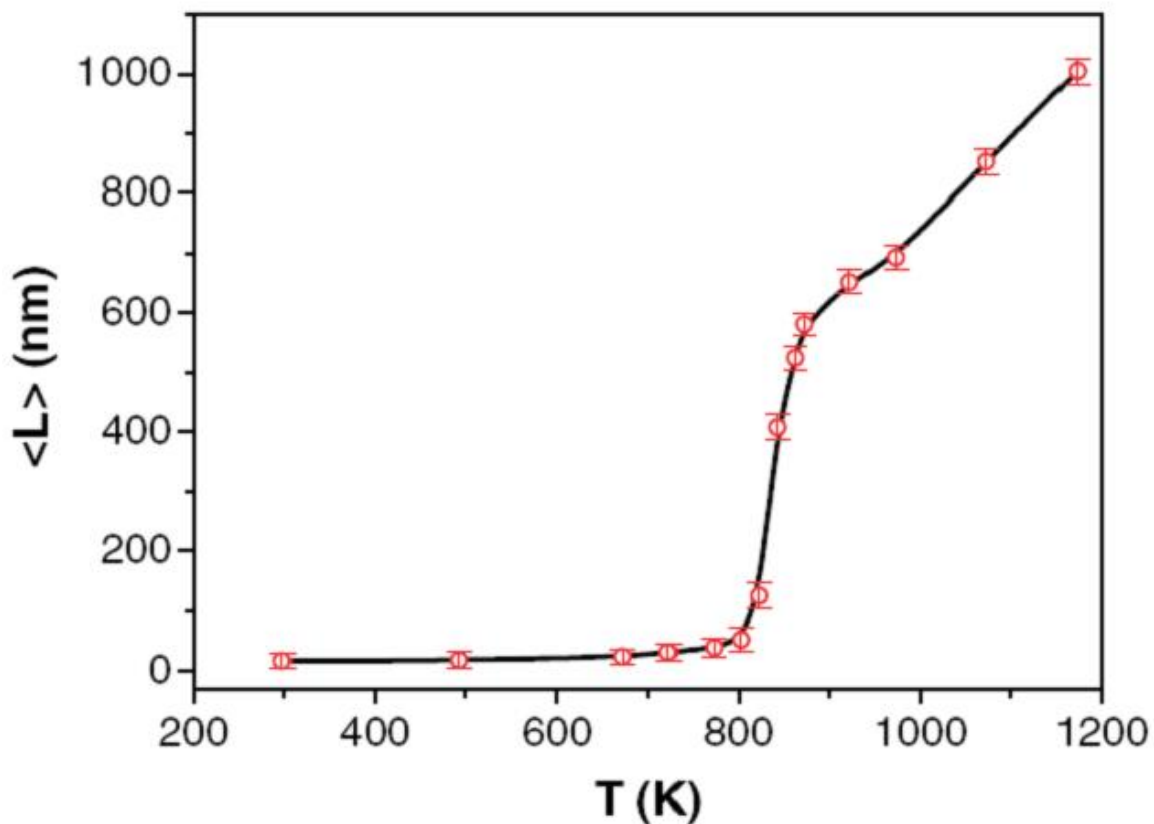
Fig. 2.6 Change of the mean grain size (the linear intercept) with annealing temperature, measured in pure nanocrystalline Co. (Reprinted with permission from Elsevier)

The unique issues of grain growth during sintering can be studied by examining the grain size versus relative density relationship. In one of the earliest studies of the sintering and grain growth of nanosized ceramic powders in the 1990s, Owen and Chokshi[105] and Averback et al. [106] showed that oxides densify without significant grain growth until the density reaches approximately 90% of the bulk density. Then the grain growth becomes very rapid. This phenomenon is observed in many different materials [40, 43, 107, 108]. A typical relationship between grain size and density during nanosintering is schematically shown in Fig. 2.7. This relationship implies that the grain growth during sintering consists of two stages: the early stages of sintering, before the
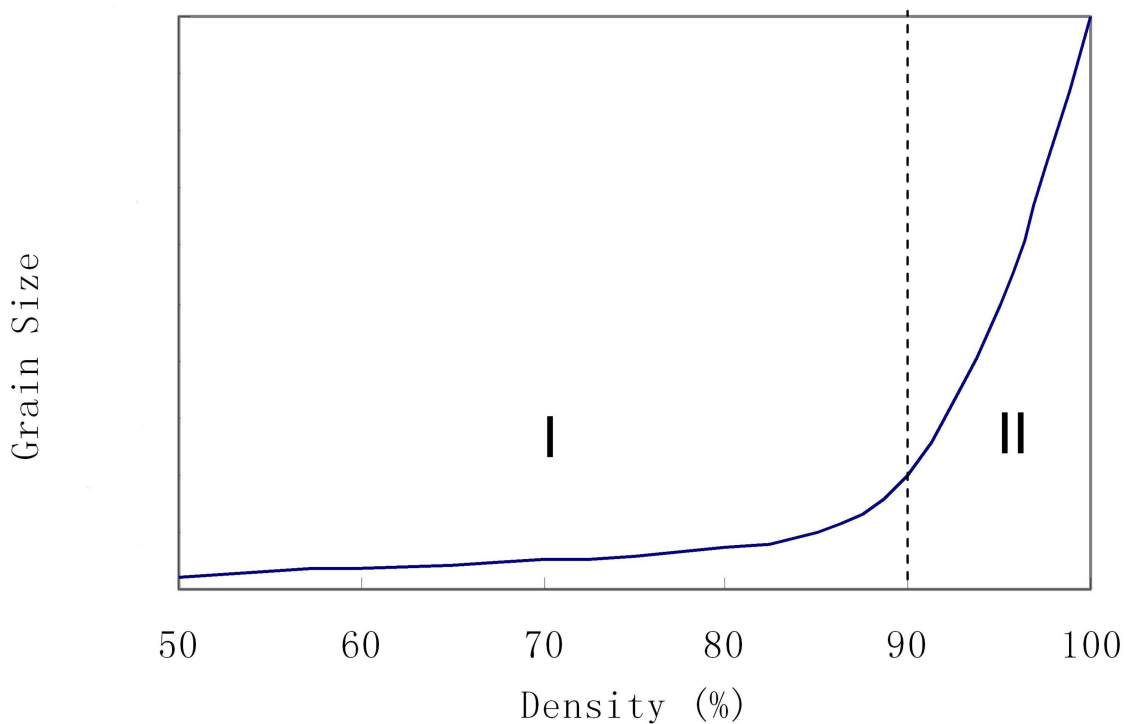
Fig. 2. 7 Relationship between grain growth and densification during nanosintering. I. early stage of grain growth; II. late stage of grain growth

powder compact reaches 90% relative density; and the late stages of sintering, when relative density is greater than 90%. It is believed that the late stages of grain growth can be viewed as "*normal*" grain growth, similar to that in bulk materials by boundary migration, but incorporating the effect of pinning by closed pores. In contrast, the early stage of grain growth during sintering is often referred to as "*coarsening*".

Fig. 2.8 shows another example of grain growth versus densification during the sintering of nanocrystalline Y_2O_3 materials [109]. This work demonstrated that the normal grain growth stage during sintering, the mechanism of which will be discussed later in this section, can be controlled. The result also shows that at the starting point for
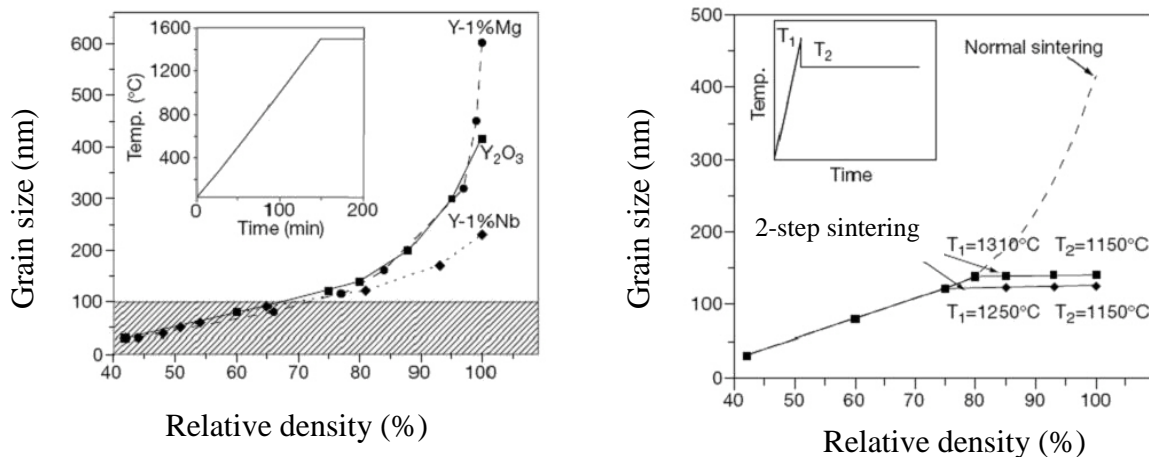
Fig. 2. 8 Sintering trajectories for normal and two-step sintering. (a). Increasing grain size of Y_2O_3 with density in normal sintering. (Heating schedule shown in inset). Even with fine starting powders (30 nm), the final grain size of dense ceramics is well over 200 nm regardless of whether dopant was used. The shaded area indicates the grain size regime commonly defined as nanostructured materials. At lower densities, the mean grain (particle) size was estimated on the fracture surface. At higher densities, the grain size was obtained by multiplying by 1.56 the average linear intercept length of at least 500 grains. (b). Grain size of Y_2O_3 in two-step sintering. (Heating schedule shown in inset.) Note that the grain size remains constant in the second sintering step, despite density improvement to 100%. (Reprinted with permission from Nature Publishing Group)

the normal grain boundary controlled grain growth, grain size has grown to 4 to 6 times the initial grain size of the nanosized powder. This part of grain growth is attributed to coarsening.

In short, from a kinetic perspective of grain growth as a function of time, experimental observations as described above suggest that the grain growth of nanosized particles during sintering can be treated as consisting of two steps: a dynamic grain growth process that occurs during heating up and at the beginning of isothermal duration, and the static grain growth during isothermal holding. From another perspective of the interrelations of grain growth to densification, the grain growth during sintering consists of two stages: first, when the relative density is lower; and, second, when the relative density is greater than 90%. It should be emphasized that although the late stage of grain growth, when relative density is greater than 90%, accounts for the majority of total grain growth, early stage grain growth that occurs during heating (when relative density is still lower than 90%) is significant and sufficient to reach beyond nanoscale. Thus, if grain size is to be maintained at nanoscale, this part of grain growth must be controlled. However, it appears from the search of open literature that although the early stage of grain growth process is critical to nanosintering, few published studies to date focus on this aspect of grain growth. In the following sections, the issues of grain growth during nanosintering in both the "normal" and "initial" stages will be examined.

2.2.2 Normal Grain Growth During Nanosintering

when Rel. Density >90%

In general, when the relative density is greater than 90% during sintering of micron sized particles, bonding between powder particles by neck growth is well developed and

the majority of pores within a sintered body are closed and isolated. Grain growth during the continued sintering densification process is akin to that of bulk materials during heat treatment, although the remaining pores can still hinder the kinetic rate of grain growth during this stage. Consequently, this stage of grain growth is referred to as "normal" grain growth. Typically, because the properties of sintered materials depend on their final grain sizes, the final stage of grain growth during sintering has received, therefore, the most attention.

2.2.2.1 Grain Growth Law – Kinetics of Normal Grain Growth

Classic treatment of grain growth in solid materials was reviewed in several studies [37, 110, 111]. It is generally believed that the mechanism of grain growth in bulk materials is by curvature driven grain boundary migration. The basic assumption is that the driving force of grain growth is a function of the grain boundary curvature and the migration rate of grain boundary is proportional to the driving force [112]

$$v = MF \tag{2.12}$$

where v is migration velocity of a grain boundary, which is related to the changing rate of grain size $v \propto \dfrac{dG}{dt}$; M is the mobility, and the mobility of a grain boundary is determined by the diffusivity of the material and temperature.; F is the driving force of grain growth $F \propto 1/G$, G is the grain size.

Hence,

$$\frac{dG}{dt} = \frac{cM}{G} \tag{2.13}$$

where c is a constant. By integrating over time, the classic parabolic grain growth law is

$$G(t)^2 - G_0{}^2 = kt \qquad (2.14)$$

where $k = k_0 \exp\left(-\dfrac{Q}{RT}\right)$ is the rate constant of grain growth that is a function of the

mobility of grain boundary; k_0 is a constant; Q is activation energy for grain boundary

migration; R is gas constant; T is absolute temperature.

In practice, accounting for the fact that the experimental observed grain growth data

do not always fit equation (2.14) with the exponent equals to 2, the parabolic grain

growth law is usually generalized as

$$G(t)^n - G_0{}^n = kt \qquad (2.15)$$

Equation (2.15) is thus termed as *generalized parabolic grain growth model* [113]. When

n is variable, grain growth kinetics can be better described by equation (2.15).

Considering the effect of factors such as segregation of impurities on grain

boundaries that mitigate grain growth, the dependence of grain size on time is further

modified as [114-116]

$$\frac{G_0 - G(t)}{G_\infty} + \ln\left(\frac{G_\infty - G_0}{G_\infty - G(t)}\right) = kt \qquad (2.16)$$

where G_∞ denotes the grain size when the grains cease to grow at $t \to \infty$. This is also

termed as *grain growth model with impediment* [113].

In the process of grain growth, the volume fraction of grain boundaries decreases; therefore, the concentration of solute and impurity atoms segregated to the grain boundary is expected to increase, resulting in a grain size dependent retarding force on grain boundary migration. On this basis Michels et al. [117] proposed a *grain growth model with size dependent impediment*.[113]

$$G(t) = \sqrt{G_\infty^2 - \left(G_\infty^2 - G_0^2\right)\exp(-kt)} \tag{2.17}$$

In a detailed study of the grain growth of nanocrystalline Fe prepared by pulsed electrodeposition, Natter [113] applied all three grain growth models to the data of grain size versus time as shown by Fig. 2.9. It was noted that the generalized parabolic growth model appropriately fits the data at low temperature, with unrealistically large grain growth exponents n>10. The growth model with impediment yields the best fit among the three models considered. Using the adjustable parameters contained in these models, the authors calculated the rate constants and, hence, the activation energies for grain growth of nanocrystalline Fe. It was concluded that, although the generalized parabolic model yielded a good fit with variable "n" values, the activation energy calculated based on that fit was unreasonably high (220kJmol[-1]) for what is assumed to be grain boundary diffusion in nanocrystalline Fe. Therefore, it was declared by the authors that the generalized parabolic model failed.
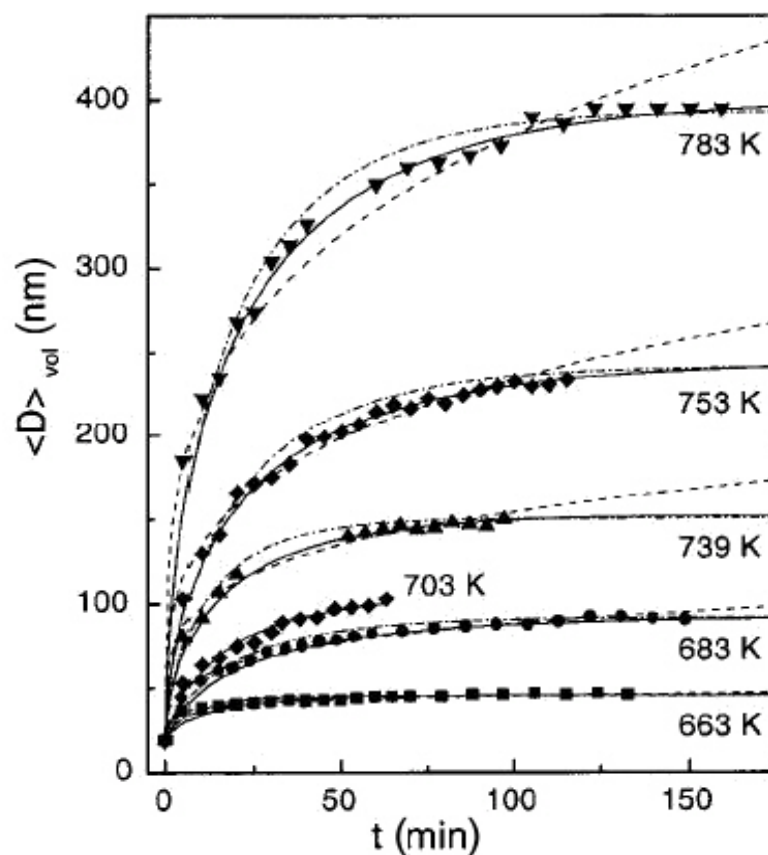
Fig. 2. 9 Temperature and time evolution of the volume-weighted average crystallite diameters of nano-Fe; the lines represent fit with different kinetic grain-growth models. Dashed lines represent fit with the generalized parabolic grain-growth model; solid lines represent fit with the grain-growth model with impediment; dashed-dotted lines represent fit with size-dependent impediment. (Reprinted with permission from American Chemical Society)

The activation energies calculated, based on the rate constant deduced from the impediment model, however, yielded an activation energy value of 170 kJmol^{-1}, which is in agreement with other published values for grain boundary diffusion [118, 119]. Thus, based on the calculated activation energies, the authors summarized that the grain growth model with impediment was a good candidate for describing the isothermal kinetics of grain growth of nanocrystalline metals.

As discussed earlier in this article, an approach that uses activation energy values to gain insight about the grain growth or densification mechanisms is inherently limited because the models contain varying parameters which can result in mathematical flexibility that would enable the model to fit almost any data. It is very difficult, however, to assign physical meaning to the parameters n and k. The fact that the grain growth of nanoparticles during sintering may be attributed to multiple mechanisms makes the matter even more complicated.

In a different approach of applying the generalized parabolic grain growth models, Feng Liu et al. [120] analyzed grain growth data in separate "domains," meaning different stages of grain growth at different sequential time periods. For each time period, a fixed value of n=2 and/or 3 is used in modeling. The overall grain growth equation is expressed as follows:

$$G(t)^2 - G_0{}^2 = \begin{cases} k_1 t & t \leq t_1 \\ k_1 t + k_2(t-t_1) & t_2 > t > t_1 \\ \Lambda & \Lambda \\ \Lambda & t_{n-1} > t > t_{n-2} \\ k_1 t + k_2(t-t_1) + \Lambda + k_n(t-t_{n-1}) & t_n > t > t_{n-1} \end{cases} \qquad (2.18)$$

According to this model, the rate constant k and activation energies change as grain growth progresses. Specifically, activation energies increase as grain size increases. This is attributed to the increasing segregation of impurities on grain boundaries which reduces grain boundaries hence the driving force for grain growth. Within each growth time period, or "domain," the activation energies and rate constants k hold constant. Compared to conventional parabolic models, this model takes into account the effect of

the changes in thermodynamic properties on the kinetics of grain growth. The assumption of the model is that the grain growth is fully accomplished by grain boundary diffusions. Direct evidence of the mechanisms of grain growth of nanoparticles during sintering is, however, still sorely needed.

2.2.2.2 Effect of Pores on Grain Growth in the Late Stages of Sintering

As in sintering of coarser particles, in the final stage of sintering of nanoparticles, grain growth will be affected by remaining pores that pin the grain boundaries and reduce the kinetic rate of grain growth. The effect of pores on grain growth during the final stage of conventional sintering is reviewed by Rahaman and Kang [37, 111].

In the final stage of sintering, isolated spherical pores are situated at the grain boundaries, in particular, at triple junctions. Pores are considered to be a second phase with an inhibiting force against boundary movement. The interaction between pore and boundary determines the conditions for either pore attachment or separation, which, in turn, determines the rate of grain growth during the final stage of sintering.

As grain grows, the moving boundary applies force on the pore at the final stage of sintering. As force is applied on the pore, the shape change, resulting in chemical potential difference between atoms at the leading and trailing surfaces, driving the flux of atoms from the leading surface to trailing surface. Thus, the pore will migrate with the grain boundaries. The mechanism of pore movement includes surface diffusion, lattice diffusion and evaporation/condensation.

Similar to grain boundary motion, the pore velocity v_p is expressed as

$$v_p = M_p F_p \tag{2.19}$$

where M_p is the pore mobility, which depends on the mechanism of pore migration [37, 48, 111, 121, 122]. F_p is the driving force for the migration of pores. Due to the presence of the pores at grain boundaries, the driving force of boundary migration is decreased due to the inhibition force of the pore against boundary migration. Thus, the velocity of boundary migration can be written as

$$v_b = M_b F = M_b \left(F_b - NF_p \right) \tag{2.20}$$

where M_b is the boundary mobility, and F is the effective driving force on the boundary $F = \left(F_b - NF_p \right)$. F_b is the driving force of boundary migration with no pores at boundaries. N is the number of pores per unit grain boundary area.

A comparison between the velocity of the pore migration and the velocity of the boundary migration reveals whether the pore attaches to the boundary or the pore separates from the boundary as grain grows during the final stage of sintering. The condition for pore attachment to the boundary is $v_b = v_p$, which can be expressed as

$$v_b = v_p = M_p F_p = M_b \left(F_b - NF_p \right) \tag{2.21}$$

and hence

$$v_b = \frac{M_p M_b}{NM_b + M_p} F_b \tag{2.22}$$

Two limiting cases can be considered [121, 123]:

a) A system containing many pores with low mobility, i.e., $NM_b \gg M_p$

b) A system containing fewer pores with high mobility, i.e., $NM_b \ll M_p$

In the first case, pore migration controls boundary migration, which is referred to as *pore control*.

$$v_b = \frac{M_p}{N} F_b \tag{2.23}$$

In the second case, the presence of the pores has almost no effect on the boundary velocity, so the migration of the grain boundary is controlled by its intrinsic mobility. This condition is referred to as *boundary control*.

$$v_b = M_b F_b \tag{2.24}$$

The condition under which a pore can separate from the boundary is $v_p < v_b$, which can also be expressed as

$$M_p F_p < M_b \left(F_b - N F_p \right) \tag{2.25}$$

Rearranging the equation, it can be written as

$$F_b > \left(\frac{M_p}{M_b} + N \right) F_p \tag{2.26}$$

Equation (2.26) reveals that the inhibition force of the pore cannot balance the driving force on the boundary; therefore, the separation of pore/boundary occurs. Once the

boundary breaks away from the inhibition of the pore, the rate of grain growth will significantly increase.

Due to the presence of large number of pores in the system at the beginning of the final stage of nanosintering, the boundary is at first dragged by the pore and the rate of grain growth is slow. But as sintering proceeds, both the number and the size of the pore decreases as a result of densification. When the density reaches the specific point at which pore/boundary separation occurs, grain growth accelerates dramatically.

2.2.2.3 Ostwald Ripening

The generalized grain growth law describes another category of grain growth which is based on Ostwald ripening. The theory of Ostwald ripening was originally developed for the coarsening of precipitates in two phase materials. The mechanism of the coarsening of second phase particles is solution-and-reprecipitation. During liquid phase sintering, the solution-reprecipitation mechanism is responsible for increased average grain size due to the growth of larger particles at the expense of smaller particles. The term "coarsening" is also used in a more general sense to describe the increase of grain sizes, as well as particle sizes, during sintering. At isothermal conditions, the kinetics of grain growth by solution-reprecipitaiton is also given by the polynomial law as follows:

$$G(t)^n - G_0{}^n = kt \qquad (2.27)$$

where n is the grain growth exponent. Usually n = 3 for diffusion controlled processes and n =2 for interface controlled processes.

2.2.2.4 Two Step Sintering: Decoupling of Grain

Growth from Densification

As an example of understanding and controlling normal grain growth during nanosintering, Chen and Wang [109] developed a clever approach to decoupling grain growth from densificaton of nanosized particles, using a pressureless sintering process to fully densify nanocrystalline Y_2O_3. In a simple two step process, the compact is briefly heated to 1310^oC; the temperature is then lowered to 1150^oC and held at that temperature for a long time. As a result, the material can be sintered to full density with minimum grain growth. If the lower temperature is applied at the onset, complete densification would not be possible. It is reasoned, then, that suppression of the final stage grain growth is achieved by exploiting the difference in kinetics between the grain boundary diffusion and the grain boundary migration. Grain growth requires grain boundary migration which requires higher activation energy than grain boundary diffusion. At a temperature that is high enough to overcome the energy hurdles for grain boundary diffusion, but low enough to deactivate grain boundary migration, the densification will proceed via grain boundary diffusion without triggering significant grain growth. This phenomenon was further studied in multiple publications of Kim et al.[124-126]

It is noted, once again, that in this work to successfully decouple grain growth from densification by exploiting difference in grain boundary mechanisms, the authors explicitly showed that at the beginning of the second sintering step, the grain size increases 4 to 6 times larger than the original size of the powder, which is attributed to coarsening during the first sintering step (Fig. 2.8). The following section will focus on coarsening, or in other words, the initial grain growth of nanoparticles.

2.2.3 Initial Grain Growth (Coarsening) of Nanoparticles

During Early Stages of Sintering (Rel. Density < 90%)

The above discussion provides evidence of an initial stage of grain growth. This part of grain growth occurs in the beginning of the sintering, often during heating up when the relative density is less than 90%. In conventional sintering of micron sized powders, the initial stage of grain growth is not significant and is often ignored in the analysis of experimental data because its contribution to the final grain size is relatively minor, compared to normal grain growth during latter stages of sintering. For nanosintering, however, two important points must be made with regard to the initial stage of grain growth:

1). The amount of grain growth during nanosintering is significant, and sufficient in many cases to cause the material to lose nanocrystalline characteristics;

2). The initial grain growth can be described by the generalized classic parabolic grain growth law only if very large values of growth exponent are used, which represent no physical processes. This implies that the mechanism of grain growth in the initial stage may be different from that of the normal grain growth stage.

2.2.3.1 Neck Formation and Coarsening of Contacting Nanoparticles

To understand initial grain growth, the key issue is the interaction between ultrafine particles at the start of sintering. According to classical sintering theories by Kuczynski [88], Kingery [84], Coble [127], Johnson [128], necks will form and grow between adjacent particles, which are assumed to have equal diameter. Densification is modeled as the approach of the centers of the two particles. Under these situations, no grain growth occurs at the beginning of sintering. Fig. 2.10 illustrates that when very fine particles are
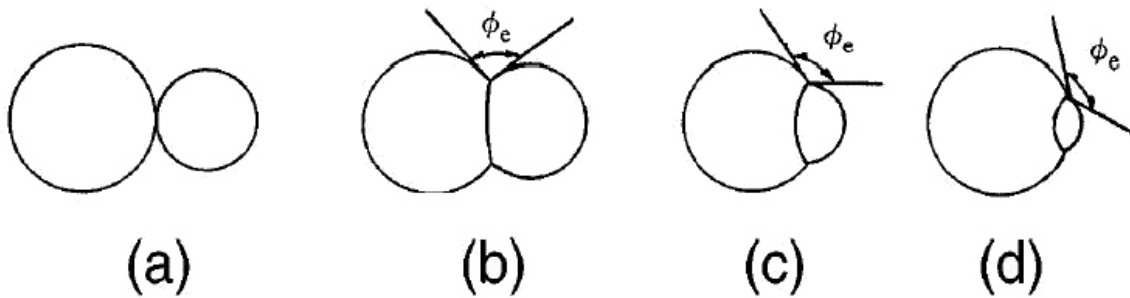
Fig. 2. 10 A linear array of two spheres of initial radii of r_1 and r_2 ($r_1 > r_2$): (a) just in touch without the formation of interface, (b) when $r_1/r_2 < R_c$, (c) $r_1/r_2 = R_c$, and (d) $r_1/r_2 > R_c$. (After Ref. 59)

in contact, if the particle sizes are not uniform, interparticle diffusion will lead to coarsening of particles in addition to formation of the neck. Large particles will grow at the expense of small particles. The coarsening of particles can be understood using the criteria as shown by equation (2.28), which was first expressed by Lange [58] based on Kingery's initial concept in pore stability [47].

$$R_c = -\frac{1}{\cos \phi_e} \qquad (2.28)$$

R_c is called critical particle size ratio for boundary migration, ϕ_e is the dihedral angle relating surface energy and grain boundary energy. Lange explained that when the size ratio between two particles is larger than the critical size ratio R_c, grain boundary migration will occur, resulting in grain growth. When actual size ratio is less than R_c, boundary migration will yield an increase in the grain boundary area and is energetically unfavorable. In this situation, interparticle mass transport will happen first to increase the size ratio between adjacent particles. This coarsening process will not stop until the size

ratio $R=r_1/r_2$ reaches R_c, then grain boundary migration will take over because the condition for grain boundary migration is now energetically satisfied.

The studies by Lange and Kingery aimed to explain the stability of pores in the intermediate stage of sintering. Shi further applied the critical size ratio criteria to the initial sintering of ultrafine particles [59, 60]. It was shown that the driving force for neck growth and interparticle diffusion are given respectively is as follows

$$\Delta\mu_n = \gamma_s\Omega\left(\frac{1}{X} - \frac{1}{r}\right) \tag{2.29}$$

$$\Delta\mu_c = 2\gamma_s\Omega\left(\frac{1}{r_1} - \frac{1}{r_2}\right) \tag{2.30}$$

$\Delta\mu_n$ and $\Delta\mu_c$ are chemical potential for neck formation and mass transport between two particles; γ_s is surface energy; Ω is atomic volume; X is radius of the neck; r is radius of particles (r_1 and r_2 are radii of two particles with different sizes). Equation (2.30) indicates that if a difference of the radius of curvature exists, mass transport would take place from the area of larger curvature to the area of smaller curvature. This process is related to the particle coarsening.

Considering equations (2.29) and (2.30) together, both the neck growth and coarsening, driven by the surface tension between the particles, can take place concurrently. However, the magnitude of the driving force for the two processes is different. Assuming the interface energy is not considered, then $\Delta\mu_n < \Delta\mu_c$, which implies that neck formation takes place before coarsening.

On the other hand, if the interface energy between particles is considered in the analysis of the driving forces as an energy barrier to neck growth, Shi showed that equation (2.29) becomes

$$\Delta\mu_n{}' = \gamma_s\Omega\left(\frac{1}{X} - \frac{1}{r}\right) - \gamma_b f(r,\phi,\phi_e) \tag{2.31}$$

where γ_b is boundary energy, ϕ is the contact angle, ϕ_e is the equilibrium dihedral angle. From a thermodynamic point of view, when $\phi = \phi_e$, the driving force for the neck growth is zero. Intuitively it is possible under certain conditions when $\phi < \phi_e$, driving force for coarsening may equal that for neck growth. Hence, coarsening by interparticle mass transport may take place significantly prior to the achievement of the equilibrium dihedral angle and the beginning of grain boundary migrations.

With regard to the issues of initial grain growth, a two step qualitative growth model was developed [129]. When particles of different sizes are in contact, the first step in grain growth is coarsening due to interparticle mass transport via the growth of larger particles into smaller particles, which result in the increase of the material's average grain size regardless of whether the size ratio r_1/r_2 is larger or smaller than R_c. During the coarsening and sintering progress, the size ratio between particles can increase. When the condition of size ratio $r_1/r_2 > R_c$ is reached, grain boundary migration will occur, leading to the second step of grain growth by the grain boundary migration. Fig. 2.10 and Fig. 2.11 schematically illustrate the two step process.
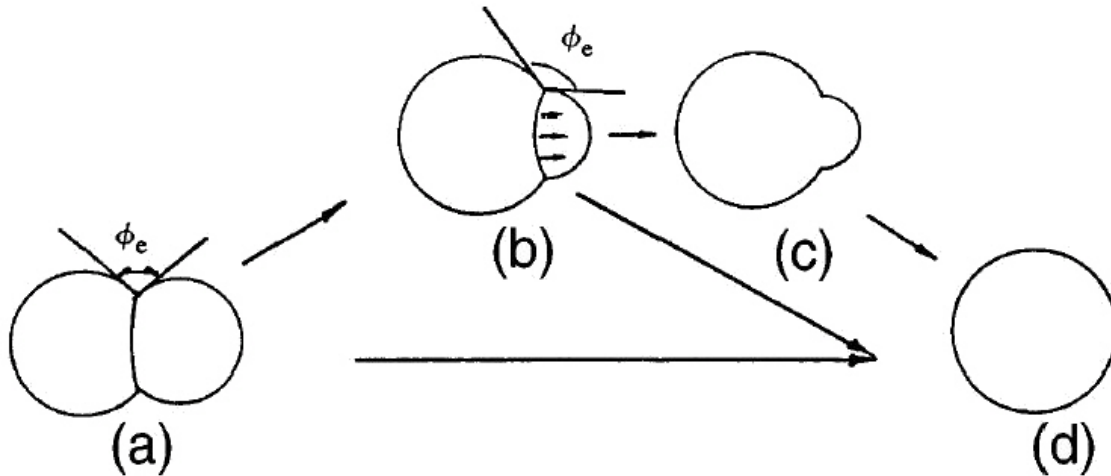
Fig. 2. 11 Particle configuration change after the formation of a dihedral angle shown in Fig 2.10: (a) the configuration when $r_1/r_2 <R_c$ (boundary cannot move); (b) the configuration resulted from the mass transport between particles before boundary motion; (c) the transient configuration after boundary motion where r_1/r_2 becomes $>R_c$; (d) final configuration either directly by mass transport or by combined mass transport and boundary motion. (After Ref. 59)

The differences in grain growth kinetics at different stages of sintering suggest differences in grain growth mechanisms, which would also be a function of specific material systems. The mechanism for normal grain growth is widely believed to be grain boundary migration. However, as indicated in the above discussion, the mechanism of coarsening, or initial grain growth, could be different depending upon the specific situation with regard to relative particle size ratios and dihedral angles. Possible mechanisms of initial grain growth are discussed in the following sections.

2.2.3.2 Initial Grain Growth Mechanisms

Based on conventional grain growth theories, several possible grain growth mechanisms for grain growth during nanosintering exist, including: 1) grain boundary migration, 2). surface diffusion, 3). solution reprecipitation, and 4). coalescence.

Understandably, surface diffusion is expected to be a highly probable mechanism, due to the extremely fine particle sizes.

It has been demonstrated that surface diffusion leads to grain growth of nanosized particles. In a study of the sintering $BaTiO_3$, Shi observed that the contacting particles become one particle via surface diffusion as shown in Fig. 2.12 [61]. Surface diffusion transported the atoms from the dissolving small particle to be redeposited on the surface of the larger particle. This is direct evidence of the role of surface diffusion in the coarsening of nanoparticles at the beginning of sintering. Although surface diffusion induced grain growth is not a widely recognized grain growth mechanism, it could play an important role in the initial grain growth. It is noted that surface diffusion causes coarsening of larger particles by consuming small particles, i.e., grain growth without requiring either grain boundary migration, rotation, or grain boundary diffusion.

Considering that the initial grain growth during sintering is the result of the coarsening of nanoparticles due to interparticle diffusions, there are other interparticle diffusion mechanisms, other than surface diffusion, that could also contribute to coarsening of particles. In particular, there is a relaxation period for migration, redistribution, and annihilation of the defects due to the fact that nanoparticles are usually not at equilibrium states and are likely to contain excess amounts of various defects that are created during the production of nanoparticles. Owing to the nonequilibrium structure of nanoparticles, diffusivity is dramatically enhanced during the relaxation process [130-133]. This may contribute to dynamic grain growth at the beginning of sintering. Dynamic grain growth usually dominates during the heat up stage and the first few minutes after reaching a preset isothermal holding temperature. Therefore, rapid dynamic
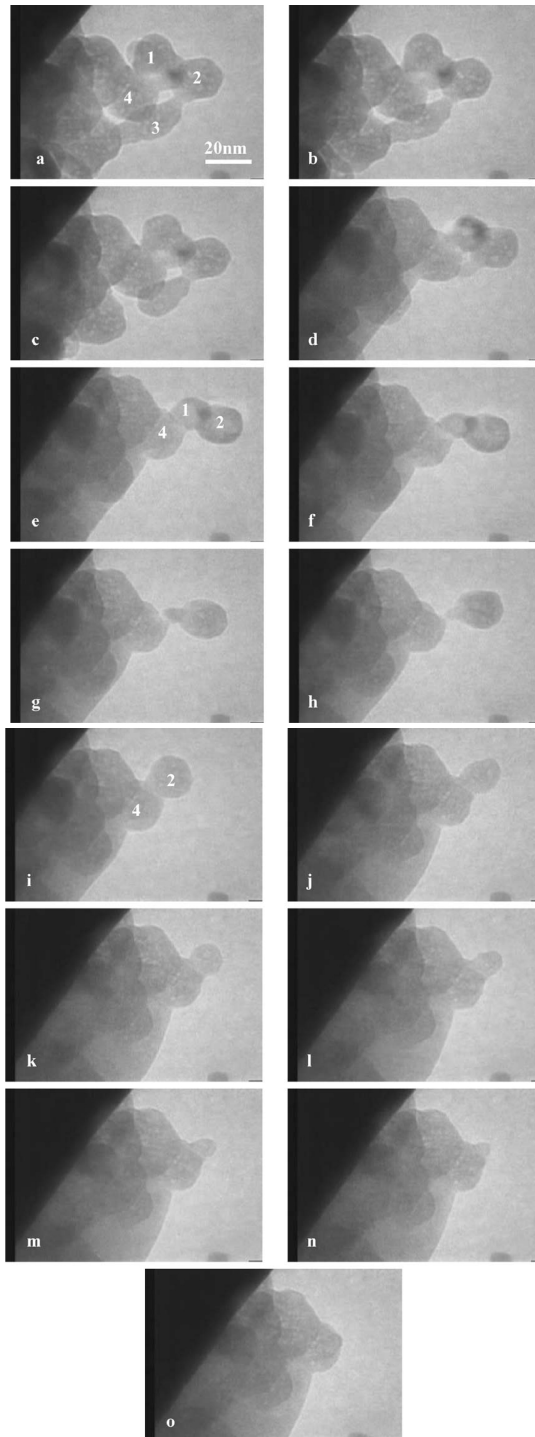
Fig. 2. 12 Observations of the grain growth in BaTiO3 powder at different temperatures from 940°C (a), 950°C ((b), (c)) to 960°C ((d) to (o)). Grains grow through reduction of smaller grains and enlargement of larger ones. The distance between the particle centers decreases simultaneously. (Reprinted with permission from Springer Science and Business Media)

isothermal holding is several times of the initial grain size. The relaxation time depends on materials, nanoparticles production methods, and temperature.

The role of grain boundary migration should also be considered in discussing the initial grain growth during nanosintering. Grain boundary migration is, of course, the most recognized grain growth mechanism for solid bulk monophase materials. The driving force for grain boundary migration is the curvature of grain boundaries. Grain boundaries migrate in the direction of the center of the curvature. Grain boundary migration can be accomplished by either volume or grain boundary diffusion. The activation energy is primarily determined by the volume diffusion. For single phase materials at later stages of sintering, when relative density is great than 90%, grain boundary migration is the most logical mechanism of grain growth as that for in bulk single phase materials. Grain boundary migration has also been observed during early stages of sintering of nanosized Al_2O_3 [64].

Coalescence is another grain growth mechanism that is often cited to explain rapid grain growth qualitatively. Coalescence is a term that is often loosely used to describe various phenomena. For example, coalescence is sometimes used interchangeably with the term "sintering" to describe the growth of particles during particle synthesis and growth process [134-137]. For clarity in this article, coalescence is used strictly to describe the increase of grain size due to the merging of two grains by eliminating the common grain boundaries between them. Differing from other grain growth processes which may also be described as the merging of two grains, the two original grains should not demonstrate significant change from their morphology prior to coalescence.

The term coalescence, as defined above, describes a unique way of grain growth, which is accomplished only through various diffusion mechanisms. Possible mechanisms for coalescence include grain boundary diffusion, dislocation climb along grain boundaries, or even grain rotations. In liquid phase sintering systems, it is believed that the solution-reprecipitation mechanism may also help facilitate the coalescence of grains. Direct evidence of coalescence is, however, very difficult to get identify. Fang et al. [138] studied the grain growth of nano WC during sintering, and found the growth of nanosized tungsten carbide grains with aggregates via coalescence, as shown in Fig. 2.13. It has been speculated that when nanoscales are approached, atomic mechanisms become more obvious. For example, the rotation and alignment of nanosized grains may be easier than
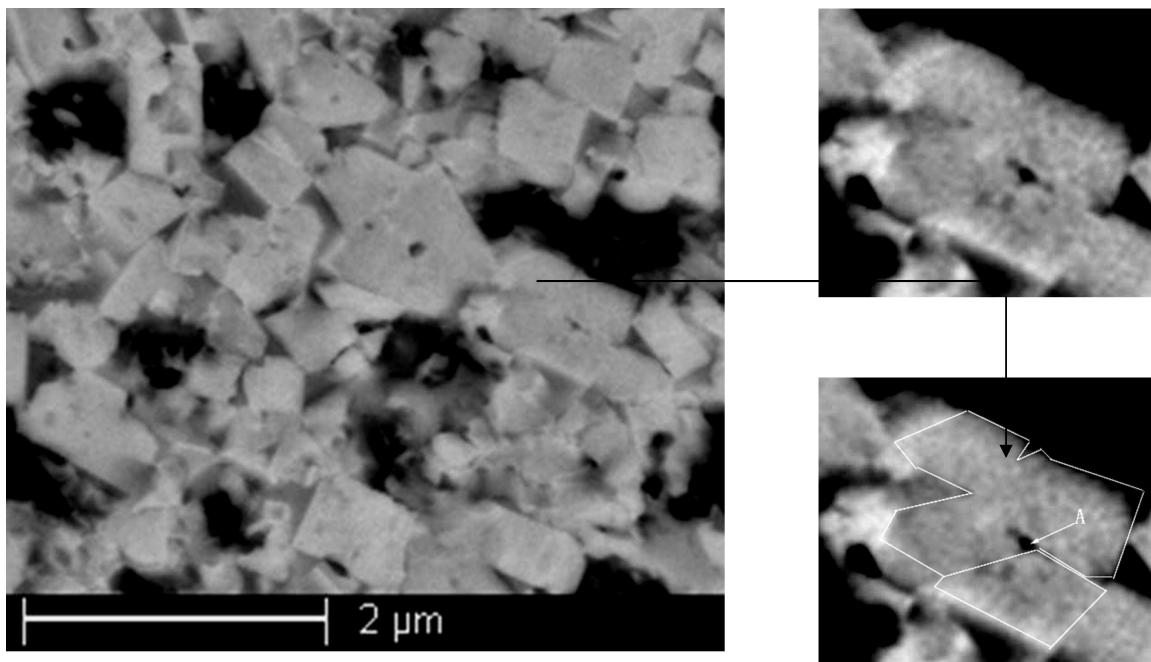
Fig. 2. 13 Coalescence of two platelet shaped grains of a nanocrystalline WC-Co compact heated up to 1200 ºC at a heating rate of 10 ºC/min. and held for 1 min. (After Ref. 138)

coarse grains [40]. Kumar and Fang's analysis of the sintering of WC-Co composites suggests that the lattice shift along low-energy CSL grain boundaries is a viable mechanism for materials with high degree of crystallographic anisotropy [139].

2.2.3.3 Effects of Agglomerates on Initial Grain Growth

Another important factor in grain growth mechanisms during nanosintering is the role of agglomerates in grain growth. Mayo [43] pointed out that grain size is often related to the size of agglomerates at the beginning of sintering. As Mayo summarized, the larger the agglomerate size, the higher the sintering temperature required to eliminate the large interagglomerate pores. By contrast, the crystallite size has little effect on the temperature required to reach full density. The same temperatures, however, promote grain growth to such an extent that the grain size can easily balloon to the agglomerate size.

To explain the effect of agglomerates, Lange [46] classified the structure of a powder compact as a hierarchical structure of agglomerates, domains, and primary particles, as shown by Fig. 2.14. Defining the coordination number as the number of particles surrounding the pore, Lange explained that pores within domains have the lowest coordination number, pores between domains have higher, and pores between agglomerates have the highest coordination number. Fig. 2.15 shows schematically the volume distribution of the three classes of pores as a function of coordination number. When $N<N_c$, a pore is unstable. Otherwise, grain growth, or coarsening of particles within agglomerates, will be necessary for elimination of the pore and continuation of the sintering. This explains the correlation between grain growth and the size of agglomerates.
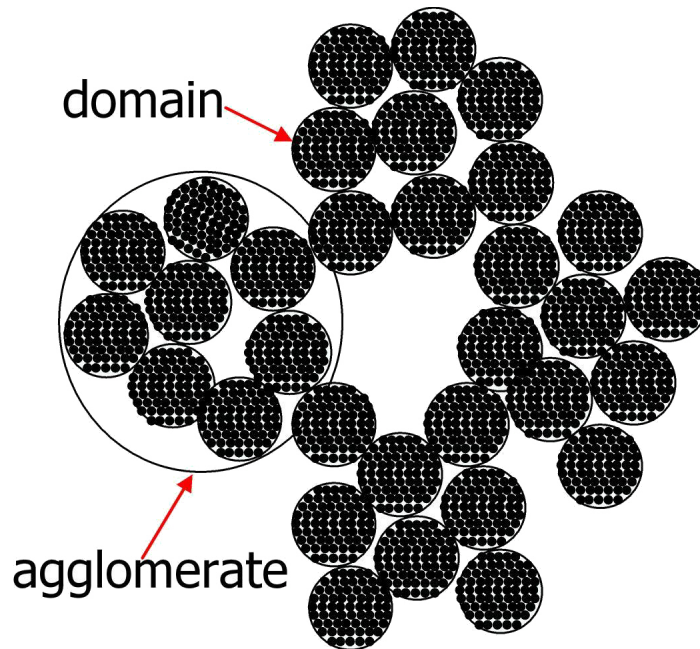
Fig. 2. 14 Schematic diagram of the hierarchical structure of agglomerates (large circle), domains (small circle), and primary particles (dots within small circles).
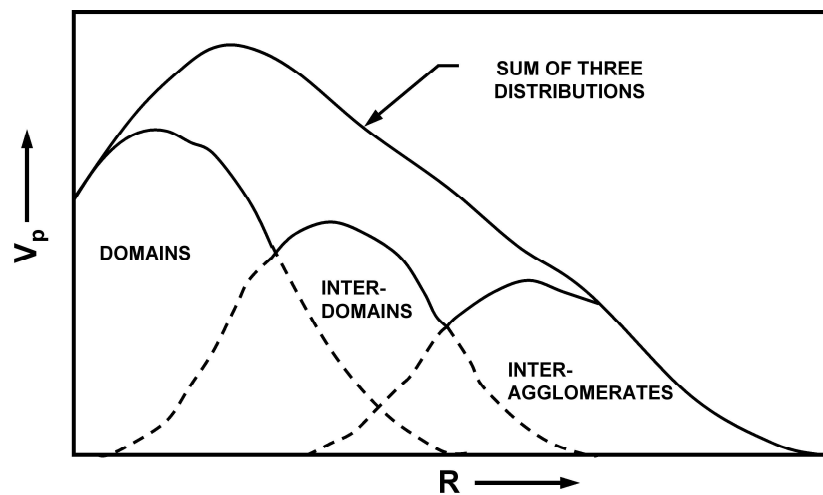
Fig. 2. 15 Schematic of pore coordination number distribution of agglomerated powder indicating three classes of pores, i.e., those within domains, those between domains, and those between agglomerates. (R stands for coordination number). (After Ref. 46)

2.3 References

[1]   German RM. Sintering Theory and Practice: Wiley-Interscience, 1996.

[2]   Campbell CT, Parker SC, Starr DE. Science 2002;298:811.

[3]   Nanda KK, Maisels A, Kruis FE, Fissan H, Stappert S. Phys Rev Lett 2003;91:106102.

[4]   Lee H-Y, Riehemann W, Mordike BL. J Eur Ceram Soc 1992;10:245.

[5]   Hahn H. Nanostruct Mater 1993;2:251.

[6]   Skandan G. Nanostruct Mater 1995;5:111.

[7]   Mayo MJ. Materials & Design 1993;14:323.

[8]   Zhou YC, Rahaman MN. J Mater Res 1993;8:1680.

[9]   Rabe T, Waesche R. Nanostruct Mater 1995;6:357.

[10]   Alymov MI, Maltina EI, Stepanov YN. Nanostruct Mater 1994;4:737.

[11]   Lee JS, Kim TH. Nanostruct Mater 1995;6:691.

[12]   Trusov LI, Lapovok VN, Novikov VI. Problems of Sintering Metallic Ultrafine Powders. In: Uskokovic DP, Plamour III H, Spriggs RM, editors. Science of Sintering. New York: Plenum Press; 1989.

[13]   Dominguez O, Champion Y, Bigot J. Metall Mater Trans A 1998;29A:2941.

[14]   Malewar R, Kumar KS, Murty BS, Sarma B, Pabi SK. J Mater Res 2007;22:1200.

[15]   Oda E, Ameyama K, Yamaguchi S. Mater Sci Forum 2006;503-504:573.

[16]   Attarian Shandiz M, Safaei A, Sanjabi S, Barber ZH. J Phys Chem Solids 2007;68:1396.

[17]   Buffat P, Borel JP. Phys Rev A 1976;13:2287.

[18]   Castro T, Reifenberger R, Choi E, Andres RP. Phys Rev B 1990;42:8548.

[19]   Couchman PR. Philos Mag A 1979;40:637.

[20]   Couchman PR, Jesser WA. Nature 1977;269:481.

[21]   Couchman PR, Ryan CL. Philos Mag A 1978;37:369.

[22]   Jiang Q, Zhang S, Zhao M. Mater Chem Phys 2003;82:225.

[23] Olson EA, Efremov MY, Zhang M, Zhang Z, Allen LH. J Appl Phys 2005;97:034304.

[24] Qi WH, Wang MP. Mater Chem Phys 2004;88:280.

[25] Ross J, Andres RP. Surf Sci 1981;106:11.

[26] Shi FG. J Mater Res 1994;9:1307.

[27] Solliard C. Solid State Commun 1984;51:947.

[28] Wautelet M. Solid State Commun 1990;74:1237.

[29] Wautelet M. Eur J Phys 1995;16:283.

[30] Wautelet M. Phys Lett A 1998;246:341.

[31] Yang P, Jiang Q, Liu X. Mater Chem Phys 2007;103:1.

[32] Troitskii VN, Rakhmatullina AZ, Berestenko VI, Gurov SV. Sov Powder Metall Met Ceram 1983;22:12.

[33] Jiang Q, Shi FG. J Mater Sci Technol 1998;14:171.

[34] Herring C. J Appl Phys 1950;21:301.

[35] Messing GL, Kumagai M. Am Ceram Soc Bull 1994;73:88.

[36] Yan MF, Rhodes WW. Mater Sci and Eng 1983;61:59.

[37] Rahaman MN. Ceramic Processing and Sintering, Second Edition. New York: CRC, 2003.

[38] Pan J. Philos Mag Lett 2004;84:303.

[39] Jiang Q, Zhang SH, Li JC. Solid State Commun 2004;130:581.

[40] Groza JR. Nanocrystalline Powder Consolidation Methods. In: Koch CC, editor. Nanostructured Materials - Processing, Properties and Potential Applications. William Andrew Publishing/Noyes; 2002.

[41] Gutmanas EY. Prog Mater Scie 1990;34:261.

[42] Gutmanas EY, Trusov LI, Gotman I. Nanostruct Mater 1994;4:893.

[43] Mayo MJ. Int Mater Rev 1996;41:85.

[44] Petersson A, Agren J. Acta Mater 2005;53:1673.

[45]   Lange FF. J Am Ceram Soc 1989;72:3.

[46]   Lange FF. J Am Ceram Soc 1984;67:83.

[47]   Kingery WD, Francois B. Sintering of Crystalline Oxide, I. Interactions Between Grain Boundaries and Pores. In: Kuczynske GC, Hooton NA, Gibbon GF, editors. Sintering and Related Phenomena. New York; 1967.

[48]   Johnson DL. J Appl Phys 1969;40:192.

[49]   Theunissen GSAM, Winnubst AJA, Burggraaf AJ. J Eur Ceram Soc 1993;11:315.

[50]   Bacmann JJ, Cizeron G. J Am Ceram Soc 1968;51:209.

[51]   Li C-R, Tang TB. J Mater Sci 1999;34:3467.

[52]   Ozawa T. J Therm Anal 1970;2:301.

[53]   Flynn JH, Wall lA. Polym Lett 1966;4:191.

[54]   Vergnon P, Astier M, Teichner SJ. Polymer Preprints, Division of Polymer Chemistry, American Chemical Society 1974:299.

[55]   Ewsuk KG, Ellerby DT, DiAntonio CB. J Am Ceram Soc 2006;89:2003.

[56]   Panigrahi BB. Mater Sci Eng A 2007;460-461:7.

[57]   Dabhade VV, Rama Mohan TR, Ramakrishnan P. Mater Sci Eng A 2007;452-453:386.

[58]   Lange FF, Kellett BJ. J Am Ceram Soc 1989;72:735.

[59]   Shi JL. J Mater Res 1999;14:1378.

[60]   Shi JL. J Mater Res 1999;14:1389.

[61]   Shi J-L, Deguchi Y, Sakabe Y. J Mater Sci 2005;40:5711.

[62]   Krill III CE, Helfen L, Michels D, Natter H, Fitch A, Masson O, Birringer R. Phys Rev Lett 2001;86:842.

[63]   Carim AH. Microstructure in Nanocrystalline Zirconia Powders and Sintered Compacts. In: Hadjipanayis GC, Siegel RW, editors. Nanophase materials : synthesis, properties, applications Dordrecht, The Netherlands: Kluwer Academic Publishers; 1994.

[64]   Bonevich JE, Marks LD. Mater Res Soc Symp Proc 1993;286:3.

[65]   Ying JY, Chi LF, Fuchs H, Gleiter H. Nanostruct Mater 1993;3:273.

[66]   Zhu H, Averback RS. J Eng Appl Sci 1995;A204:96.

[67]   Zhu H, Averback RS. Mater Manuf Processes 1996;11:905.

[68]   Xing Z, Shaoqing W, Caibei Z. J Mater Sci Technol 2006;22:123.

[69]   Koparde VN, Cummings PT. J Phys Chem B 2005;109:24280.

[70]   Tsuruta K, Omeltchenko A, Kalia RK, Vashishta P. Europhys Lett 1996;33:441.

[71]   Raut JS, Bhagat RB, Fichthorn KA. Nanostruct Mater 1998;10:837.

[72]   Win-Jin C, Te-Hua F, Jun-Wei C. Microelectr J 2006;37:722.

[73]   Hai D, Kyoung-Sik M, Wong CP. J Electron Mater 2004;33:1326.

[74]   Pan J. Int Mater Rev 2003;48:69.

[75]   Olevsky EA, Tikare V, Garino T. J Am Ceram Soc 2006;89:1914.

[76]   Ashby MF. Acta Metallurgica 1974;22:275.

[77]   Beere W. Acta Metallurgica 1975;23:139.

[78]   Coble RL. J Appl Phys 1961;32:787.

[79]   Exner HE. Rev Powder Metall Phys Ceram 1979;1:11.

[80]   Exner HE. Powder Metall 1980;23:203.

[81]   Exner HE, Arzt E. Sintering Processes. In: Cahn RW, Haasen P, editors. Physical Metallurgy, vol. 3. Amsterdam: Elsevier Science; 1996.

[82]   Exner HE, Kraft T. Review on computer simulations of sintering processes. Powder Metallurgy World Congress & Exhibition 1998, vol. 2. Shrewsbury, UK, 1998. p.278.

[83]   Frenkel J. J Phys 1945;9:385.

[84]   Kingery WD, Berg M. J Appl Phys 1955;26:1205.

[85]   Mackenzie JK, Shuttleworth. Proceedings of the Physical Society. Section B 1949;12:833.

[86]   Olevsky EA. Mater Sci Eng R 1998;23:41.

[87]   Scherer GW. J Am Ceram Soc 1977;60:236.

[88]   Kuczynski GC. JOM 1949;1:169.

[89]   Matsubara H. J Ceram Soc Jpn 2005;113:263.

[90]   Rao Madhavrao L, Rajagopalan R. J Mater Res 1989;4:1251.

[91]   Braginsky M, Tikare V, Olevsky E. Int J Solids Struct 2005;42:621.

[92]   Tikare V, Braginsky M, Olevsky EA. J Am Ceram Soc 2003;86:49.

[93]   Luque A, Aldazabal J, Martin-Meizoso A, Martinez-Esnaola JM, Sevillano JG, Farr R. Model Simulat Mater Sci Eng 2005;13:1057.

[94]   Malow TR, Koch CC. Grain growth of nanocrystalline materials - a review. TMS Annual Meeting-Synthesis and Processing of Nanocrystalline Powder. Anaheim, CA, USA: Minerals, Metals & Materials Soc (TMS), Warrendale, PA, USA, 1996. p.33.

[95]   Malow TR, Koch CC. Mater Sci Forum 1996;225-227:595.

[96]   Malow TR, Koch CC. Acta Mater 1997;45:2177.

[97]   Song X, Zhang J, Li L, Yang K, Liu G. Acta Mater 2006;54:5541.

[98]   Shen ZJ, Peng H, Liu J, Nygren M. J Eur Ceram Soc 2004;24:3447.

[99]   Okuda S, Kobiyama M, Inami T, Takamura S. Scr Mater 2001;44:2009.

[100] Chen DJ, Mayo MJ. Nanostruct Mater 1993;2:469.

[101] Dickenscheid W, Birringer R, Gleiter H, Kanert O, Michel B, Guenther B. Solid State Commun 1991;79:683.

[102] Hibbard G, Aust KT, Palumbo G, Erb U. Scr Mater 2001;44:513.

[103] Klemm R, Thiele E, Holste C, Eckert J, Schell N. Scr Mater 2002;46:685.

[104] Zhou F, Lee J, Lavernia EJ. Scr Mater 2001;44:2013.

[105] Owen DM, Chokshi AH. Nanostruct Mater 1993;2:181.

[106] Averback RS. Z Phys D Atom Mol Cl 1993;26:84.

[107] Li JG, Ye YP. J Am Ceram Soc 2006;89:139.

[108] Vassen R. CFI-CERAM FORUM INT 1999;76:19.

[109] Chen IW, Wang XH. Nature 2000;404:168.

[110] Atkinson HV. Acta Metallurgica 1988;36:469.

[111] Kang S-JL. Sintering: Densification, Grain Growth and Microstructure: Butterworth-Heinemann 2005.

[112] Burke JE, Turnbull D. Progr Met Phys 1952;3:220.

[113] Natter H, Schmelzer M, Loeffler MS, Krill CE, Fitch A, Hempelmann R. J Phys Chem B 2000;104:2467.

[114] Grey EA, Higgins GT. Acta Metallurgica 1973;21:309.

[115] Burke JE. Trans. Metall. Soc. AIME 1949;180:73.

[116] Burke JE. Trans. Metall. Soc. AIME 1950;188:1324.

[117] Michels A, Krill CE, Ehrhardt H, Birringer R, Wu DT. Acta Mater 1999;47:2143.

[118] Mehrer H. Diffusion in solid metals and alloys. Berlin; New York: Springer-Verlag, 1990.

[119] Guiraldenq P, Lacombe P. Acta Metallurgica 1965;13:51.

[120] Liu F, Yang GC, Wang HF, Chen Z, Zhou YH. Thermochim Acta 2006;443:212.

[121] Brook RJ. J Am Ceram Soc 1969;52:56.

[122] Hsueh CH, Evans AG, Coble RL. Acta Metallurgica 1982;30:1269.

[123] Nichols FA. J Am Ceram Soc 1968;51:468.

[124] Kim H-D, Park Y-J, Han B-D, Park M-W, Bae W-T, Kim Y-W, Lin H-T, Becher PF. Scr Mater 2006;54:615.

[125] Lee Y-I, Kim Y-W, Mitomo M, Kim D-Y. J Am Ceram Soc 2003;86:1803.

[126] Polotai A, Breece K, Dickey E, Randall C, Ragulya A. J Am Ceram Soc 2005;88:3008.

[127] Coble RL. J Am Ceram Soc 1958;41:55.

[128] Johnson DL, Cutler IB. J Am Ceram Soc 1963;46:541.

[129] Greskovich C, Lay KW. J Am Ceram Soc 1972;55:142.

[130] Kornelyuk LG, Lozovoi AY, Razumovskii IM. Diffus Defect Data. Pt A 1997;143/1:1481.

[131] Wuerschum R, Reimann K, Farber P. Diffus Defect Data. Pt A 1997;143/1:1463.

[132] Perevezentsev VN. Theoretical Investigation of Nonequilibrium Grain Boundary Diffusion Properties. In: Michael Zehetbauer, Valiev RZ, editors. Nanomaterials by Severe Plastic Deformation. WILEY-VCH; 2002.

[133] Nazarov A. Phys Solid State 2003;45:1166.

[134] Nakaso K, Shimada M, Okuyama K, Deppert K. J Aerosol Sci 2002;33:1061.

[135] Lehtinen KEJ, Zachariah MR. J Aerosol Sci 2002;33:357.

[136] Koch W, Friedlander SK. J Aerosol Sci 1989;20:891.

[137] Mukherjee D, Sonwane CG, Zachariah MR. J Chem Phys 2003;119:3391.

[138] Fang Z, Maheshwari P, Wang X, Sohn HY, Griffo A, Riley R. Int J Refract Met Hard Mater 2005;23:249.

[139] Kumar V, Fang Z, Wright S, Nowell M. Metall Mater Trans A 2006;37:599.

CHAPTER 3

RESEARCH SCOPE AND OBJECTIVES

Sintering of nanosized powders is a viable approach to manufacture of bulk nanocrystalline materials. The goal of sintering of nanosized powders is not only to achieve full densification but also to retain nanoscale grain size at full densification. However, the challenge of sintering of nanosized powder is the rapid grain growth during consolidation, leading to loss of nanocrystalline grain size after sintering. Therefore, the densification and grain growth behavior during sintering of nanosized powders have to be clearly understood including their kinetics and mechanisms, as well as their differences from those of micronsized powders. Then strategies to enhance densification and inhibit grain growth can be provided.

In order to examine the characteristics of densification and grain growth of nanosized powders, and identify the differences in sintering behavior between nanosized powder and coarse sized powder, this study is designed using tungsten as an example material to investigate the following issues:

1. Experimental examination of effects of particle size on sintering behavior

2. Experimental examination of the characteristics of densification and grain growth of sintering nanosized powders

3. Analyze and understand the characteristics and the origin of the differences in sintering behavior between nanosized and micronsized powders

4. Provide more insights into the densification and grain growth process for future solutions to inhibit grain growth during sintering of nanosized powder, especially the initial and intermediate stages when the sintered densities are less than 90% relative density.

For the purpose of this research, a number of sintering experiments are designed and carried out under various conditions. The detailed experimental processes are given in Chapter 4 and the results are provided in the following chapters. Chapter 5 deals with the effects of particle size on sintering behavior using different sized tungsten powders. Chapter 6 focuses on densification and grain growth of nanosized tungsten powder in order to identify the characteristics of nanosintering. Chapter 7 concentrates on kinetics analysis and mechanisms of densification and grain growth in order to understand nanosintering. Chapter 8 concludes the research with proposing method for reducing grain growth during nanosintering.

CHAPTER 4

EXPERIMENTAL

This chapter describes experimental procedures for studying the effects of particle size on sintering and further examining the characteristics of densification and grain growth of nanosized powders. The experimental procedures included preparation, compaction and sintering of nanosized tungsten powders as well as characterization of powders and sintered samples.

4.1 Production of Nanosized Tungsten Powders

Production of nanosized powders was accomplished using a unique one-of-a-kind planetary ball milling machine (Fig. 4.1). With its large gyration radius and independent controlled motors for gyration and revolution, the milling energy potential reaches 60g force under normal conditions. The machine is capable of 100g acceleration force. Compared to commercial high energy ball milling machines such as Fritzsch planetary ball mills and Union Process attritor mills, the custom designed planetary mill, has much higher milling energy and efficiency, which in turn translates into unique opportunities for effective reduction of particles size to nanoscale.

Fig. 4. 1 The dual drive planetary ball milling machine for nanoparticle production

For this study, tungsten was selected as an example material, and high energy milling technology was applied to produce nanosized tungsten powders. The purpose of the study was to examine the following issues:

- Effects of particle size on sintering

- The characteristics of grain growth and densification of nanosized powders.

Various tungsten powders with different particle sizes were prepared by high energy milling. The detailed preparation processes are described as follows:

1. *Preparation of powders for examining effects of particle size on sintering*

Two raw tungsten materials provided by Kennametal Inc. were used for studying the effects of particle size on sintering. Both of the raw materials were produced by the reduction of tungsten oxide. One had a particle size of ~500 nm ("C500", "C" denotes "chemical synthesis"); the other had a particle size of ~50 nm ("C50"). Both C500 and C50 powders were put into separate canisters with milling media and the canisters were filled with heptane. The powders were then subjected to ultra high energy milling for 6 hours using the high energy planetary ball milling machine. Tungsten carbide balls were used as milling media and the ball-to-powder weight ratio was 6:1. The milled powders were denoted as "MC500" and "MC50" respectively ("M" stands for "milled"). The two raw W powders, C500 and C50, and the two milled W powders, MC500 and MC50, were used for studying effects of particle size on sintering behavior. The designations of all four powders and their preparations are tabulated in Table 4.1.

- C500: the as received chemically synthesized submicron powder;

- C50: the as received chemically synthesized nanosized powder;

- MC500: the high energy milled C500 powder;

- MC50: the high energy milled C50 powder.

Table 4. 1 The designations of the powders for examining effects of particle size on sintering

Raw tungsten powder	High energy milled powder-6 hours
C500	MC500
C50	MC50

2. *Preparation of powders for examining densification and grain growth of nanosized powders*

C50 powder was selected as the starting material for studying the characteristics of densification and grain growth of nanosized powders. In order to further reduce particle size and enhance the sinterability, the as received C50 tungsten powder was subsequently subject to high energy ball milling for 12 hours. The milling of the as received powder was carried out in canisters filled with heptane. Tungsten carbide balls were used as milling media with ball-to-powder weight ratio 6:1. In addition to 12 hours milling, 6 hours milling was also carried out in order to examine the effects of milling time on sintering and grain growth of nanosized tungsten powders. Table 4.2 list the powders used for studying the densification and grain growth of nanosized powder.

- A-W: as-received C50 W powder

- M6-W: 6 hours milled C50 W powder

- M12-W: 12 hours milled C50 W powder

The 12 hours milled powder "M12-W" are focused to examine the characteristics of densification and grain growth of nanosized powder.

Table 4. 2 Nanosized tungsten powders produced for studying densification and grain growth during sintering.

Milling time Raw materials	6h	12h
C50 (A-W)	√ (M6-W)	√ (M12-W)

4.2 Compaction and Sintering of Tungsten Powders

The milled tungsten powders were dried in a vacuum at room temperature for 12 hours to allow for evaporation of heptane. The dried powders were collected for subsequent compaction and sintering. Compaction and sintering experiments were conducted to study effects of particle size on sintering and examine densification and grain growth of nanosized powders. The experiments were conducted as follows.

1. Compaction and sintering for studying effects of particles size on sintering

The powders in Table 4.1 were compacted under a uniaxial pressure of 240 MPa. Each sample was 10 grams in weight. The compacted specimens were round pellets 16.22 mm in diameter and 4-7 mm in height depending on different powders. Sintering was carried out in a flowing hydrogen atmosphere at temperatures of 1100 ℃, 1250 ℃ and 1400 ℃. The heating rate for all sintering temperatures was 10 ℃ /min. The specimens were held at each temperature for 0, 30 and 60 minutes. The MC50 powder was also heated up to 1000 ℃ without being held at the temperature in order to examine the entire densifications during the heating up process. Table 4.3 lists the sintering conditions for this set of experiments.

Table 4. 3 Designed sintering conditions for examining the effects of particle size on sintering behavior

t (min) T (℃)	0	30	60
1000	√ (MC50 only)		
1100	√	√	√
1250	√	√	√
1400	√	√	√

2. Compaction and sintering for studying densification and grain growth of nanosized powders

The nanosized powders listed in Table 4.2 were consolidated into green compacts using a uniaxial press machine. Each sample was 5 grams in weight. Due to the extremely fine particle size, very large friction forces were present among the nanosized powders and between powders and inside wall of the die. As a result, the typical green density for both 6 hours-milled (M6-W) and 12 hours-milled (M12-W) nanosized tungsten powders was only about 36% theoretical density of tungsten material under a pressure of 140 MPa. The dimensions of the compacted specimens were round pellets 16.22 mm in diameter and about 3.5 mm in thickness. In order to study the effects of green density on sintering and grain growth, other green densities, 31% and 40%, were also obtained for M12-W powder using different compaction pressures 50 MPa and 240 MPa. Further increasing compaction pressure did not increase green density but led to cracking problems in the green compacts, so higher pressures were not applied in this study.

Sintering studies were carried out in a tube furnace. The compacted samples were heated in a flowing hydrogen atmosphere with constant heating rate 10 ºC/min to different temperatures. A series of experiments was designed and carried out to study densification and grain growth of nanosized powder during early stage of sintering, including both nonisothermal and isothermal sintering experiments. The nonisothermal experiments were carried out by heating the green compacts to preset temperatures and then shutting down the furnace without holding at the temperature. The following temperatures were selected: 800 ºC, 900 ºC, 950 ºC, 1000 ºC, 1050 ºC, 1100 ºC, 1250 ºC

and 1400 ºC. Isothermal sintering was conducted at different temperatures to obtain detailed densification and grain growth behavior of nanosized powder. The temperatures for isothermal sintering were 950 ºC, 1000 ºC, 1050 ºC, 1100 ºC and the holding times were 15, 30, 45 and 60 mins at each temperature. The detailed sintering temperature and time are listed in Table 4.4. For comparison, both M6-W and M12-W powders were sintered with same sintering conditions to study effects of milling time on sintering behavior. Further, the effects of different green densities on the sintering and grain growth behavior of nanosized powder were also examined through nonisothermal heating experiments using M12-W samples. The detailed information is listed Table 4.5.

4.3 Characterization of Powders and Sintered Samples

The following section describes methods used in this study for characterizing powders and sintered samples. These methods included X-ray diffraction (XRD), Scanning Electron Microscope (SEM), BET method, Light scattering method, Archimedes method. Each is described below.

Table 4. 4 Designed sintering temperature and time for studying densification and grain growth of nanosized tungsten powder

T (ºC) \ t (min)	0	15	30	45	60
800	√				
900	√				
950	√	√	√	√	√
975	√	√	√	√	√
1000	√	√	√	√	√
1050	√	√	√	√	√
1100	√	√	√	√	√
1250	√				
1400	√				

Table 4. 5 Designed experiments for studying effect of green density on densification and grain growth of nanosized tungsten powders

t (min)	0		
T (ºC)	Effect of green density		
	31%	36%	40%
800	√	√	√
900	√	√	√
950	√	√	√
1000	√	√	√
1050	√	√	√
1100	√	√	√
1250	√	√	√
1400	√	√	√

XRD. To determine the grain sizes of as received and milled powders, the X-ray diffraction line broadening techniques was applied. Due to the intense mechanical energy input during milling, strain energy was inevitably stored within the crystal lattice. In order to quantify the grain size accurately considering the effects of the internal strains, Williamson-Hall method [1] was applied using the following formula:

$$\beta = \beta_d + \beta_\varepsilon = \frac{0.89\lambda}{d\cos\theta} + 4\varepsilon\tan\theta \qquad (4.1)$$

where β is full width at half maximum (FWHM) of the diffraction peak after instrument correction; β_d and β_ε are FWHM caused by small grain size and internal stress, respectively; and d and ε are, respectively, grain size and internal stress or lattice distortion. The experimentally determined line broadening was corrected for $K\alpha_1$-$K\alpha_2$ separation and instrumental line broadening using coarse W powder (average grain size

about 40 μm). To determine both d and ε from equation (4.1), line broadening data corresponding to several 2θ values were used. Grain size and internal strain were calculated by plotting $\beta\cos\theta$ *vs. $\sin\theta$*. The grain size and lattice strain were obtained from the intercept and the slope of the linear plot. In this study, XRD method (Siemens D5000 X-ray Diffractometer) was applied to the following samples: C50, MC500, MC50, A-W, M12-W.

SEM. A high resolution scanning electron microscope (FEI Nova NanoSEM 630) was used to characterize the morphology of the milled powder as well as the sintered samples. Grain sizes of the powder and sintered samples were calculated quantitatively using linear intercept method. For each sample, three fracture images were used for grain size measurement. A total of more than 600 grains were measured for each sample and the mean grain size value was used as the grain size for this sample ($\overline{G}_{sample}$). Further, the distribution of grain sizes was also obtained for each sample. The error bar for each grain size data was determined by the differences between $\overline{G}_{sample}$ and $\overline{G}_{image}$ ($\overline{G}_{image}$ is mean grain size for each field of view). All the samples in this study were characterized by SEM method.

BET. C500, C50, MC500 and MC50 powders were characterized using a BET surface area analysis instrument (Micromeritics ASAP 2010). Particle size of the powders was calculated based on the BET specific surface area using a modified formula that incorporates surface roughness and pore area factors,

$$d_{BET} = k(D/2) \times 6/(S_{BET} \times density) \tag{4.2}$$

where d_{BET} is calculated particle size, k is a constant related to pore area (equal to 1.5 [2]), D is fractal dimension value of surface roughness (equal to 2.58 [2]), S_{BET} is specific surface area, *density* is theoretical density of a material. The particle size was also determined by SEM method d_{SEM} for comparison.

Light scattering. A light scattering method was used for examining the agglomerates of powders. This technique is not available in our lab, so in this study, the powders A-W and M12-W were sent out for doing this examination.

Archimedes method. In this study, green density was determined by calculating the weight divided by the volume of the specimens, while sintered density was determined using the Archimedes method. It follows the principle that the partial loss in weight of the material in water due to buoyancy effect is a measure of the volume of the material. Porous samples were soaked in oil in vacuum before density measurements was taken so that the pores were sealed with oil. The density, ρ, is given by the relation:

$$\rho = \frac{w_{air}}{w_{oil} - w_{water}} \times \rho_{water} \tag{4.3}$$

where w_{air} is the weight in air of the sample, w_{oil}, is the weight after oil infiltration, and w_{water}, is the oil infiltrated sample immersed in water. Care was taken to dry the sample of oil after infiltration, to ensure accurate weight measurement.

The samples and the corresponding characterization methods used in this study are listed in Table 4.6.

Table 4. 6 A summary of different characterization methods used in this study

Sample / Method	For studying particle size effects					For studying nanosintering and grain growth			
	C500	C50	MC500	MC50	Sintered sample	A-W	M6-W	M12-W	Sintered sample
XRD		√	√	√		√		√	
BET	√	√	√	√					
SEM	√	√	√	√	√	√	√	√	√
Light Scattering						√		√	

4.4 References

[1]   Williamson GK, Hall WH. Acta Metallurgica 1953;1:22.

[2]   Jiqiao L, Baiyun H. Int J Refract Met Hard Mater 2001;19:89.

CHAPTER 5

EFFECTS OF PARTICLE SIZE ON DENSIFICATION
BEHAVIOR OF TUNGSTEN POWDERS

5.1 Introduction

This chapter deals with the effects of particle size on sintering behavior of tungsten powders. Before going to the detailed results, I will firstly introduce the background and importance of studying size effects on tungsten sintering.

Tungsten, the example material for this study, is an excellent candidate for many applications owing to its attractive properties such as high melting point and high density [1]. However, the sintering of tungsten powders is usually very difficult because of its high melting point. For example, tungsten powder with a particle size of 1.8 μm can be sintered to only 76% of its theoretical density at 1650 ºC [2]. Often temperatures well over 2000 ºC must be utilized to manufacture bulk tungsten materials by sintering [2-7].

There are typically two approaches to improve the sinterability of tungsten. One is by the addition of small amount of transition metals such as Ni, and Pd [8-11] as activators, which can reduce the sintering temperature to the range of 1200 to 1500 ºC. However, since the addition of transition metals could alter properties of sintered tungsten, this approach has limited applications. The other approach is by particle size refinement. The sintering temperature of tungsten was reported to decrease with decreasing particle size [2, 12-14]. For example, Staab et al. [2, 14] and Vasilos et al. [2, 14] found that fine

tungsten powders with particle sizes from 400 nm to 800 nm could be sintered to over 90% theoretical density at around 1700 ºC. Malewar et al. showed that the sintering temperature of nanosized tungsten powders produced by high energy mechanical milling was 1700 ºC compared to 2500 ºC for conventional powders with 95% theoretical density after sintering [12]. Further, Oda et al. showed that nanosized tungsten powder could be sintered at 1000 ºC under pressure of 200 MPa using a SPS sintering technique [13].

As shown above, the sintering of tungsten is very sensitive to the particles' size. In order to further explore the effects of particle size on densification of tungsten powders as well as the effects of mechanical milling, the sintering of tungsten with different particle sizes prepared by either chemical methods (C500, C50) or high energy milling (MC500, MC50), are investigated and discussed in the following.

5.2 Results and Discussion

5.2.1 Powder Characteristics

Fig. 5.1 shows SEM images of the four different sized tungsten powders: C500, C50, MC500, and MC50. The figure shows that the particle sizes of the milled powders – MC500 and MC50 – are, as expected, much smaller than their corresponding original powders. The grain sizes, lattice strains, specific surface areas and particle sizes of all the powders are summarized in Table 5.1. Calculated particle sizes from specific surface area d_{BET} are listed in comparison to that of by SEM method d_{SEM}. It is evident that the values of d_{BET} particle sizes are close to that of d_{SEM}. In this study, d_{SEM} was used for discussion hereafter. The as received submicron powder C500 had the largest grain size, particle size and lowest specific surface area, while the milled powder, MC50, had the smallest grain size, particle size and highest specific area. It is noted that the milled submicron powder
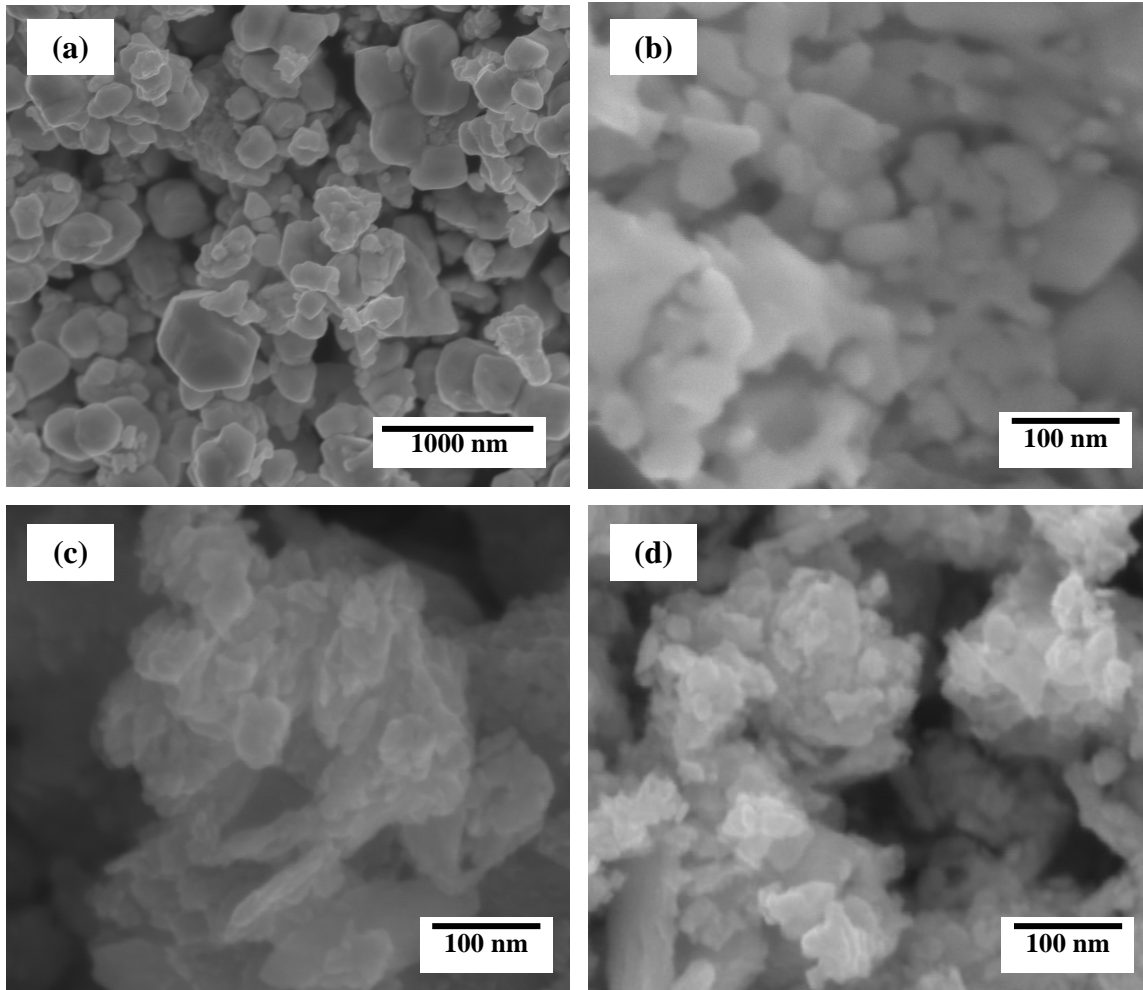
Fig. 5. 1 SEM micrographs of different sized tungsten powders: (a) C500; (b) C50; (c) MC500; (d) MC50

(MC500) and the as received 50 nm (C50) had similar specific surface areas (around 10 m^2/g) and particle size, but the grain size of MC500 was smaller than that of C50. Further, the two milled powders MC500 and MC50 have approximately equal grain size, while the specific surface area of MC50 was much higher than that of MC500. Based on Table 5.1, the relative comparison of the particle sizes of the four powders were $P_{MC50} < P_{MC500} \approx P_{C50} < P_{C500}$, and the relative comparison of their grain sizes were $G_{MC50} \approx G_{MC500} < G_{C50} < G_{C500}$.

Table 5. 1 Grain size, lattice strains, and specific surface area of as received and milled W powder

Sample	Production method	Grain Size (nm)	Lattice Strain (%)	Specific Surface Area (m²/g)	Particle size (nm)	
					d_{BET}	d_{SEM}
C500	Chemical synthesis	260	–	2.93	205	260
MC500	High energy milling	21	0.135	10.33	58	52
C50	Chemical synthesis	45	0.095	9.39	64	57
MC50	High energy milling	19	0.107	16.79	37	36

The comparison of lattice strains in all powder samples shows, however, that the differences between different powders are relatively small, especially that the lattice strains in C50, the 50 nm powder produced by chemical method, are only slightly lower than those of milled powder MC500 and MC50. This is consistent with the findings by Staab et al. that dislocation density in chemically produced W has strong dependence on particle sizes [2]. In their study, the results showed that a submicron powder reduced at lower temperature may have one magnitude higher dislocation density than that of a micron sized powder reduced at high temperatures. Therefore, the powders produced by chemical method could also present a number of defects when the reaction temperature is very low. Nanosized powders need to be produced at low temperatures during chemical synthesis, so they might contain many dislocations after reaction.

5.2.2 Isothermal Sintering Behavior

Fig. 5.2 shows the evolution of sintered densities as functions of time at various temperatures from 1100 ℃ to 1400 ℃. At 1100 ℃ (Fig. 5.2 (a)), submicron sized powders C500 did not experience densification. The MC500 and C50 had only moderate densification after extended holding time. Compared to the as received 50 nm powder C50, the milled submicron powder MC500, which has similar particle size as C50, had relatively higher density after holding for 1 hour; yet, the density of the sintered MC500 is still only 75% of the theoretical density of tungsten. In contrast, the relative density of the milled nano powder (MC50) reached 97% after holding at 1100 ℃ for 1 hour. Clearly, MC50 had superior sinterability compared to the other three powders. This result for the first time shows that tungsten powder can be sintered to near full density at a temperature as low as 1100 ℃ using a conventional pressureless sintering process in a hydrogen atmosphere.

The sintering behaviors at 1250 ℃ and at 1400 ℃ are shown in Fig. 5.2 (b) and Fig. 5.2 (c). The figures show that the as received C500 and C50 powders were still not well densified at these relatively high temperatures, though the relative density of sintered C50 powder (91%) was slightly higher than that of sintered C500 powder (89%) after holding for one hour at 1400 ℃. In contrast, the milled powders, both MC500 and MC50, achieved near full densification after sintering at these temperatures. Specifically, the relative density of both sintered MC500 and MC50 powders reached 97-99% of the theoretical density of tungsten. According to Fig. 5.2, MC 50 has the best sinterability; C500 has the worst sinterability; MC500 and C50 have moderate sinterability, but the sinterbility of MC500 is better than that of C50.
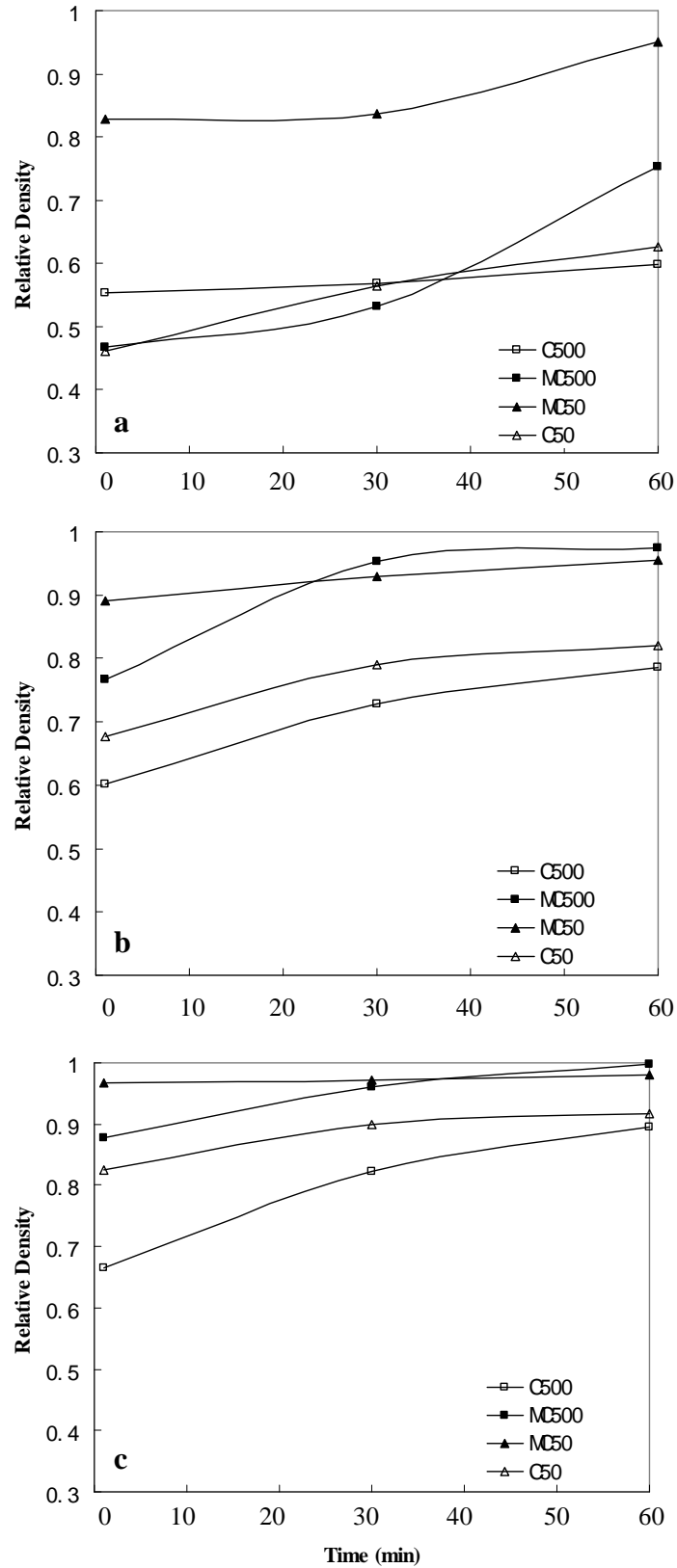
Fig. 5. 2 Evolution of relative densities of different sized tungsten powders sintered at various temperatures. (a) 1100 ºC; (b) 1250 ºC; (c) 1400 ºC

The above results suggest that the densification of tungsten powders is affected by two factors – particle size and milling. The poor sinterability of C500 can be attributed to its relatively coarse particle size. The poor sinterability of C50, however, was unexpected considering the fact that the original particle size of C50 powder was 50 nm. As shown in Table 5.1, C50 had similar particle size to that of MC500 which is the milled submicron powder. After sintering at 1400 ℃ for 1 hour, however, C50 did not achieve high density, while MC500 had extensive densification (99%) when sintered at 1400 ℃. This suggests strongly that milling is a critical factor affecting the sintering of nanosized W powders. Specifically, the ultrahigh energy milling method that was used to prepare MC500 and MC50 greatly enhanced the sinterability of tungsten. The effect of milling may be partially attributed to the deagglomeration of particles, in addition to continued refining of particle and grain sizes of the powder. However, because both MC500 and C50 powders were still agglomerated after synthesis based on SEM images (Fig. 5.1 (b) and (c)), milling may also have additional effects on sintering. Furthermore, comparing the results of MC50 and MC500, it seems that the particle size of raw materials before high energy milling also plays an important role in affecting the sinterability of the milled powders. The finer the initial particle size is, the better the sinterability of the milled powder will be.

5.2.3 Nonisothermal Sintering Behavior

To further understand the sintering behavior of nanosized W powders, the densification of the powders as a function of temperature was examined with respect to densification during the heat up stage of a sintering cycle as well as the onset temperature of densification. First of all, Fig. 5.3 shows significant differences among the four
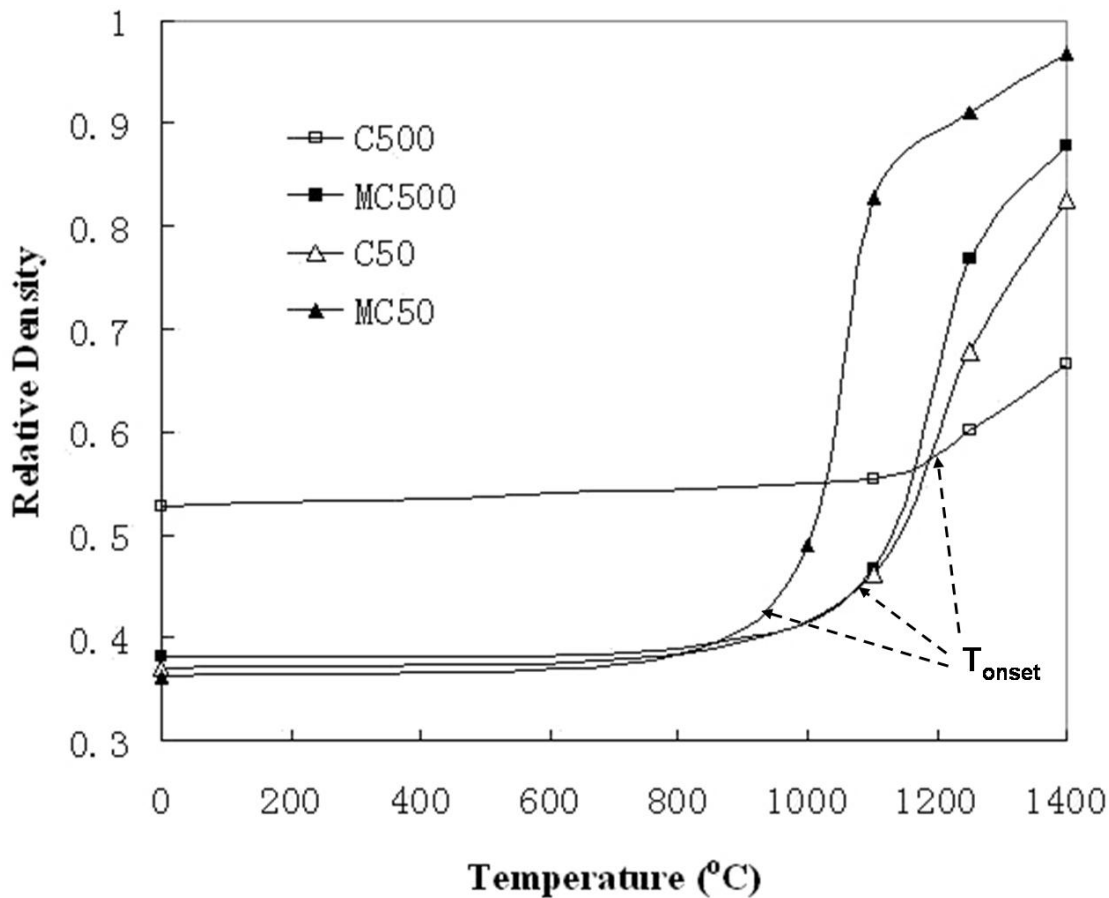
Fig. 5. 3 Densification evolution of different sized tungsten powder during heating up process

powders with respect to the densification that was achieved during the heat up stage of the sintering. Specifically, most of the densification of MC50 was achieved during heating up before reaching 1100 ℃, while other powders did not have significant densification before 1100 ℃. In addition, it is noted that green densities of the tungsten powders after compaction varied from 0.53 for C500 to 0.36~0.38 for C50, MC500 and MC50 due to different initial particle sizes.

Figure 5.3 also shows that the onset temperatures of the sintering of powders with different initial particle size are significantly different. Onset temperature of sintering is

defined as the temperature at which sintering starts and proceeds. In this study, the onset temperature is determined as the temperature at which 10% relative fraction of densification is achieved, i.e., when $(\rho - \rho_0)/(\rho_{th} - \rho_0) = 10\%$, where ρ , ρ_0 and ρ_{th} are sintered density, green density and theoretical density, respectively. Based on this definition and the data in Fig. 5.3, it is clear that C500 has the highest onset temperature; MC500 and C50 have intermediate, and MC50 has the lowest onset temperature. The onset temperature of sintering is related to particle size and the dependence of the onset temperature of sintering on particle size can be described by the following expression [15-17]: $T_{onset}(d) \propto \exp[-k/d]$, where T_{onset} is onset temperature of sintering; d is particle size; k is a constant determined by the properties of the material. This relationship predicts a sharp decrease of the onset temperature of sintering as particle size decrease to the nanoscale.

5.2.4 Scaling Law

The effects of particle size on sintering behavior can be further elucidated by examining the dependence of sintering temperature on particle size using the scaling law. In this study, the sintering temperature is defined as the temperature at which over 95% relative sintered density can be achieved by holding for less than 1 hour. The scaling law describes the relationship between sintering temperature and particle size by the following equation [15, 18, 19]:

$$n\ln(\frac{d_1}{d_2}) = \frac{Q}{R}[\frac{1}{T_2} - \frac{1}{T_1}] \qquad (5.1)$$

where d_1, d_2 are particle sizes, T_1 and T_2 are corresponding sintering temperatures, R is the gas constant, Q is the activation energy, and n is an exponent dependent of diffusion mechanisms: $n=1/2$ for volume diffusion and $n=1/3$ for grain boundary diffusion. With respect to sintering of tungsten powder, the dominant mechanism for densification is grain boundary diffusion based on reported studies in literature [14], thus n is taken as 1/3. By regression fitting of experimental data to equation of sintering shrinkage, German[20] and Johnson[21] calculated the value of Q/R for tungsten sintering to be 4407 K. Another reported study in the literature [2] found that tungsten powder with a particle size of 400 nm was able to be sintered to over 95% theoretical density at 1650 ºC within one hour. Based on the above data, the dependence of sintering temperature on particle size is analyzed and illustrated in Fig. 5.4. It shows that the sintering
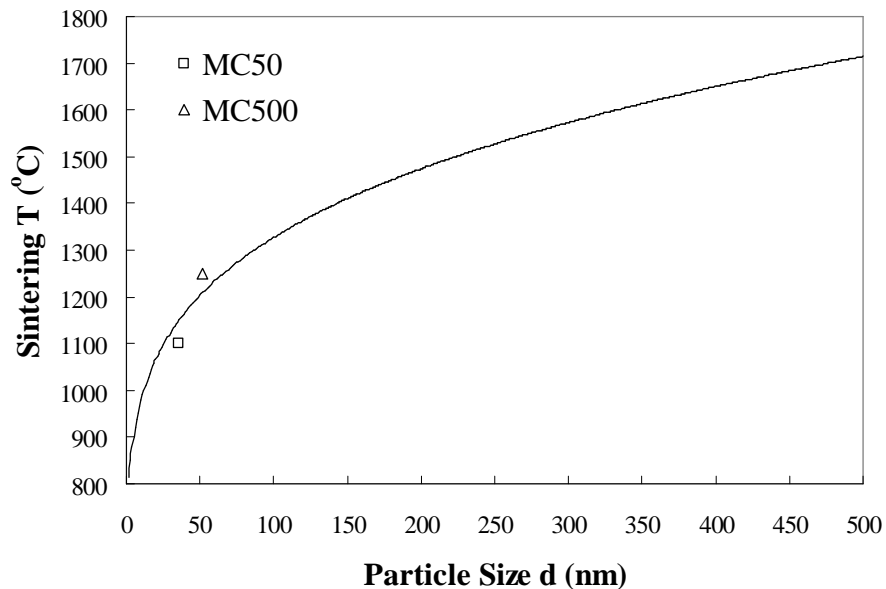
Fig. 5. 4 Dependence of sintering temperature of the milled tungsten powder on particle size described by scaling law, along with the experimental data of MC500 and MC50 in this study

temperatures of MC50 and MC500 powders in this study are very close to the prediction of the scaling law by using the above equation. Therefore, the scaling law is applicable to study the relationship between sintering temperature and particle size of high energy milled tungsten powders.

Finally, the sinterablity of a powder depends not only on its particle size, but also on its grain size and internal strains. Comparing the as received 50 nm powder (C50) to the milled submicron powder (MC500) which has almost the same particle size (similar specific surface area) and the same onset of sintering temperature, one can see that the sinterability of MC500 is better than that of C50 (see Fig. 5.2 (b) and (c), Fig. 5.3). This result can be explained in terms of the grain size of these two powders. After milling, although the particle size of MC500 is similar to that of C50, the grain size of MC500 is smaller than that of C50 (Table 5.1). The smaller grain size results in more grain boundaries, hence more grain boundary diffusion during sintering of MC500 powder than during sintering of C50 powder, which leads to higher relative density for sintered MC500 than for C50. Further, because the MC500 powder was produced by ultrahigh energy milling, it is reasonable to expect that the MC500 powder had a large amount of internal strain energy. However, the data in Table 5.1 showed that the differences of lattice strains in these two powders were relatively small suggesting that the internal strain energy was not the most critical factor that determined the differences in their sintering behaviors. Nonetheless if a powder has all the attributes that are favorable for sintering, including the nanoscale particle size, nanoscale grain size, and internal strain energy, the sinterability of the powder would be most enhanced. The MC50 powder in this study is such an example with the most enhanced sinterability.

5.3 Conclusion

In summary, the present work, for the first time, showed that nanocrystalline tungsten powders can be pressurelessly sintered to near full density at a temperature as low as 1100 ℃ under a hydrogen atmosphere. The ultrahigh energy method of milling was found to be critical to the sinterability of the powder. Ultrahigh energy milled nanosized tungsten powder exhibited extraordinary sintering enhancement compared to chemically synthesized nanosized tungsten powder. The enhanced sinterability can be attributed to the combined effects of nanoscaled particle size, grain size, deagglomeration, and internal strain energy.

5.4 References

[1]   Smith WF. Structure and Properties of Engineering alloys. New York: McGraw Hill, 1993.

[2]   Staab TEM, Krause-Rehberg R, Vetter B, Kieback B, Lange G, Klimanek P. J Phys Condens Matter 1999;11:1787.

[3]   Lassner E, Schubert W-D. TUNGSTEN - Properties, Chemistry, Technology of the Element, Alloys, and Chemical Compounds. New York, Boston, Dordrecht, London, Moscow: Kluwer Academic / Plenum Publishers, 1999.

[4]   Trzaska M. International Int J Refract Met Hard Mater 1996;14:235.

[5]   Uray L. Int J Refract Met Hard Mater 2002;20:319.

[6]   Uray L. Int J Refract Met Hard Mater 2002;20:311.

[7]   Grueger A, Vassen R, Mertens F. Int J Refract Met Hard Mater 1998;16:37.

[8]   Amato I. Mater Sci Eng 1972;10:15.

[9]   German RM, Munir ZA. Metall Trans A 1976;7A:1873.

[10] Panichkina VV, Radchenko PY, Skorokhod VV. Sov Powder Metall Met Ceram 1983;22:442.

[11] Panichkina VV, Skorokhod VV, Pavlenko NP. Sov Powder Metall Met Ceram 1977;16:950.

[12] Malewar R, Kumar KS, Murty BS, Sarma B, Pabi SK. J Mater Res 2007;22:1200.

[13] Oda E, Ameyama K, Yamaguchi S. Mater Sci Forum 2006;503-504:573.

[14] Vasilos T, Smith JT. J Appl Phys 1964;35:215.

[15] Fang ZZ, Wang H. Int Mater Rev 2008;53:326.

[16] Jiang Q, Shi FG. J Mater Sci Technol 1998;14:171.

[17] Troitskii VN, Rakhmatullina AZ, Berestenko VI, Gurov SV. Sov Powder Metall Met Ceram 1983;22:12.

[18] Messing GL, Kumagai M. Am Ceram Soc Bull 1994;73:88.

[19] Yan MF, Rhodes WW. Mater Sci Eng 1983;61:59.

[20] German RM, Ma J, Wang X, Olevsky E. Powder Metall 2006;49:19.

[21] Johnson JL. Proc. 2008 Int. Conf. on Tungsten, Refractory and Hardmaterials VII. Washington DC, 2008. p.5.57.

CHAPTER 6

SINTERING AND GRAIN GROWTH OF NANOSIZED

TUNGSTEN POWDERS

6.1 Introduction

Chapter 5 discussed the size dependence of sintering behavior for different sized tungsten powders produced by chemical synthesis and mechanical milling. The results indicate that the particle refinement by high energy milling is a very effective approach to enhancing densification of tungsten powder, and the sinterability of nanosized tungsten powder produced by high energy milling is evidently superior to that of coarse tungsten powders. But, in Chapter 5, the detailed information regarding densification and grain growth of nanosized tungsten powder was not revealed. Therefore, in this chapter, the sintering and grain growth behavior of nanosized tungsten powder are examined and highlighted in order to identify the uniqueness in sintering of nanosized powder. Since most kinetic processes during sintering of nanosized powder have been completed before reaching normal sintering temperature (e.g., MC50 in Fig 5.3), this chapter place a great emphasis on studying densification and grain growth during early stage of sintering at low temperatures.

6.2 Powder Characteristics

As introduced in Chapter 4, the powders used for this section are A-W: as-received tungsten powder, M6-W: 6 hours milled tungsten powder and M12-W: 12 hours milled tungsten powder. The characteristics of "A-W" and "M12-W" powders are compared with respect to particle morphology, particle size and agglomeration.

Fig. 6. 1 contains SEM images of A-W and M12-W powders showing particle size
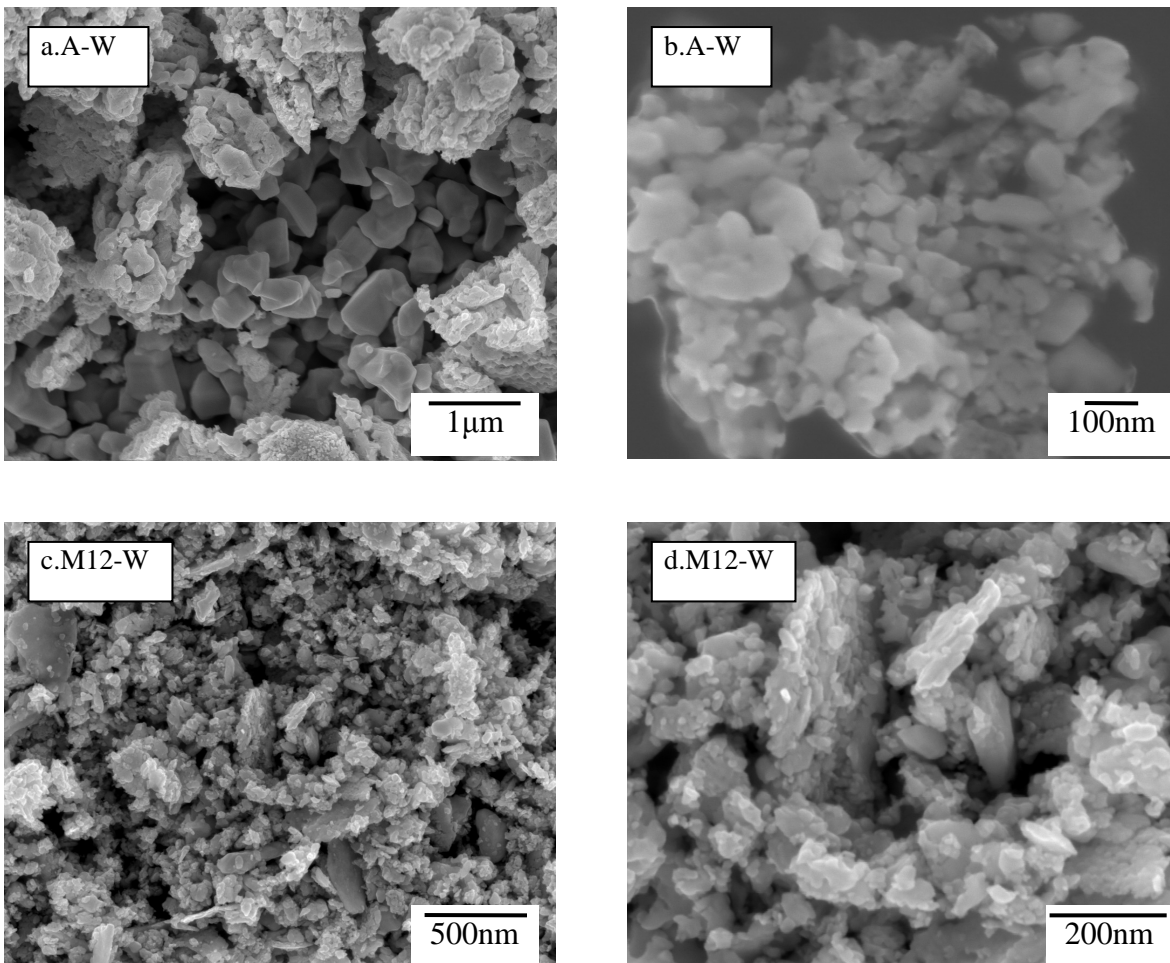
Fig. 6. 1 SEM images of both A-W powder (a, b) and M12-W powder (c, d) with different magnifications

and particle morphology. The A-W powder exists in two forms (Fig. 6. 1 a): one consists of some relative large particles (< 500nm); the other is agglomerates of very fine particles (the agglomerate size is about 1 micron), and this form is more common. The fine particles in an agglomerate are outlined in Fig. 6. 1 b and its size is less than 100nm. After milling, both particles and agglomerates in A-W were crushed down to extremely fine powders (Fig. 6. 1 c). But agglomerates are still present, with size reduced from 1~2 μm to approximate 200 nm (Fig. 6. 1 d).

The A-W and M12-W powders were also subject to light scattering examination for particle size distribution and the result is shown in Fig. 6.2. It is clear that the A-W sample contains much coarser particles than the M12-W sample and the particle size
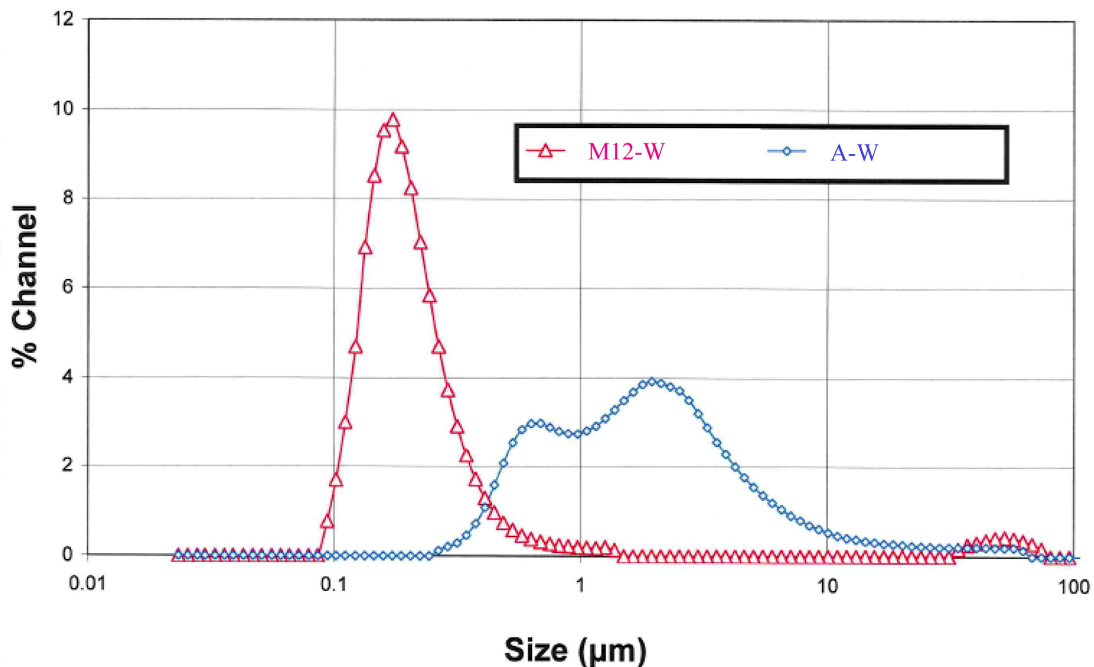
Fig. 6. 2 Size distribution curves based on light scattering examination of A-W and M12-W

distribution is bimodal and wide in the A-W sample in contrast to unimodel and sharp distribution in the M12-W sample. The detailed information is summarized in Table 6.1. The b_{80} in the Table 6.1 is an indicator of the width of distribution, the larger the value the wider the distribution. It can be seen that the results of light scattering test reasonably reflected the observation results on SEM images in Fig. 6.1 as discussed above.

The bimodal distribution in the A-W sample corresponds to the two forms of particle morphology in A-W: large particles and agglomerates of fine particles respectively. Fig. 6.1 a and Table 6.1 show that mode 0.528-µm corresponds to large particles in A-W and mode 2.07-µm reflects agglomerates in A-W. It can be seen that the mode 2.07-µm, i.e., agglomerate, plays major role in A-W due to its high volume percentage (>80%). For the milled powder M12-W, the dominent mode 0.177-µm (>97 volume percentage) in Table 6.1 is related to the agglomerates observed in Fig. 6.1 d, with the agglomerates' size by

Table 6. 1 Agglomerate size distribution measured by light scattering method

| Sample | Microtrac, (µm) | | | | $b_{80}=(b_{90}-b_{10})/b_{50}$ |
	10%	50%	90%	Distribution	
A-W	0.546	1.69	6.01	bimodal	3.23
				Mode 2.07-µm (82.1 vol.%), width 3.85-µm	
				Mode 0.528-µm (17.9 vol.%), width 0.22-µm	
M12-W	0.122	0.180	0.366	«almost» unimodal	1.356
				Mode 48.6-µm (3.2 vol.%), width 23.8-µm	
				Mode 0.177-µm (96.8 vol.%), width 0.14-µm	

SEM observation corresponding well to mode size. Based on the light scattering results and SEM observation, it can be concluded that light scattering method can reflect precisely agglomerate size instead of primary particle size. The primary particle size needs to be determined using SEM images. In the following text, "agglomerate size" refers to the light scattering results and "particle size" refers to SEM results which will be discussed below.

Table 6.2 lists particle size and grain size of A-W and M12-W powders by SEM and XRD measurement. It can be seen that particle size by SEM is similar to grain size by XRD method for A-W powder, implying each particle is a single crystallite. But for M12-W powder, the measured particle size by SEM is little larger than the calculated grain size by XRD. The difference between XRD results and SEM results for M12-W powder may be due to the measuring error for SEM method because the extremely tiny particles are not clearly shown in SEM images. However, it can be seen that the difference between SEM and XRD is small and in the range of measuring error, so the starting grain size of M12-W powder can be reasonably believed to be around 20~30 nm in the following study. Comparing M12-W with A-W, we can see that milling process reduced both particle size and grain size from about 50 nm to 20~30 nm and crushed 2 μm

Table 6. 2 Particle size by SEM and grain size by XRD

Sample	Particle size (nm) by SEM	Grain size (nm) by XRD
A-W	42	45
M12-W	30	18

agglomerates down to 200 nm. The refinement by milling is very important in enhancing sinterablity of milled powder as described in Chapter 5.

6.3 Densification of Nanosized Tungsten Powders

Densification behavior is a primary concern for producing bulk nanocrystalline materials via sintering of nanosized powder because the purpose of sintering is to achieve fully densified parts. It has been usually found that due to the high surface to volume ratio, the densification behavior of nanosized powders is different from that of micron sized powders, e.g., the lower onset temperature of sintering, the faster densification rate. Besides these commonly observed differences, however, it is still necessary to further explore the detailed sintering behavior of nanosized powder and to determine if there is any other uniqueness or any different mechanism involved during sintering of nanosized powder. With this concern, the detailed densification process of nanosized tungsten powders (M12-W) during both nonisothermal heating process and isothermal holding period is presented in the following. Attention is paid to the unique characteristics during the early stage of sintering process. In addition, the effects of milling time and green density on densification of nanosized powder are also provided.

6.3.1 Nonisothermal Densification

Fig. 6.3 shows the change of the relative density of nanosized tungsten powder (M12-W) compacts upon heating from 800 ℃ to 1400 ℃. The density vs. temperature curve exhibits the typical "S" shape, illustrating the slow densification at low temperatures, very rapid densification after the temperature reaches above 1000 ℃, and the final stage
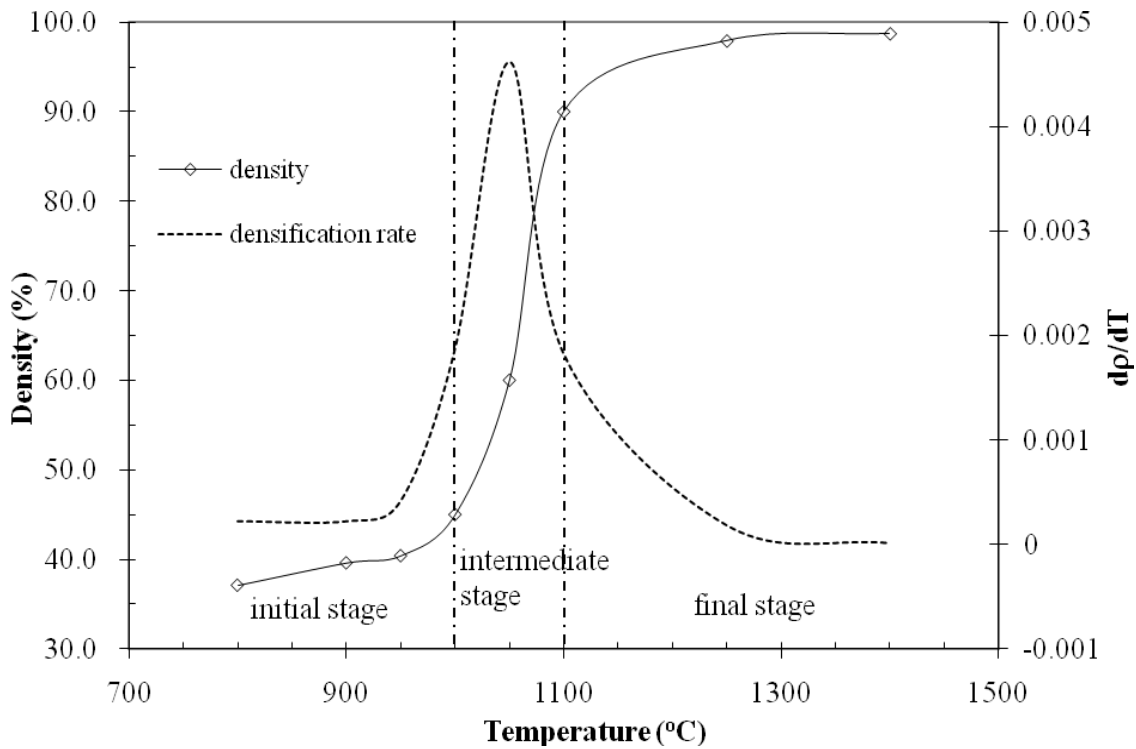
Fig. 6. 3 Nonisothermal densification behavior during heating up nanosized tungsten powder from 800 °C to 1400 °C

during which the rate of densification slows considerably after the relative density reaches above 90% at high temperatures (>1100 ℃).

Based on Fig. 6.3, the evolution of density as a function of temperature can be viewed as consisting of three stages similar to sintering of micron sized powders: the initial, intermediate, and final stages. As shown in Fig. 6.3, the initial stage of sintering refers to the gradual increase of density at temperatures below 1000 ℃. The corresponding density change during this period is from 36% (green density) to 50%. The intermediate stage includes the rapid densification period between 1000 ℃ and 1100 ℃. The majority of densification are completed during this stage, density being increased from 50% to 90%.

The final stage of sintering involves the continued densification with a decreased densification rate. Full or near full densification is achieved during this stage.

One surprising result from Fig. 6.3 is that, with such a low green density (~36%), the compact can be sintered to near full densification. The low green density is the typical characteristic of nanosized powders. Unlike micron sized powder which can usually obtain more than 60% green density, nanosized powder can only achieve 30%-40% green density. The differences in green densities between micron sized powder and nanosized powder lead to different initial compact structures: micron sized powders have a relatively dense compact structure while nanosized powders have a very porous compact structure. So it is reasonable to believe that nanosized powders might have a different densification process compared with micron sized powders in the initial stage of sintering. Traditionally, the initial stage of sintering is considered to be a neck building process for micron sized powders, but for nanosized powders, the initial stage of sintering should experience not only neck bonding process but also other processes owing to the very porous initial structure. This issue will be further examined in following isothermal densification section.

6.3.2 Isothermal Densification

In order to further understand the sintering behavior of nanosized tungsten powders, isothermal experiments were carried out at different temperatures so that different sintering stages could be revealed, particularly initial stage. The isothermal densification evolution at different holding temperatures is shown in Fig. 6.4. The obvious feature in Fig. 6.4 is the clearly different sintering behaviors at low temperatures compared with high temperatures. At low sintering temperatures 950 ℃ and 975 ℃, the sintered

densities increase slowly with a nearly linear relationship between sintered densities and holding time, implying an almost constant sintering rate during this period. This linear increase in density with time is uncommon and cannot be explained by traditional sintering theories. This phenomenon indicates that the initial stage of sintering of nanosized powders, as discussed in the previous section, is indeed different from that of micron sized powders due to the low green density. It can be seen that the sintered densities are still low after one hour's sintering at these low temperatures, 51% for 950 ℃ and 67% for 975 ℃. At high temperatures 1050 ℃ and 1100 ℃, the sintering curves
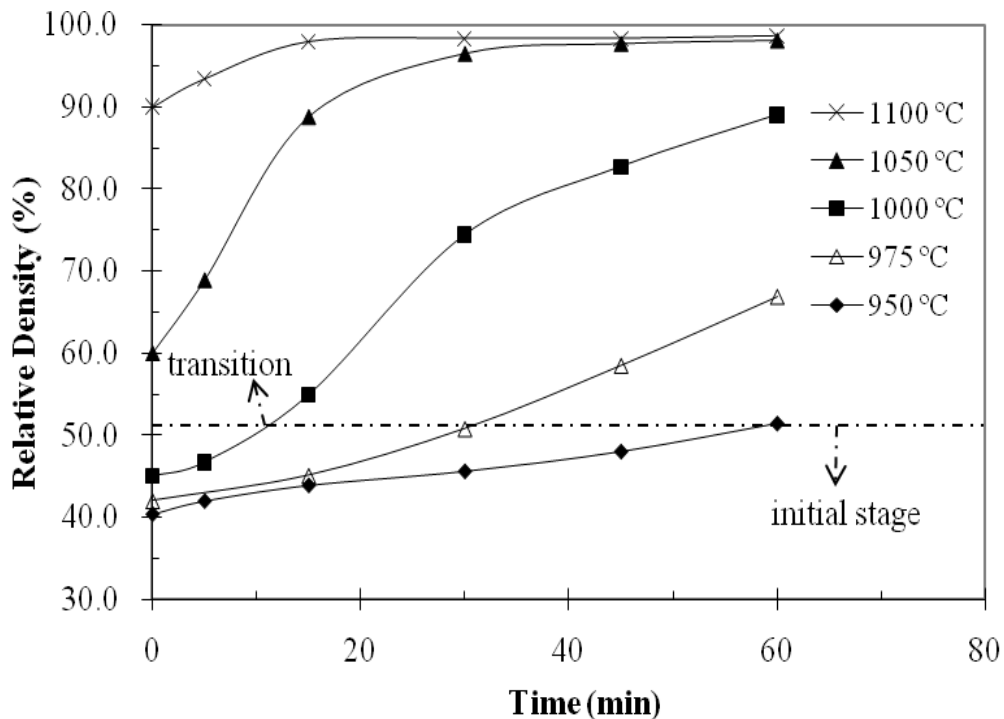
Fig. 6. 4 Isothermal densification behavior of nanosized tungsten powder at different holding temperatures

appear to be normal, with densification rate decreasing with time. For example, at the beginning of sintering at 1050 ℃, the densification rate is very rapid, then decreases continuously with time, and finally becomes close to zero when near full densification is achieved after 30 minutes holding. At 1100 ℃, full densification is able to be obtained within only 15 minutes holding. Again, it should be emphasized that sintering at low temperatures shows very different densification behaviors compared with sintering at high temperatures.

Besides the sintering temperatures 950 ℃, 975 ℃, 1050 ℃, 1100 ℃, a very special temperature needs to be discussed separately, i.e., 1000 ℃. Unlike the sintering behavior at either low temperatures 950 ℃, 975 ℃ or high temperatures 1050 ℃, 1100 ℃, the densification curve at temperature 1000 ℃ appears to be a combination of densification behaviors at both lower temperatures and higher temperatures. It can be seen that the curve at 1000 ℃ exhibits linear densification at the beginning of holding and then transforms into normal densification after a transition period. Fig. 6.4 shows that the transition from linear densification to normal densification seems to be occurring at around 50% density which actually corresponds to transition from initial stage of sintering to intermediate stage of sintering illustrated in Fig. 6.3. Accelerated densification starts after the transition. The sintered density at 1000 ℃ starts with a value about 45% and ends with a value close to 90% after 1 hour holding, which exactly covers two stages of sintering – initial stage before 50% density and the entire intermediate stage between 50% and 90% densities.

Based on the above results, we can summarize the characteristics of densification behavior during sintering of nanosized tungsten powders:

1. Nanosized powders have very low green densities which affect densification behavior during sintering, especially initial stage of sintering.

2. Sintering of nanosized powder can also be divided into three stages – initial stage, intermediate stage and final stage, but each stage may be different from that of micron sized powder due to the low green densities and small particle sizes.

3. During initial stage of sintering at low densities (<50% relative density), the kinetics of densification appears to be linear, which is different from the kinetics at intermediate and final stages of sintering when density is higher than 50%.

4. A transition from the nearly linear densification behavior to normal densification behavior can be found between initial and intermediate stages of sintering, which may indicate different mechanisms for these stages.

5. Intermediate stage of sintering is very rapid and majority of densification is completed during this stage.

6. Full densification can be achieved even with very low initial green densities (e.g., 36%).

6.3.3 Effects of Milling Time on Densification

In order to explore the effects of milling time on densification, 6 hours milled powder (M6-W) and 12 hours milled powder (M12-W) were sintered under the same nonisothermal and isothermal conditions for comparison.

Fig. 6.5 shows the nonisothermal densification behaviors for both powders from 800 ℃ to 1400 ℃. It can be seen that both powders have similar densification behaviors, especially during initial stage of sintering before 1000 ℃ and final stage of sintering after 1250 ℃. The main difference results from the intermediate stage of sintering, during which the acceleration of densification for 6 hours milled powder is behind that for 12 hours milled powder, implying sinterablility is more enhanced for 12 hours milled powder. But with respect to final sintered densities, both powders can achieve same and near full densification after being heated to high temperatures. Based on the nonisothermal experimental results, the effects of milling time on sintering are primarily
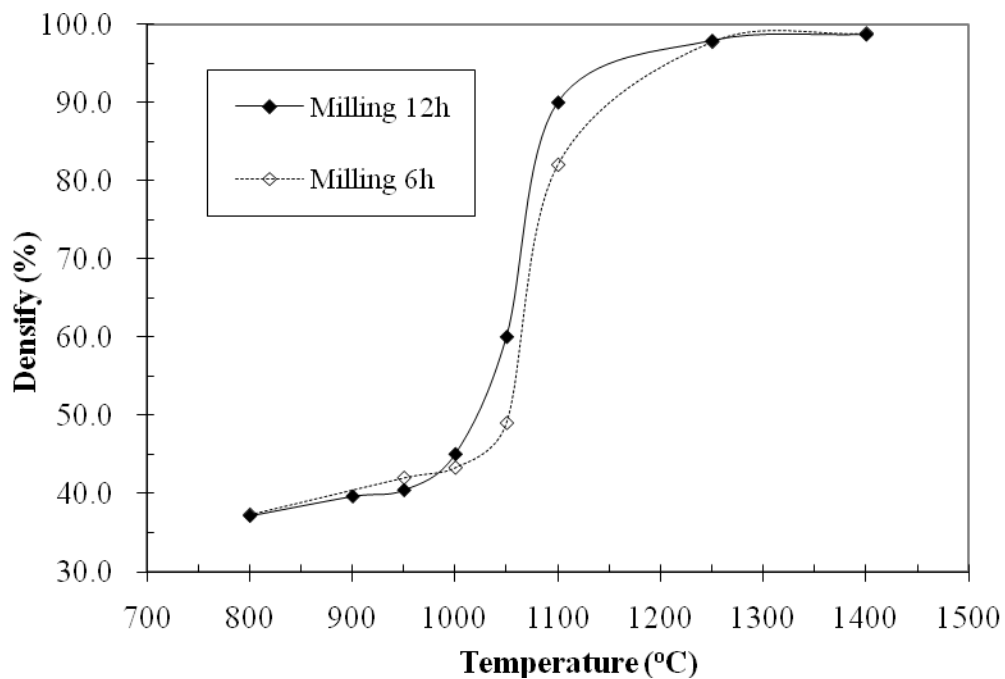
Fig. 6. 5 Effects of milling time on densification during nonisothermal heating 6 hours and 12 hours milled powders

located at intermediate stage of sintering, and there is no effect on final sintered densities.

The effects of milling time on densification were further examined by isothermal sintering experiments. The isothermal sintering behaviors for both powders are compared in Fig. 6.6. It can be seen that both powders show nearly the same linear densification behaviors at 950 ℃, indicating linear densification behavior during initial stage of sintering is not affected by milling time. At 1000 ℃, both powders also exhibit similar sintering behavior – initially linear densification at the beginning of holding and then normal densification behavior after transition from initial stage of sintering to intermediate stage of sintering. However, 12 hours milled powders can reach higher
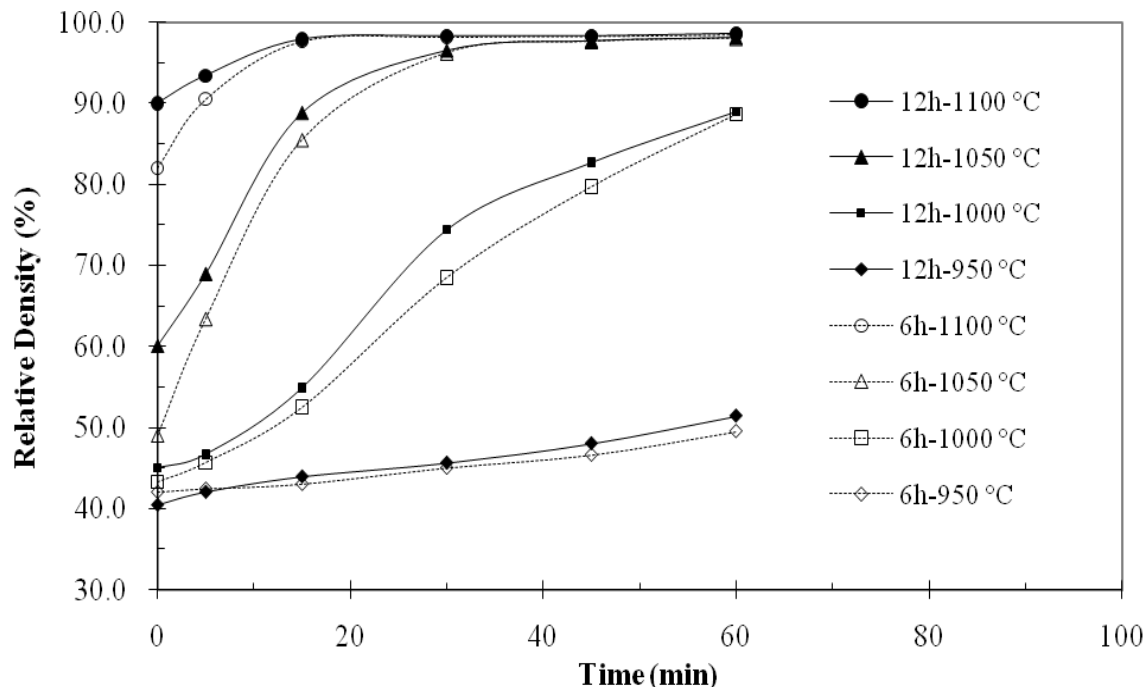
Fig. 6. 6 Effects of milling time on isothermal densification at different holding temperatures for 6 hours and 12 hours milled powders

sintered densities than 6 hours milled powders especially during intermediate stage of sintering, which is in accordance with the findings in Fig. 6.5 for nonisothermal densification behavior. The differences in sintered densities during the intermediate stage of sintering are also observed at 1050 ℃ and 1100 ℃. Nevertheless, when the sintered density exceeds 90%, the differences in sintered densities for the two powders diminish and both powders can reach full densification at the same time (see the curves at 1050 ℃ and 1100 ℃ in Fig. 6.6).

In short, based on the above results, the overall sintering behaviors for 6 hours milled powder and 12 hours milled powder have no substantial differences, and the milling time has only limited effects on the intermediate stage of sintering and no effect on the final sintered density.

6.3.4 Effects of Green Density on Densification

The effect of green density on sintering behavior was examined by heating samples with different green densities (31%, 36%, 40%) to a series of temperatures then cooling down directly without holding, see Table 4.5. Using this method, the density evolutions as a function of temperature for the samples during heating up are recorded and compared in Fig. 6.7.

It can be seen from Fig. 6.7 the initial differences in green density remained very well at the beginning of sintering before 1000 ℃; then once the intermediate stage of sintering started after 1000 ℃, accelerated densification decreased partial differences in density between temperature 1000 ℃ and 1100 ℃; finally the differences in density were diminished and eliminated after 1250 ℃ during late stage of sintering. According to this result, it can be summarized that the effect of green density on sintered density is
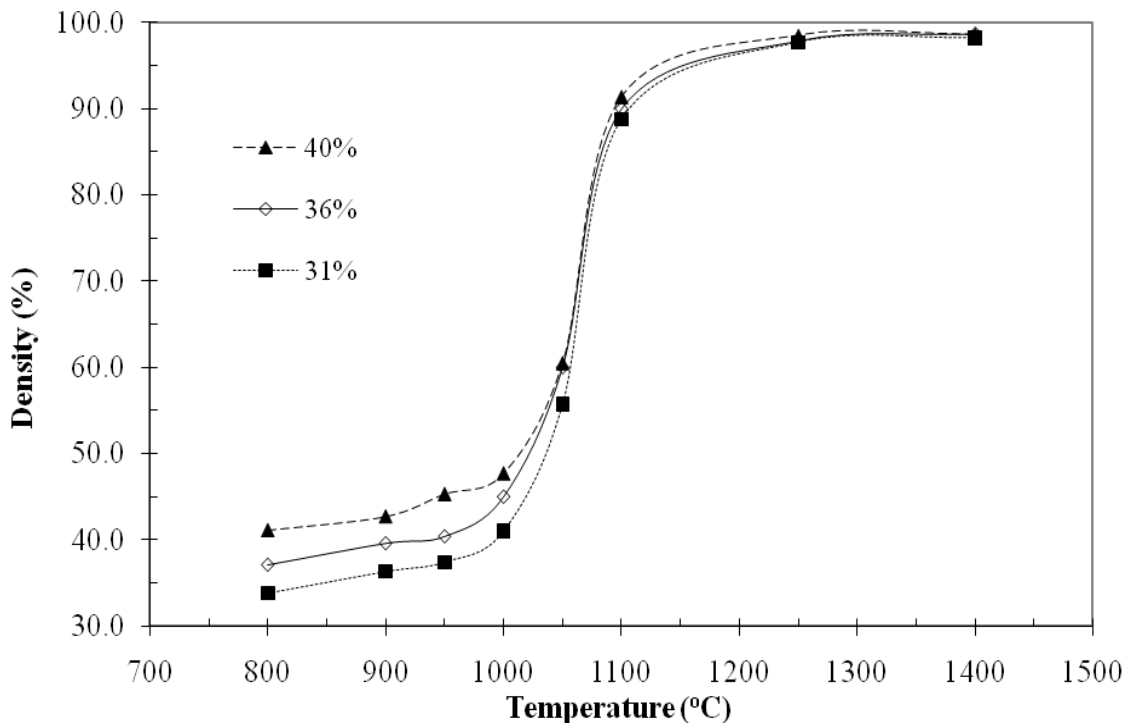
Fig. 6. 7 Effects of green density on densification during heating up process

apparent during initial and intermediate stages of sintering, the higher green density leading to the higher sintered density during these processes; while the initial differences in green density are depleted during late stage of sintering, resulting in convergence of three curves in Fig. 6.7 eventually. It should be mentioned that all the samples can achieve nearly full densification at 1400 ℃ regardless of initial different green densities, which indicates the excellent sinterability of high energy milling treated tungsten powder.

In addition to the above results, Fig. 6.7 also shows another phenomenon that needs to be discussed here. Even though green density has some effects on densification especially during initial and intermediate stages of sintering, the overall densification behaviors are not altered significantly due to the three different starting densities. This

may be attributed to the fact that the difference in green densities (~10%) is not large enough to dramatically change sintering behavior of the nanosized tungsten powders. In this study, the highest green density is 40%, which is still too low to overcome the initial slow densification period before reaching 50% density, see Fig. 6.7. The author believes that if the green density is high enough to surpass the initial stage of sintering, e.g., at least larger than 50% according to Fig. 6.7, the overall sintering behavior would be evidently changed. However, increasing green density over 50% is a big challenge for the nanosized tungsten powder used in this study.

6.4 Grain Growth of Nanosized Tungsten Powders

Grain growth is a critical factor in producing bulk nanocrystalline materials from sintering nanosized powders. The goal of sintering nanosized powders is not only to accomplish fully desified sintered parts but also to retain nanoscaled grain size after sintering. However, this goal has hardly been reached in practice during the past two decades because rapid grain growth during sintering always leads to loss of nanoscaled grain size. Grain growth and densification are two very important processes during sintering. Section 6.3 discussed the densification process and showed that the densification of nanosized tungsten powder was greatly enhanced and full densification could be achieved. In order to understand and control grain growth process, this section will focus on investigating the grain growth behavior during sintering of nanosized tungsten powders. The grain growth during both nonisothermal heating and isothermal holding processes will be examined, with special emphasis on grain growth during initial and intermediate stages of sintering. Further, the effects of milling time and green density on grain growth will also be inspected.

6.4.1 Nonisothermal Grain Growth

Grain growth during heating up nanosized tungsten powders from 800 ℃ to 1400 ℃ is illustrated in Fig. 6.8. The corresponding density curve is also shown in Fig. 6.8 in order to clarify the grain growth characteristics during different stages of sintering. The initial grain size of the milled powder is around 20~30nm, which remains unchanged up to 800 ℃. From 800 ℃ to 1100 ℃, which corresponds to initial and intermediate stages of sintering, the grain growth is slow, see Fig. 6.8; but once density exceeds 90% after 1100 ℃, grain size rapidly increases and final grain size reaches around 5 µm after heating up to 1400 ℃, indicating very rapid grain growth during final stage of sintering. As Fig. 6.8 demonstrates, the grain growth before 90% density (hereafter denoted as
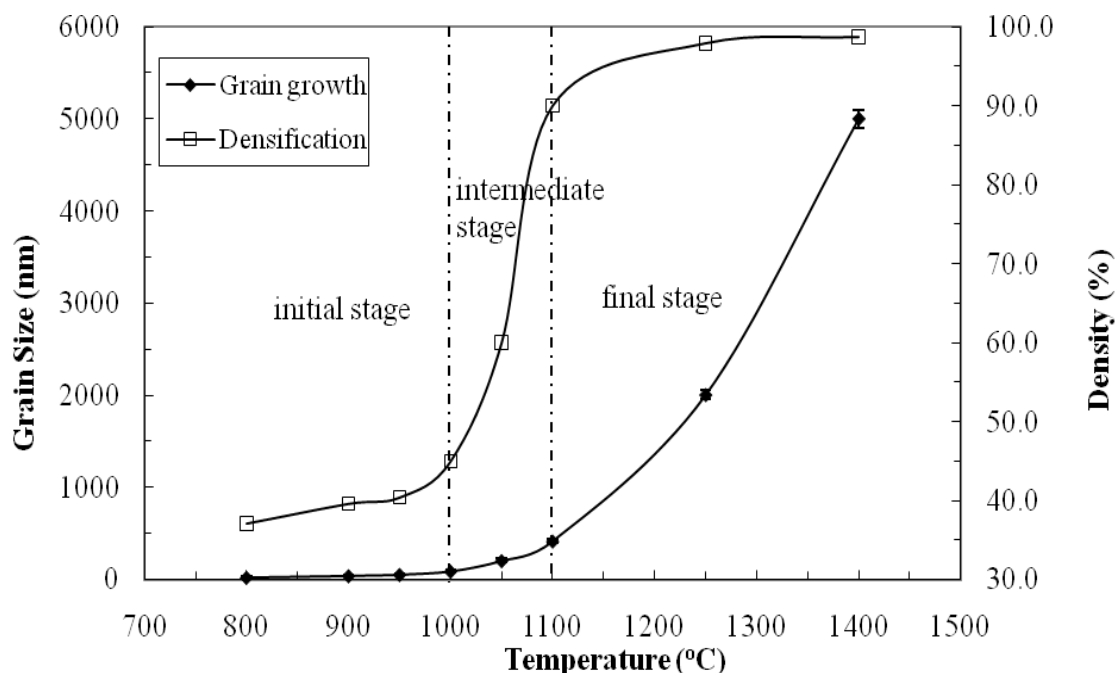
Fig. 6. 8 Grain growth during nonisothermal heating nanosized tungsten powder from 800 °C to 1400 °C

"initial grain growth") is minor compared with the grain growth after 90% density (hereafter denoted as "normal grain growth"), so more attention should be paid to the latter one in order to control grain size in the sintered state. This explains why most traditional literature dealt with normal grain growth during final stage of sintering after 90% density and why many theories have been developed for this part of grain growth. However, for sintering of nanosized powder, even though the initial grain growth is small and slow compared with normal grain growth, it may still be sufficient to lead to loss of nanoscaled grain size. For example, in this study, grain size was increased from about 20-30 nm to more than 400 nm during initial and intermediate stages of sintering before reaching 90% density, which sufficiently exceeds the required grain size for nanocrystalline materials. This phenomenon implies that the initial grain growth is also crucial for sintering of nanosized powder and can not be neglected. However, the process of the initial grain growth has been rarely studied, so the details of this part of grain growth need to be revealed.

The detailed process of initial grain growth is shown as a function of temperature during heating up in Fig. 6.9. It can be seen that grain growth is relatively slow at the beginning of sintering at low temperatures, although the grain size increased from 20-30 nm to about 100 nm when the temperature reached 1000 ℃; and then accelerated grain growth occurred resulting in the loss of nanoscale grain sizes. This initial grain growth behavior apparently has the same feature as the normal grain growth process. However, it is not clear if the mechanisms and kinetics of the initial grain growth are the same as the normal grain growth. Because of the large surface area to volume ratio of nanosized powders and the extremely porous structure of green compacts of nanosized powders, it
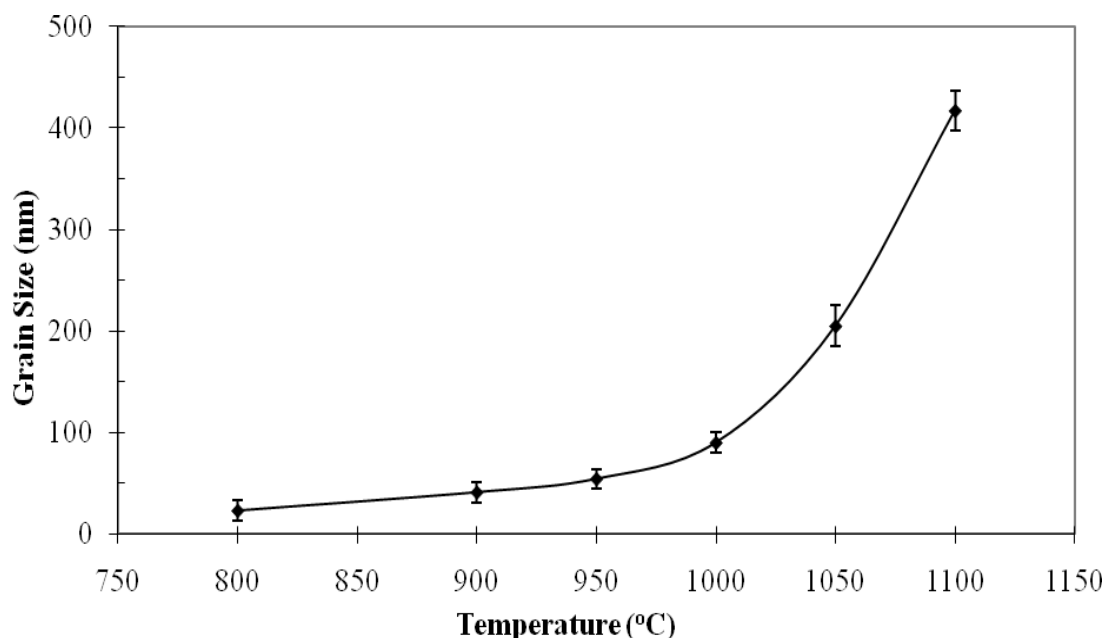
Fig. 6. 9 Grain growth during initial and intermediate stages of sintering before 90% density

is reasonable to expect the mechanisms and kinetics of the initial grain growth process may be different from those in less porous or near dense materials during the final stage of sintering. A more detailed analysis of the kinetics and mechanisms of the nonisothermal initial grain growth process will be presented in Chapter 7.

6.4.2 Isothermal Grain Growth

Although the nonisothermal sintering experiments as described above provide a realistic view of the grain growth process during sintering of nanosized powders, it is difficult, however, to study the kinetics of the grain growth directly using the nonisothermal experiments because both temperature and time change simultaneously. Isothermal sintering experiments were thus designed and carried out at different

temperatures to gain more insights on the kinetics of the initial grain growth process and compare the differences of kinetic behaviors between the initial grain growth and normal grain growth processes. Fig. 6.10 shows the results of isothermal sintering and grain growth experiments at 950 ℃, 1000 ℃, 1050 ℃ and 1100 ℃, respectively. The corresponding density changes are 40%-51% at 950 ℃, 45%-89% at 1000 ℃, 60%-98% and 90%-98% at 1100 ℃, respectively.

The sintering was in the initial stage at 950 ℃, initial to intermediate stage at 1000 ℃, intermediate to final stage at 1050 ℃, and final stage at 1100 ℃. Fig. 6.10 shows that
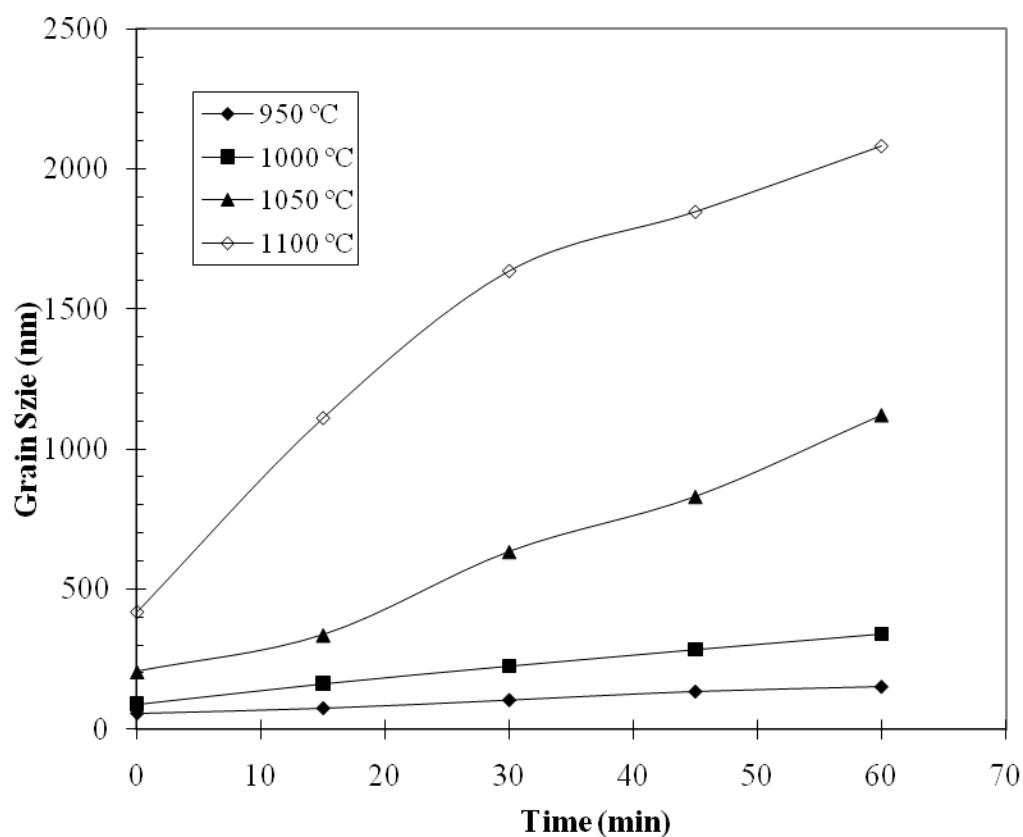
Fig. 6. 10 Grain growth during isothermal holding at different temperatures

grain growth appears to be linear with time at low temperatures 950 ℃, 1000 ℃, and 1050 ℃, but becomes normally parabolic when the temperature surpasses 1100 ℃. These results imply that the kinetics of grain growth during the initial, intermediate and even the beginning of the final stages of sintering is different from that of the grain growth during the final stage of sintering at high temperatures. The difference in kinetic behavior between initial and normal grain growth during isothermal sintering is a significant finding that may suggest different mechanisms of grain growth during the initial stages of sintering. In Chapter 7, detailed analysis of the grain growth data will be carried out to shed more light on the exact kinetic behavior of the initial grain growth process and possible corresponding mechanisms.

6.4.3 Effects of Milling Time on Grain Growth

The effects of milling time on grain growth were examined by comparing 6 hours milled powder with 12 hours milled powder, and both of them were sintered under the same conditions. Fig. 6.11 shows the nonisothermal grain growth behaviors for both powders from 800 ℃ to 1400 ℃. It can be seen that the overall grain growth behaviors were similar for both powders during entire sintering process. The only difference is that the 12 hours milled powder starts leading in grain size compared to the 6 hours milled powder from 1000 ℃ until temperature 1400 ℃ where both powders reach similar grain size again. This lead in grain size for 12 hours milled powder is possibly related to its earlier occurrence of rapid densification during nonisothermal heating, see Fig. 6.5.
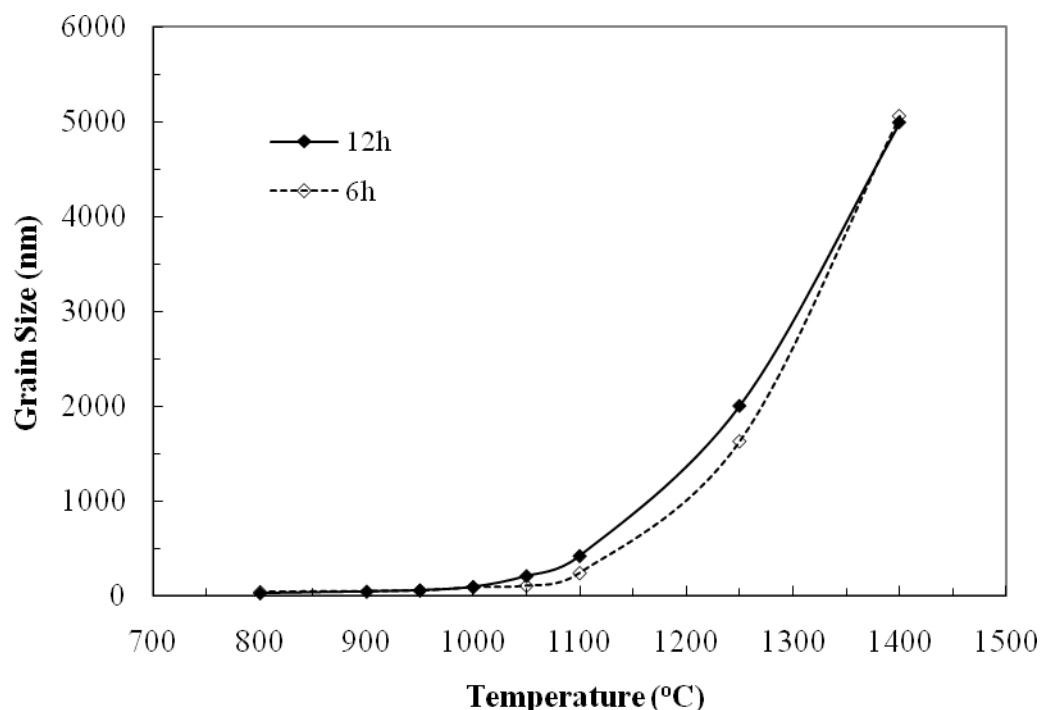
Fig. 6. 11 Effects of milling time on nonisothermal grain growth during heating up

The effect of milling time on grain growth is further examined by isothermal experiments as well, see Fig. 6.12. It is clear that both powders show linear grain growth behavior at temperature 950 ℃, 1000 ℃, 1050 ℃ and parabolic grain growth behavior at temperature 1100 ℃. The isothermal experiments show once again that the overall trend in grain growth is similar for both powders. It should be mentioned here that the uncommon linear grain growth behavior at low temperatures is present not only for 12 hours milled powder but also for 6 hours milled powder. Fig. 6.12 also illustrates that, at 1050 ℃ and 1100 ℃, grain growth curves for 6 hours milled powder are deviated from those for 12 hours milled powder, which is also in accordance with the previous
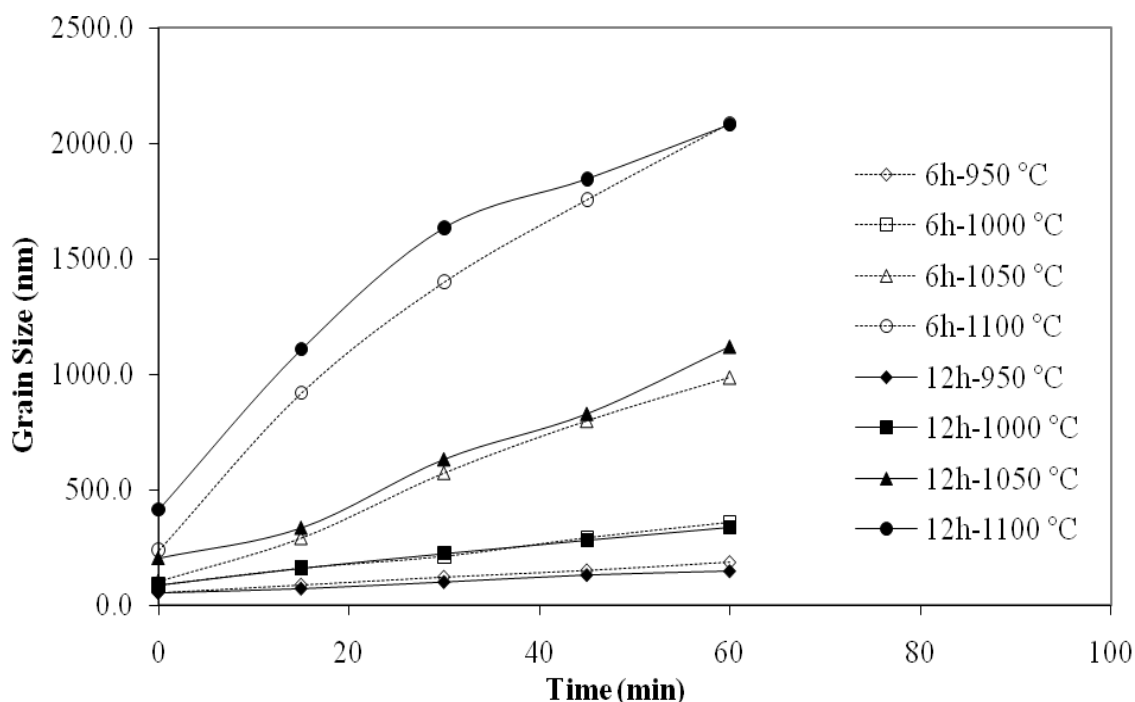
Fig. 6. 12 Effects of milling time on isothermal grain growth at different temperatures

nonisothermal results that 12 hours milled powder started leading in grain size once the intermediate stage of sintering began after 1000 ℃.

In general, the effects of milling time on grain growth are not substantial. The grain sizes during intermediate stage of sintering are slightly affected by the milling time, but the overall grain growth behavior and the final grain size after sintering are insensible of milling time, especially at low temperature sintering.

6.4.4 Effects of Green Density on Grain Growth

Three different initial green densities, 31%, 36%, 40%, were used to examine the effects of green density on grain growth. The samples with different green densities were

heated up to a series of temperatures then cooled down directly without holding, and then the grain sizes were measured as a function of temperature (Fig. 6.13). Fig. 6.13 illustrates the dependence of grain sizes on temperature for the samples with three different initial green densities. It can be seen that the grain sizes are similar at each temperature, which indicates that the effect of green density on grain growth is not obvious, or in other words, grain growth behavior is independent of green density.

To further examine the effects of green density on initial grain growth at low temperatures, the grain growth during initial and intermediate stage of sintering before
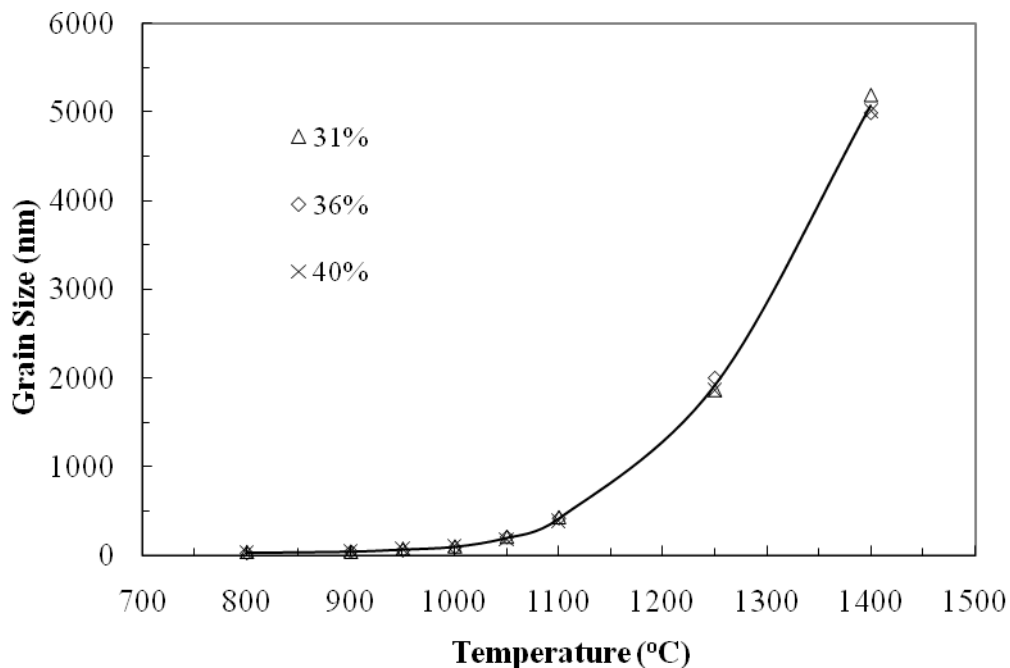
Fig. 6. 13 Effects of green density on grain growth during nonisothermal heating up process

1100 ºC is highlighted in Fig. 6.14. Fig. 6.14 shows effects of green density on initial grain growth are also negligible. In addition, Fig. 6.14 confirms the point that even the slow grain growth during the initial and intermediate stages of sintering can cause the loss of nanoscale grain size.

6.5 Relationship Between Grain Growth and Densification

In sections 6.3 and 6.4, the densification and grain growth behavior were described separately with respect to factors such as temperature and time, milling time and green density. During sintering, densification and grain growth are not independent processes,
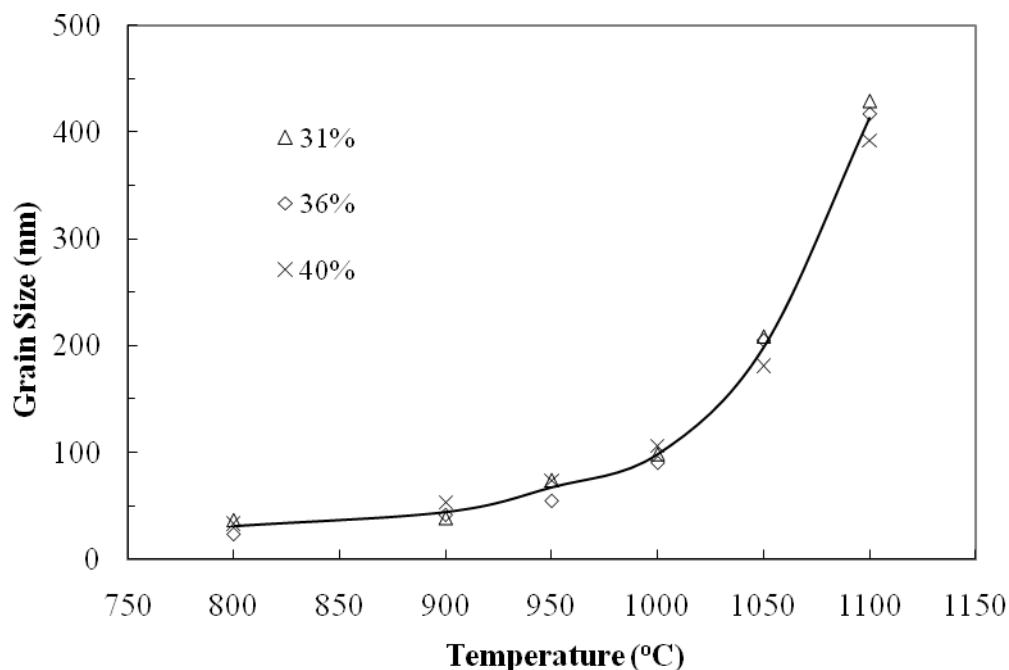
Fig. 6. 14 Effects of green density on grain growth during initial and intermediate stages of sintering before 90% density

and they take place concurrently and interact with each other. Understanding the correlation between these two intertwined processes is thus of importance for grasping the overall sintering process, especially for proposing strategies for inhibiting grain growth and enhancing densification, which are the keys to achieving the goal of sintering of nanosized powders – full densification without losing nanocharacteristic grain size. This section will focus on the relationship between grain growth and densification during sintering of nanosized tungsten powders. The relationship between grain growth and densification is typically studied by plotting grain size vs. density curve, usually called "sintering trajectory". The following will examine sintering trajectories under different conditions, such as nonisothermal heating, isothermal holding, different milling time and different green densities.

6.5.1 Nonisothermal Sintering Trajectory

The sintering trajectory during nonisothermal heating of 12 hours milled tungsten powder from 800 ℃ up to 1400 ℃ is depicted in Fig. 6.15. The corresponding temperature for each data point is labeled in the figure too. Overall, Fig. 6.15 shows the typical features of grain size versus density trajectory, i.e., minor grain growth before reaching 90% relative density and major grain growth after reaching 90% relative density. It can be seen that 1100 ℃ seems to be a critical point at which the density reaches 90% and the grain growth accelerates dramatically, suggesting a transition from the intermediate stage of sintering to final stage of sintering. Based on the grain size versus density trajectory (Fig. 6.15), the grain growth can be viewed as consisting of two stages: 1) initial grain growth during initial and intermediate stages of sintering before 90% relative density, 2) normal grain growth during the final stage of sintering after
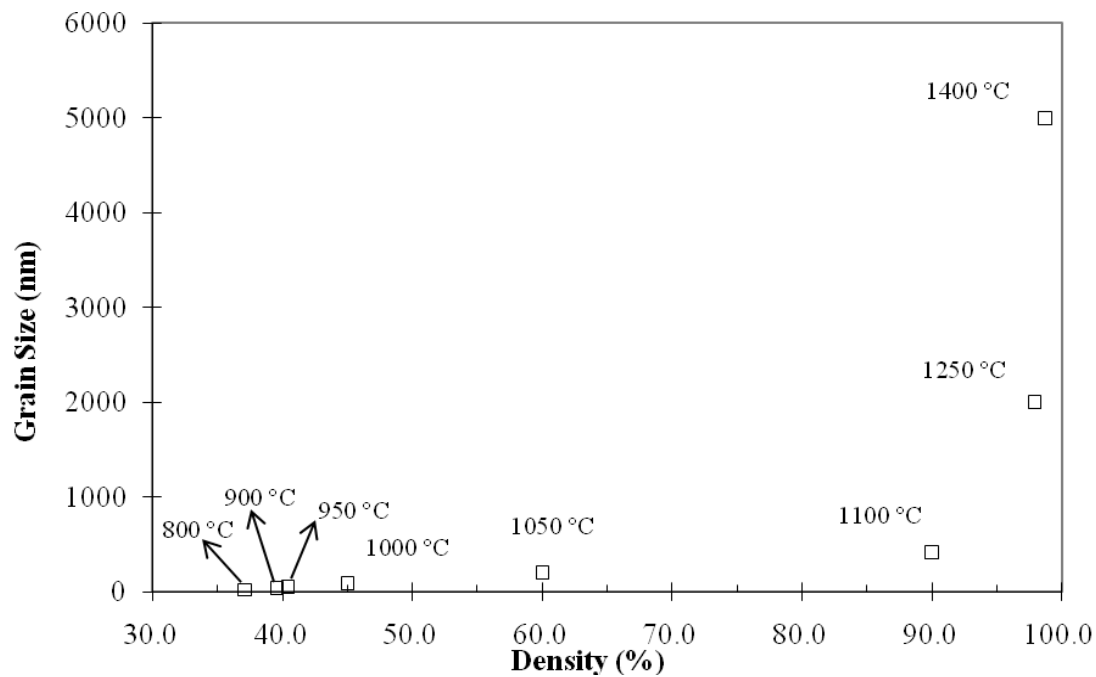
Fig. 6. 15 Grain size vs. density sintering trajectory during nonisothermal heating up from 800 °C to 1400 °C

reaching 90% relative density. The small initial grain growth before 90% density is attributed to open and interconnected pores during the initial and intermediate stages of sintering, which impede grain growth by pinning grain boundaries from migration; whereas during late stage of sintering, the pores become closed and isolated after relative density >90%, losing the ability of pinning effects on grain boundary. Rapid normal grain growth thus begins by grain boundary migration. Although the normal grain growth during final stage of sintering is dominant in the grain growth process, the initial grain growth cannot be neglected because it is still sufficient to lose nanocharacteristic grain size. Therefore, it is meaningful to study the relationship between grain growth and densification during initial and intermediate stages of sintering and investigate the

interaction between them within this period. Fig. 6.16 illustrates the dependence of grain size on density during initial and intermediate stages of sintering. It shows grain size has a linear dependence on density, and grain size increases from about 20 nm to more than 400 nm with density increase from 36% to 90%. The linear relationship between grain size and densification before 90% density has also been observed in the literature [1, 2].

6.5.2 Isothermal Sintering Trajectory

The dependence of grain size on densification during isothermal sintering is plotted in Fig. 6.17. Similar to Fig. 6.15, Fig. 6.17 also shows small grain growth during the initial
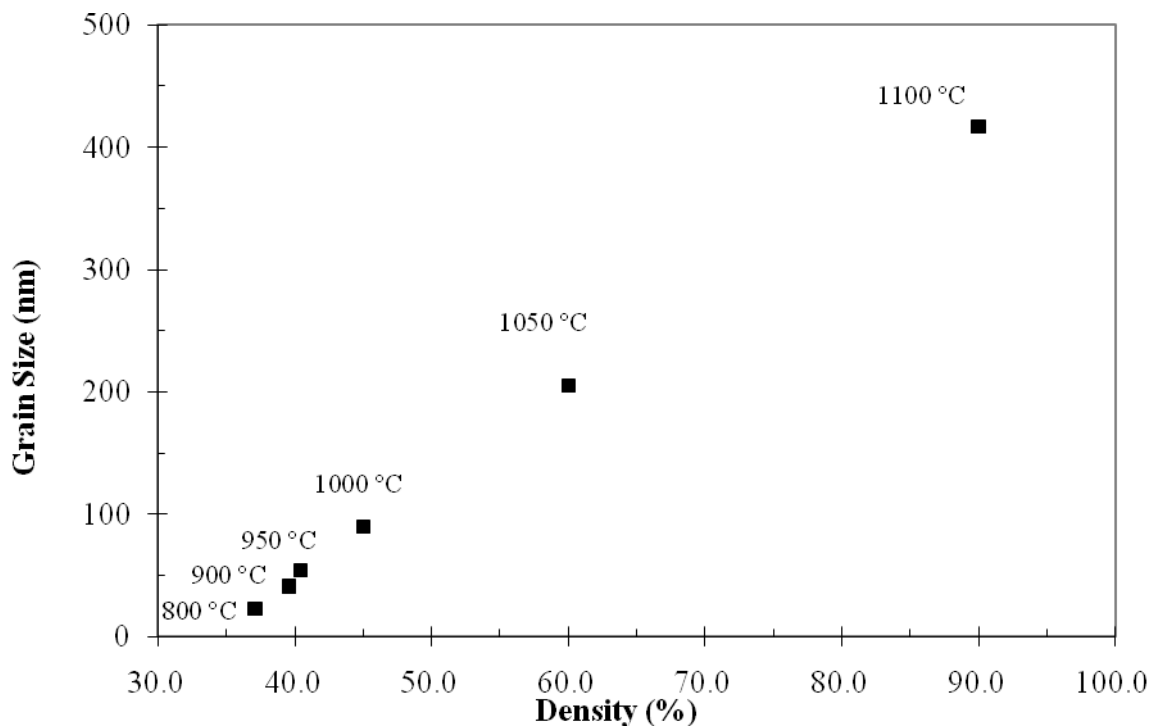
Fig. 6. 16 Grain size and density relationship during initial and intermediate stage of sintering
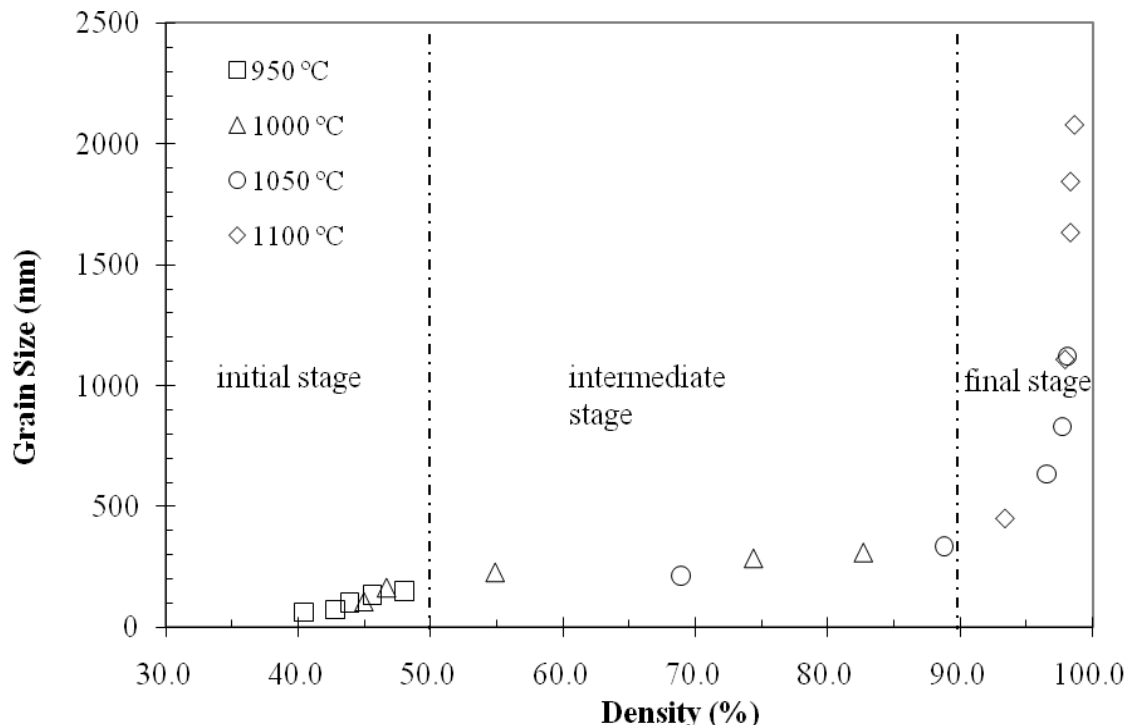
Fig. 6. 17 Dependence of grain size on density during isothermal holding at different temperatures

and intermediate stages of sintering before 90% density and significant grain growth during final stage of sintering after 90% density. But when highlighting the sintering trajectory during initial and intermediate stages of sintering before 90% density, see Fig 6.18, we find that the curve in Fig. 6.18 is not a single straight line, which is different form that in Fig. 6.16. Instead the curve in Fig. 6.18 can be viewed as consisting of two straight lines with different slopes, and a turning point can be found at around 50% density. The line before 50% density corresponding to initial stage sintering has higher slope, and the line between 50% and 90% density corresponding to the intermediate stage
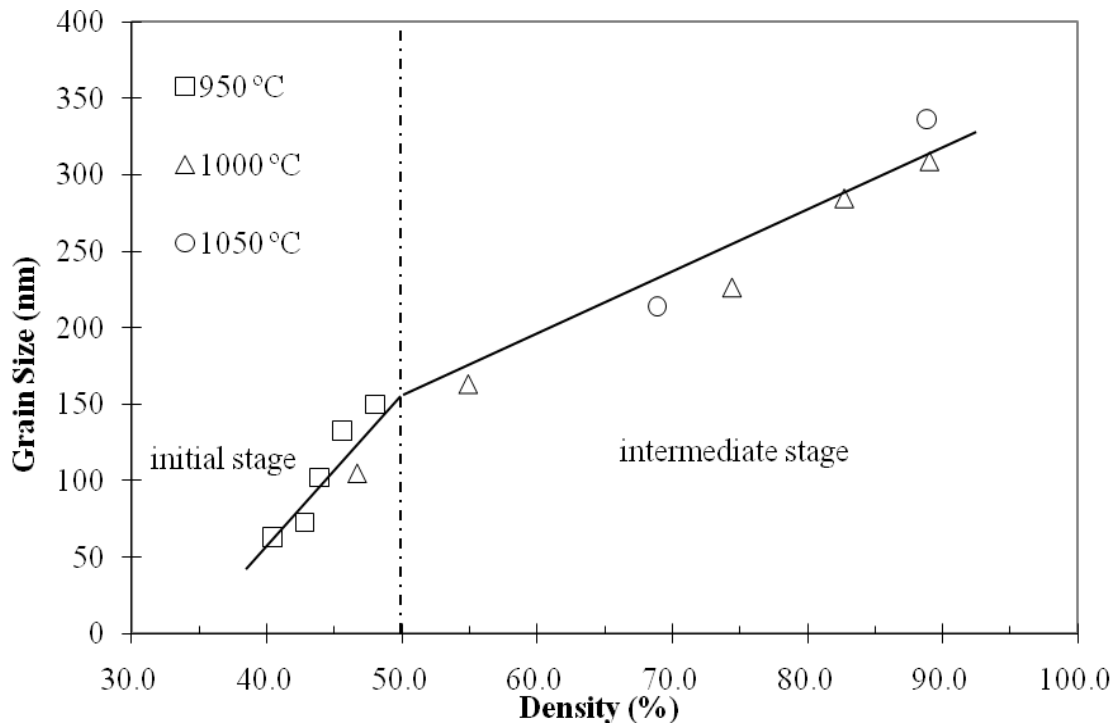
Fig. 6. 18 Relationship between grain size and density during initial and intermediate stages of sintering

sintering has lower slope. It can be seen based on Fig. 6.17 and Fig. 6.18 that the dependence of grain size on density is different for each stage of sintering, which may imply that the mechanisms for grain growth and densification are varied in different stages of sintering.

6.5.3 Effect of Milling Time on Sintering Trajectory

The effect of milling time on sintering trajectory is examined using 6 hours milled powder and 12 hours milled powder. The sintering trajectories for 6 hours milled powder and 12 hours milled powder during nonisothermal heating and isothermal holding processes are plotted in Fig. 6.19 and Fig. 6.20, respectively. Both figures show that the
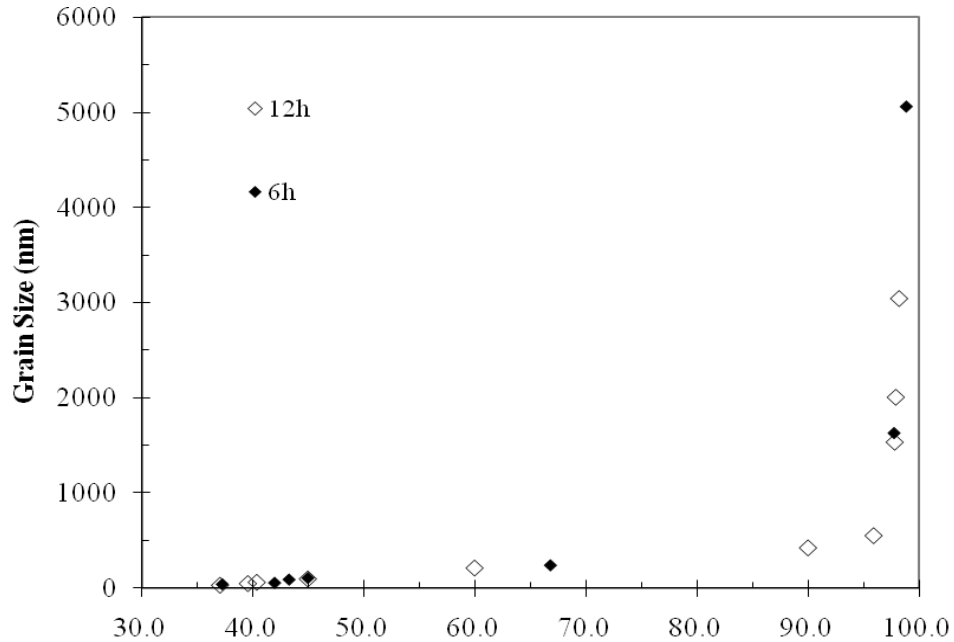
Fig. 6. 19 Effects of milling time on grain size vs. density sintering trajectory during nonisothermal heating
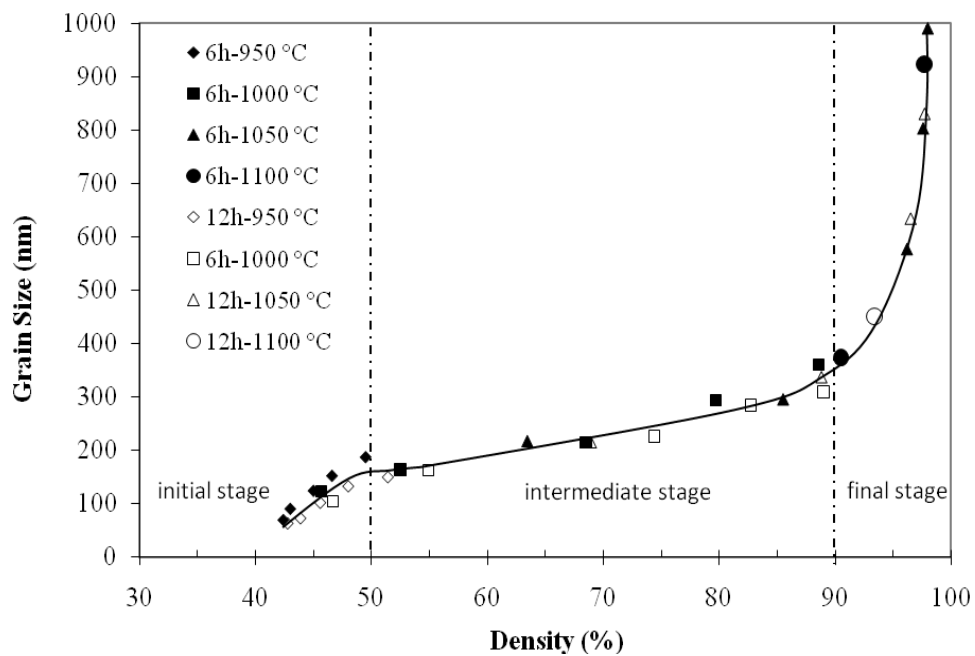
Fig. 6. 20 Effects of milling time on grain size vs. density sintering trajectory during isothermal holding at different temperatures

milling time has no effects on sintering trajectories because the shape of curves or the slope of lines remain the same for both powders. In addition, Fig. 6.20 also exhibits the dependence of sintering trajectory on sintering stages, different shapes being found corresponding to different sintering stages.

6.5.3 Effect of Green Density on Sintering Trajectory

The effect of green density on sintering trajectory is also examined in Fig. 6.21 by nonisothermal heating up. Since neither grain size nor sintered density is vulnerable to
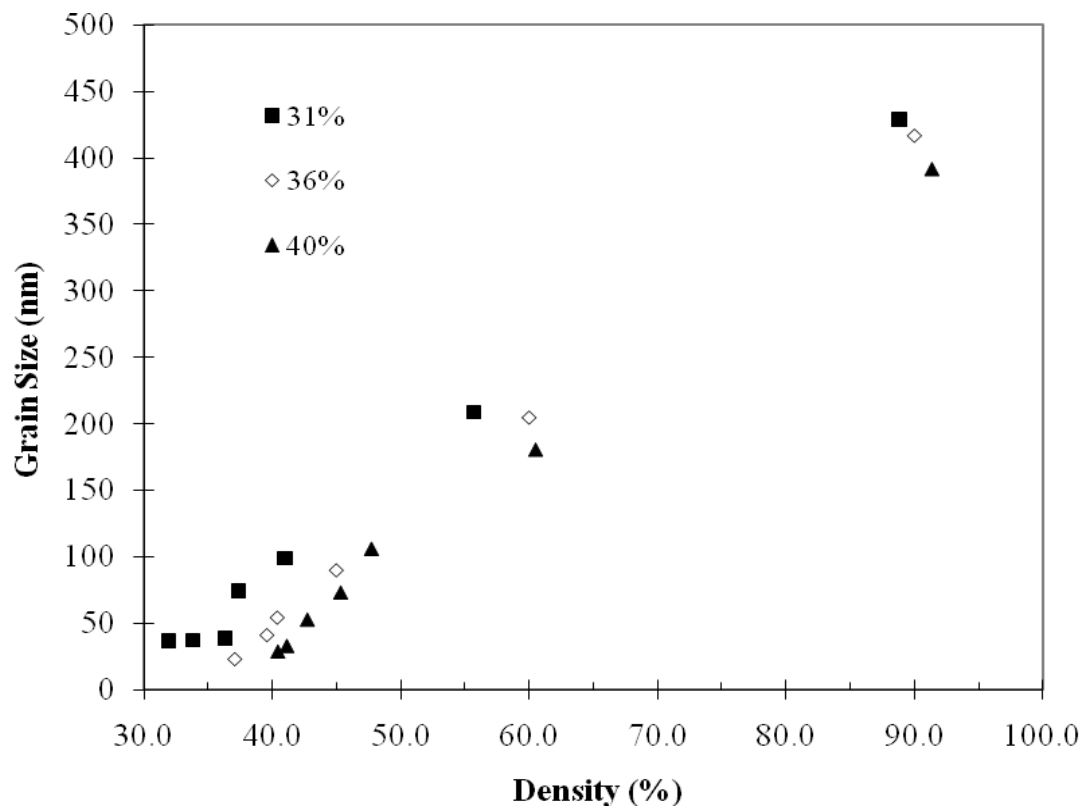
Fig. 6. 21 Effects of green density on sintering trajectories during initial and intermediate stages of sintering

green density during late stage of sintering, Fig. 6.21 focuses only on the sintering trajectory during initial and intermediate stages of sintering. It is clear that grain size and density have a linear relationship before 90% density regardless of initial green densities. Each green density corresponds to a straight line and the lines are separate but parallel to each other, implying that green density does not change the slope of the lines but only shift them. The shifting direction depends on the initial green densities, high green density shifting the line to right side and low green shifting it to the left. This shifting can be explained by the fact that sintered densities inherit the initial differences in green densities during the initial and intermediate stages of sintering but grain growth is independent of green densities. Therefore, with similar grain size, higher green density can yield higher sintered density, which accordingly shifts the grain size vs. density line to the right side, see Fig. 6.21.

Overall, the effects of green density on densification and grain growth can be summarized as follows:

- Densification is very sensitive to the initial green density with higher green density leading to higher sintered density;
- Grain growth is not affected by green density, which is dependent on temperature;
- Green density does not change the slope of sintering trajectory during initial and intermediate stages of sintering, but shifts the trajectory to the higher density side for the sample with higher green density.

These results advise us that the green density should be as high as possible so that high sintered density can be obtained with limited grain growth after the initial and intermediate stages of sintering.

In summary, this chapter described the experimental results for densification, grain growth and sintering trajectory during nonisothermal heating and isothermal holding of the milled nanosized tungsten powders. The results revealed some characteristics of sintering of nanosized powders. The sintering of nanosized powders can be divided into three stages and each stage possesses its own features. During the initial stage of sintering, both grain growth and densification are slow and show an abnormally linear increase with time, which may be due to the initial low green density. During the intermediate stage of sintering, grain growth is still linear but densification becomes normal, indicating the change of mechanisms for densification during the intermediate stage of sintering. During the final stage of sintering, grain growth becomes normal parabolic while densification slows down due to the exhausted driving force at high densities, leading to the slope of sintering trajectory increasing rapidly and becoming infinite at near 100% density.

Based on the above results, it seems that grain growth and densification during the final stage of sintering can be explained by the traditional sintering theories. However, the traditional theories fail to explain the linear grain growth behavior during initial and intermediate stages of sintering and the linear densification behavior during initial stage of sintering. The kinetics and mechanisms for these unique behaviors in grain growth and densification will be examined in Chapter 7.

6.6 References

[1]   Gupta TK. J Am Ceram Soc 1972;55:276.

[2]   Shi JL. J Mater Res 1999;14:1389.

CHAPTER 7

KINETICS AND MECHANISMS OF DENSIFICATION AND GRAIN

GROWTH OF NANOSIZED TUNGSTEN POWDER

7.1 Introduction

In Chapter 6, the experimental results for sintering of nanosized tungsten powder have been introduced with respect to basic characteristics of densification and grain growth under different conditions such as nonisothermal heating, isothermal holding. Further, the effects of milling time and green density on sintering and grain growth were also mentioned. In general, these results show the sintering of nanosized tungsten powder also consists of three sintering stages: initial stage, intermediate stage and final stage. But the initial stage is different from the traditional initial stage of micron sized powder due to the low green density of nanosized powders. The low green density results in very porous structure in green compact and thus affects the densification and grain growth behaviors during initial stage of sintering. The densification during the initial stage of sintering appears to have a linear densification behavior, which is a phenomenon that cannot be explained by classical sintering theories. Besides this phenomenon, grain growth also exhibits uncommon behaviors. The entire grain growth can be divided into two stages: initial grain growth during initial and intermediate stages of sintering and normal grain growth during final stage of sintering. The initial grain growth shows unusual linear grain growth behavior while the normal grain growth shows normal

parabolic grain growth behavior. The linear initial grain growth in this study is another phenomenon that can not be explained by traditional grain growth theories. So this chapter will focus on understanding these unique phenomena during sintering of nanosized tungsten powder. It should be noticed that the uniqueness in densification and grain growth for sintering of nanosized powder is mainly present during initial and intermediate stages of sintering. Accordingly, the densification and grain growth during initial and intermediate stages of sintering will be primarily analyzed in the following sections. The kinetics of densification and grain growth will be evaluated respectively and the corresponding mechanisms for densification and grain growth will be discussed based on the kinetic analysis. Further, the microstructure evolution during sintering will also be revealed.

7.2 Kinetic Analysis of Densification

Before analyzing the densification results, the traditional sintering theories will be firstly introduced in order to provide the background on sintering kinetics.

7.2.1 Brief Review of Sintering Theories

Sintering kinetics has been a primary concern in powder metallurgy and the ceramic field because it can be used to predict sintering progress and direct practical manufacture. Since the 1950s, there have been many studies dealing with sintering kinetics in order to understand and predict the sintering process, so there have been accumulated numerous knowledge on sintering models, sintering rate equations and so on. Generally, these theories treated sintering as consisting of three stages – initial, intermediate, final – based on characteristics of microstructure evolution in the process of sintering, each stage

corresponding to some specific microstructure features. The initial stage of sintering features rapid interparticle neck growth process at the beginning of sintering with relative density increasing from green state up to 65%; the intermediate stage of sintering features continuous porosity with equilibrium pore shape during density change from 65% to 90%; the final stage of sintering includes the rest of sintering after 90% density where the typical microstructure is the closed and isolated porosity. Since the microstructure characteristics are different for these stages, different sintering models have been developed corresponding to the different sintering stages.

Kingery and Berg [1] developed the very famous two sphere model in 1955 to describe the kinetics of neck building process between two equal sized particles, which is usually used to analyze initial sintering kinetics. The general result derived from two sphere model for the initial sintering kinetics is:

$$\frac{\Delta L}{L_0} = \left(\frac{k}{G^m} t \right)^n \tag{7.1}$$

where $\Delta L/L_0$ is the linear shrinkage, G is grain size, t is time, n is the exponent depending on the mechanism responsible for shrinkage, m is called Herring scaling law exponent, k is constant depending on temperature and the model geometry. The exponents m and n are important because their values can be used to determine the mechanism for sintering. Table 7.1 lists the values for n and m corresponding to different mechanisms. Obviously, if the values of m and n are known based on experimental data, the mechanism can be determined for the sintering.

Table 7. 1 Possible value for n and m with respect to different mechanisms during initial stage of sintering

Mechanism	n	m
Surface diffusion	2/7	4
Boundary diffusion	1/3	4
Lattice diffusion from surface	1/2	3
Lattice diffusion from grain boundary	2/5	3
Vapor transport	2/3	2
Viscous flow	1	1

In practice, density is more commonly used than shrinkage for kinetic analysis, so it is necessary to translate linear shrinkage into density. For isotropic densification, the linear shrinkage equation (7.1) can be translated into density change as the following expression:

$$\frac{\Delta L}{L_0} = \frac{1}{3}\frac{\Delta \rho}{\rho} = \frac{1}{3}\frac{\rho - \rho_0}{\rho} = \left(\frac{k}{G^m}t\right)^n \qquad (7.2)$$

where ρ is sintered density at time t, ρ_0 is the sintered density at $t=0$. The equation (7.2) is usually used to evaluate n value by plotting $\ln\left(\frac{\rho - \rho_0}{\rho}\right)$ v.s ln(t) according to following expression:

$$\ln\left(\frac{\rho - \rho_0}{\rho}\right) = n \ln t + \ln\left(\frac{k}{G^m}\right)^n \tag{7.3}$$

n is obtained from the slope of line. It should be noted that the above equations (7.1~7.3) were derived based on initial stage of sintering, but many studies in literature expanded their applications to intermediate and final stages of sintering [2], which is inappropriate.

The model for intermediate stage of densification was derived by Coble [3]. In this model, the typical microstructure for this stage was represented using tetrakaidecahedra with pore channels distributed along the edges. Based on this geometrical model, the rates of densification corresponding to grain boundary diffusion and lattice diffusion are expressed as follows, respectively:

$$\frac{d\rho}{\rho dt} = \frac{A * k(T)}{\rho(1-\rho)^{1/2} G^4} \tag{7.4}$$

$$\frac{d\rho}{\rho dt} = \frac{A * k(T)}{\rho G^3} \tag{7.5}$$

where ρ is sintered density, t is time, A is constant, G is grain size, $k(T)$ is constant related to temperature. Equation (7.4) corresponds to grain boundary diffusion dominated sintering and equation (7.5) corresponds to lattice diffusion dominated sintering. Since the relationship between G and ρ remains unknown, equation (7.4-7.5) cannot be integrated. So there is no analytical expression for the intermediate stage of sintering.

The model for final stage of sintering was also developed by Coble [3] using similar approach to that for intermediate stage of sintering. But different from intermediate stage of sintering, the geometrical model for the final stage of sintering is the

tetrakaidecanhedron with spherical monosize pores at the corners, in contract to cylindrical pores along the edges for intermediate stage of sintering. Using this model, the kinetics of the final stage of sintering for grain boundary diffusion and lattice diffusion are obtained as:

$$\frac{d\rho}{\rho dt} = \frac{A * k(T)}{\rho G^4} \tag{7.6}$$

$$\frac{d\rho}{\rho dt} = \frac{A * (1-\rho)^{1/3} k(T)}{\rho G^3} \tag{7.7}$$

Equation (7.6) is for grain boundary diffusion and equation (7.7) is for lattice diffusion. Again, without knowing the dependence of G on ρ, it is impossible to integrate the above equations and obtain analytical expressions for the final stage of sintering.

Based on Kingery's and Coble's models, there have been many further explorations to sintering kinetics in literatures. These studies used the same strategies as Kingery and Coble but with more delicate considerations from both geometrical and mechanistic aspects [4-7]. For example, Zhao and Harmer [4] introduced a parameter of the number of pores per grain to their model for the final stage of sintering; Chu et al. [5] proposed the sintering stress parameter in the expression for densification rate; Hansen et al. [6] proposed a combined stage sintering model intending to describe the entire sintering process from initial to final stage. Although these explorations improved sintering models to some extent, all of these models yield the similar results to the Coble's model except for more parameters included in the expressions. This implies that the primary factors that affect sintering kinetics are same for all of these models. So a general form can be

extracted to describe the sintering kinetics by summarizing the main factors for densification.

The general form for sintering kinetics was firstly proposed by Wang and Raj [8] based on Young and Culter [9]:

$$\frac{d\rho}{dt} = \frac{A * f(\rho) * k(T)}{G^n} \qquad (7.8)$$

where A is a constant, G is grain size, $k(T) = \frac{\exp(-Q/RT)}{T}$ is temperature related function, $f(\rho)$ is an unknown function of density, and n is the scaling exponent – 3 for lattice diffusion and 4 for grain boundary diffusion. According to equation (7.8), it can be concluded that the densification rate is mainly dependent on three factors: density, grain size and temperature. This simplicity is the result of using the unspecified $f(\rho)$, which actually contains all the complex parameters in the model. Since $f(\rho)$ is unknown and complex, it is usually assumed to be unchanged during sintering in practical kinetic analysis, especially for intermediate stage of sintering [6]. Further, if the empirical power law grain growth $G^n = G_0^n + k'(T)t$ is introduced and the initial grain size G_0 is negligible comparing with G, the equation (7.8) can be expressed as:

$$\frac{d\rho}{dt} = \frac{C * k(T)}{k'(T)t} = \frac{C * K(T)}{t} \qquad (7.9)$$

where $C = A * f(\rho)$ and $K(T) = \frac{k(T)}{k'(T)}$. After integration, a simple expression is obtained for isothermal sintering kinetics:

$$\rho = \rho_0 + k \ln(t/t_0)$$ (7.10)

where ρ_0 is the density at an initial time t_0, ρ is the density at time t, and k is a temperature dependent parameter. In practice, equation (7.10) is widely used to analyze isothermal sintering kinetics and found to be very successful in fitting the experimental data.

The traditional sintering kinetics have been briefly described from above introduction, and next section will examine the sintering kinetics of nanosized tungsten powder to determine if the traditional sintering kinetics is applicable for analyzing kinetics of nanosized powder, and then the differences/uniqueness for nanosized powder will be identified.

7.2.2 Analysis of Nonisothermal Densification

This section will evaluate the kinetics of nonisothermal sintering during heating up process. The sintering behaviors have been introduced in section 6.3.1 (Fig. 6.3). The experimental data for the samples with initial green density 36% are chosen here for kinetic analysis.

For nonisothermal sintering, the kinetics can be analyzed using equation (7.8). If the heating rate is a constant "c", the general sintering kinetics equation (7.8) can be expressed as:

$$\frac{d\rho}{dT} = \frac{Af(\rho)}{c} \times \frac{1}{TG^n} \times \exp\left(-\frac{Q}{RT}\right)$$ (7.11)

Assuming *f(ρ)* is a constant, the activation energy *Q* can be obtained using the below equation by plotting $\ln\left(TG^n \dfrac{d\rho}{dT} \right)$ vs. $\left(\dfrac{1}{T} \right)$:

$$\ln\left(TG^n \frac{d\rho}{dT} \right) = -\frac{Q}{R}\left(\frac{1}{T} \right) + \ln\left(\frac{Af(\rho)}{c} \right) \tag{7.12}$$

At each temperature *T*, the grain size *G* and densification rate *dρ/dT* are known based on experimental results, and if the value of *n* is also known, then the activation energy *Q* could be determined by plotting equation (7.12). Based on traditional sintering models, the value of *n* could be **3** for lattice diffusion and **4** for grain boundary diffusion, both of them being used for the following kinetic analysis.

Applying both *n* values for equation (7.12), the fitting results are shown in Fig. 7.1. It can be seen that, for each *n* value, there is no single line which can fit all the data, and the data need to be treated as two parts, those at low temperatures (900 ℃ -1000 ℃) and those at high temperatures (1050 ℃ - 1250 ℃). As discussed in Chapter 6, the low temperatures before 1000 ℃ represent the initial stage of sintering and high temperatures correspond to the intermediate and final stages of sintering. The fitting results show that the activation energy for high temperatures sintering (intermediate and final stages of sintering) is about 308 kJ/mol if n=3 and 498 kJ/mol if n=4; and the activation energy for low temperature sintering (initial stage of sintering) is 565 kJ/mol if n=3 and 662 kJ/mol if n=4. Comparing to the activation energy values reported in literature – 268~327 kJ/mol for surface diffusion [10-13], 383~460 kJ/mol for grain boundary diffusion [14, 15] and 507~640 kJ/mol for lattice diffusion [16-18], the following remarks can be made with respect to the nonisothermal sintering kinetics of nanosized tungsten powders:
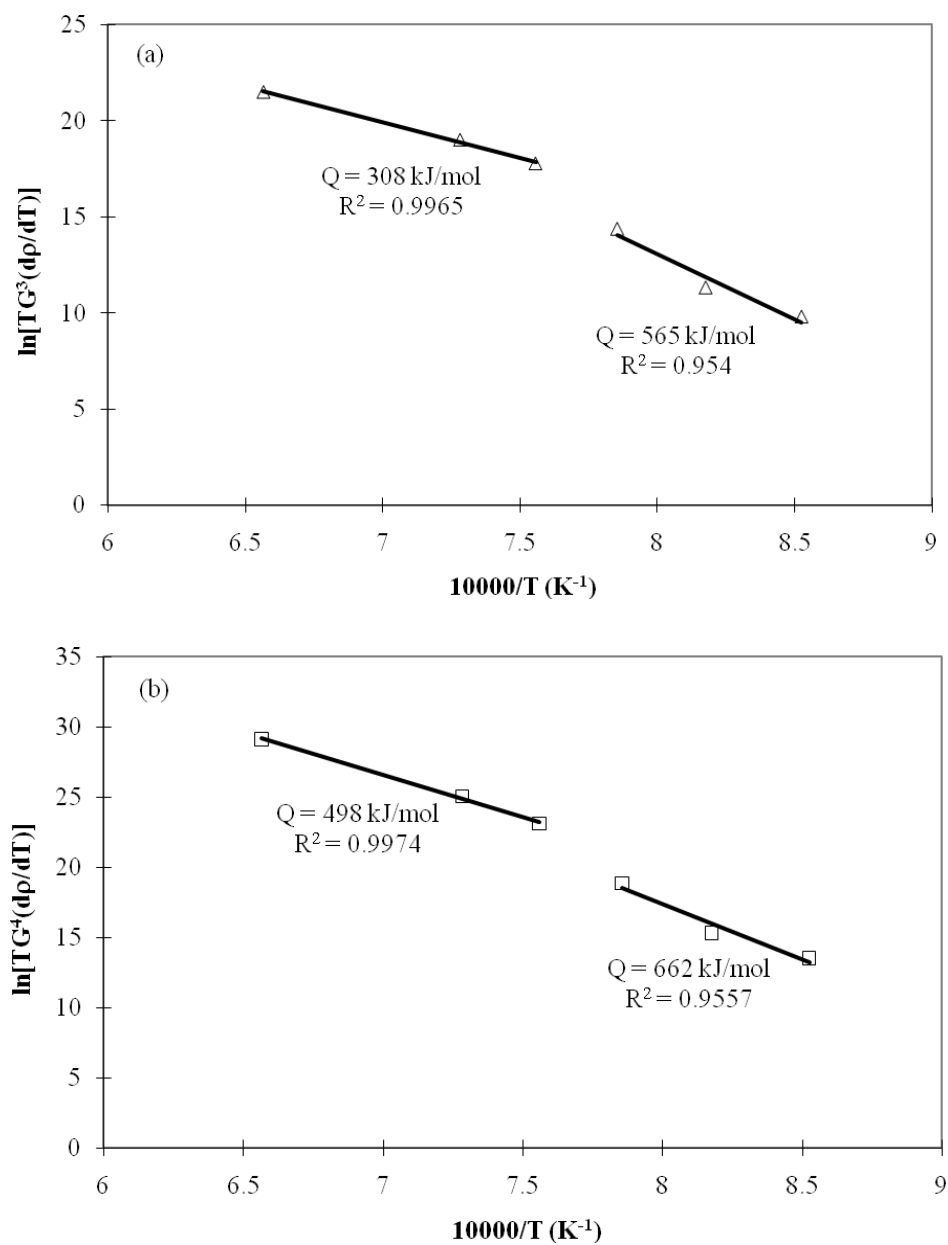
Fig. 7. 1 Evaluation of nonisothermal densification kinetics during heating up process by assuming (a) lattice diffusion and (b) grain boundary diffusion

1.) During intermediate and final stages of sintering at high temperatures, the activation energy 498 kJ/mol obtained using n=4 is reasonable because it is comparable to literature data for the grain boundary diffusion. Therefore, grain boundary diffusion should be believed to be the dominant mechanism for densification during intermediate and final stages of sintering.

2.) For the initial stage of sintering at low temperatures, both n=3 and n=4 yield very high activation energies, the values corresponding to lattice diffusion which is not reasonable for sintering tungsten at such low temperatures. Thus, the traditional sintering models fail to explain the experimental data for the initial stage of sintering of nanosized tungsten powder in this study.

The failure of traditional sintering models for analyzing the initial stage of sintering implies that initial sintering kinetics in this study does not follow the traditional sintering theory and should be explained using different doctrine. As the experimental results shown (see Fig. 6.4), the densification during initial stage of sintering appeared to exhibit a unusual linear behavior which can not be explained by traditional sintering models. In order to explore the mechanism for the densification during this stage of sintering, the linear sintering kinetics is used to evaluate this stage of sintering. The linear sintering kinetics can be expressed as:

$$\frac{d\rho}{dt} = K(T) \Rightarrow \frac{d\rho}{dT} = \frac{K(T)}{c} = C \times \frac{1}{T} \times \exp\left(-\frac{Q}{RT}\right) \tag{7.13}$$

where $K(T)$ is a function of only temperature, C is a constant. So by plotting the following relationship, the activation energy can be obtained.

$$\ln\left(T\frac{d\rho}{dT}\right) = -\frac{Q}{R}\left(\frac{1}{T}\right) + \ln(C) \tag{7.14}$$

The fitting results using the above equation (7.14) are shown in Fig. 7.2. It is interesting to find that the data at high temperature (>1050 °C) show a negative activation energy, which indicates that the linear sintering kinetics is not suitable for high temperature sintering, i.e., intermediate and final stages of sintering. On the other hand, the linear sintering kinetics fits well with the initial sintered densities at low temperatures, and the activation energy for the initial sintering is evaluated to be 284 kJ/mol. This activation energy value corresponds to surface diffusion according to literature data. Therefore, surface diffusion is believed to be the dominant mechanism for the initial linear densification, which is reasonable for the low sintering temperature. But traditional
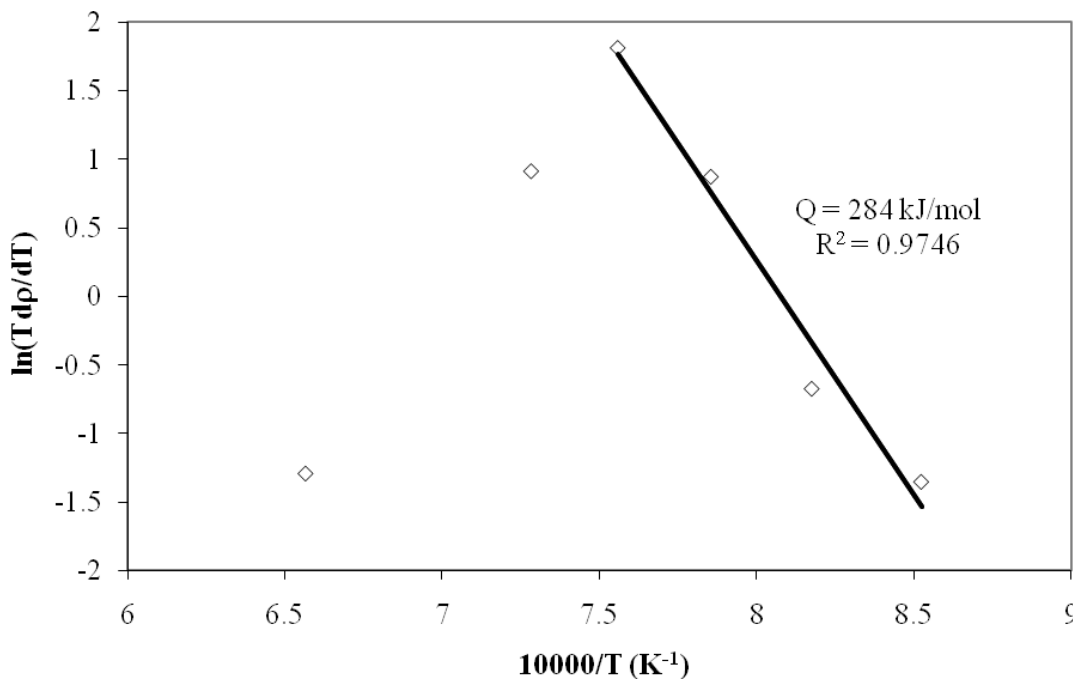
Fig. 7.2 Evaluation of nonisothermal densification kinetics using linear densification behavior

sintering theories believe that surface diffusion does not contribute to densification. This conflict will be discussed later in section 7.2.4.

7.2.3 Analysis of Isothermal Densification

After analysis of nonisothermal sintering kinetics, the primary mechanisms for different sintering stages have been recognized. This section will continue to evaluate the isothermal sintering kinetics in order to compare the analyzing results with nonisothermal sintering kinetics and further understand the sintering process at different stages. The experimental sintered density data at different holding temperatures were given in Chapter 6, see Fig. 6.4.

First, the traditional sintering equations are used to evaluate the experiment results to check their validities. As described previously in section 7.2.1, traditionally, the isothermal sintering kinetics is usually evaluated using equation (7.3) and (7.10), so these two equations are used to fit the isothermal sintered data in this study. The fitting results using both equation (7.3) and equation (7.10) are shown in Fig. 7.3 (a, b) by plotting $\ln[(\rho-\rho_0)/\rho]$ vs. $\ln(t)$ and ρ vs. $\ln(t)$, respectively. It is very clear, except for the data at 950 ºC in Fig. 7.3 (a), that both equations are not satisfied with respect to fitting the experimental data into a straight line for the holding temperatures. For the data at 950 ºC in Fig. 7.3 (a), the linear fitting yields a value of n = 0.6692, which corresponds to vapor transport mechanism according to Table 7.1. However, since tungsten has the lowest vapor pressure among the family of pure metals [19], it is believed that vapor transport is impossible to be the mechanism for sintering and densification of tungsten material. Thus, Fig. 7.3 demonstrates that the traditional fitting equations cannot be employed to evaluate the isothermal sintering data in this study.
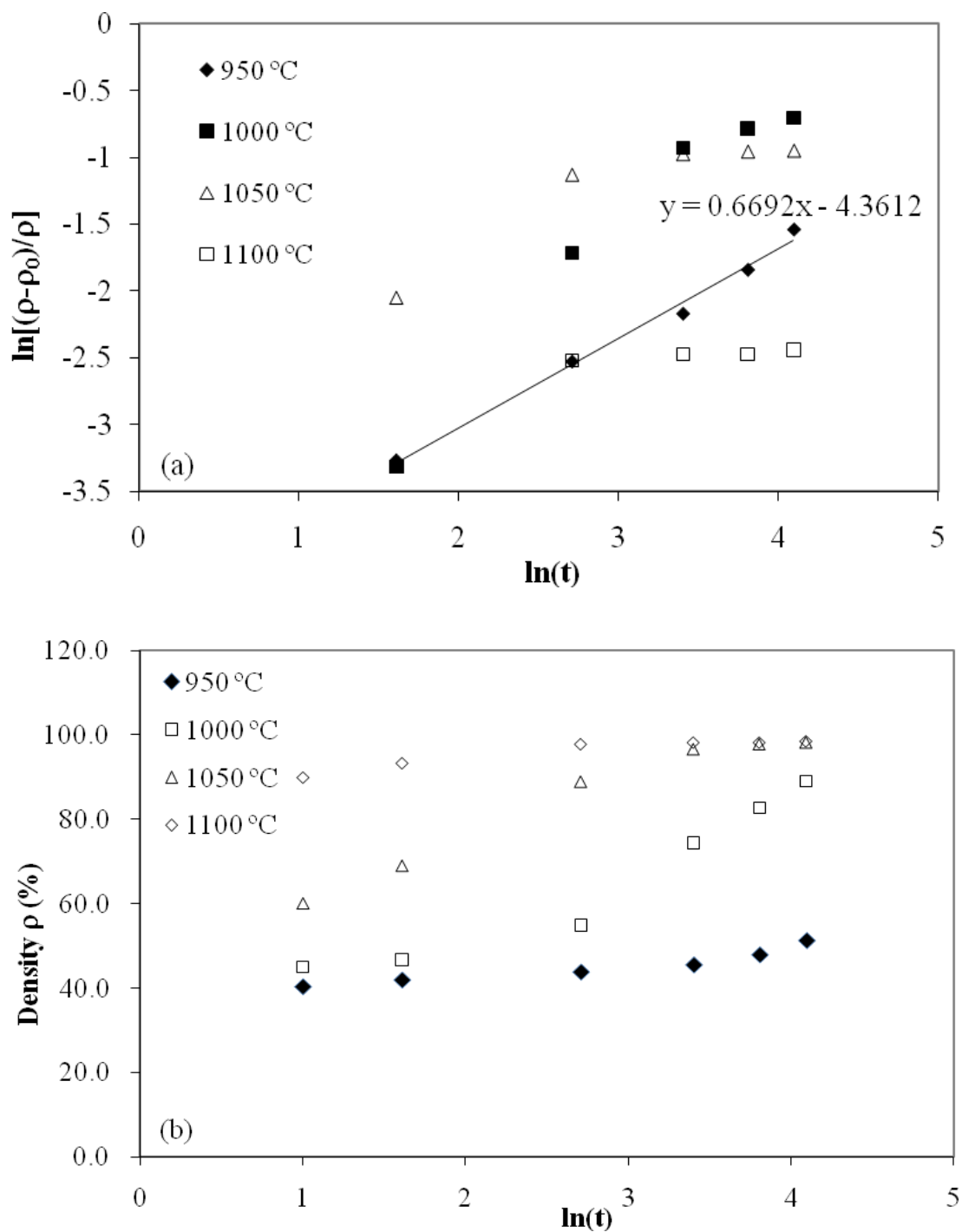
Fig. 7. 3 Analysis of isothermal densification data using traditional fitting sintering equations: (a) equation (7.3); (b) equation (7.10)

Second, since the initial sintering kinetics appears to be linear based on phenomenological observation (see Fig. 6.4), the following equation is applied to evaluate initial stage of sintering data:

$$\rho = \rho_0 + k(T)t \tag{7.15}$$

Using the above equation to fit the sintered density data at 950 °C, 975 °C and the beginning sintered densities at 1000 °C before transiting to intermediate stage of sintering, three different k(T) values are obtained corresponding to each temperature. Then by plotting ln[k(T)] vs. (1/T), the activation energy for initial stage of sintering is gained, see Fig. 7.4. The resultant activation energy is calculated to be 288 kJ/mol, which
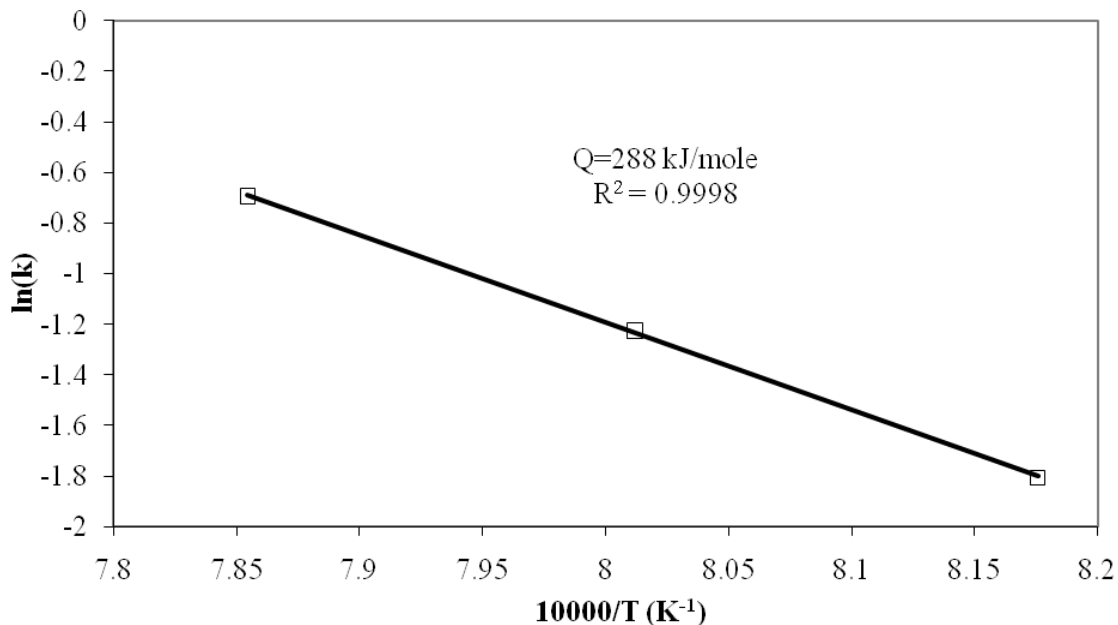
Fig. 7. 4 Evaluation results on densification during initial stage of sintering using linear sintering kinetics

is in accordance with the evaluated activation energy result from nonisothermal sintering data, both confirming that surface diffusion is the mechanism responsible for the initial linear sintering densification.

Third, for intermediate stage of sintering, since there is no integrated analytical equation available to analyze the experimental data as described in section 7.2.1, another method is introduced here in order to evaluate the isothermal sintering data. By rearranging the equation (7.8), the following expression is achieved:

$$\int \left[\frac{G^n}{A * f(\rho)} \right] d\rho = k(T)t \tag{7.16}$$

For the same density ρ, the left side of the equation (7.16) can be regarded as a constant by assuming that grain size G is only dependent on density ρ which is, in fact, approximately true based on literature [20, 21] and the results in this study. By the way, it should be mentioned that the equation (7.16) is actually the essential idea for the concept of master sintering curve proposed by Su and Johnson [20], i.e., separating microstructure from kinetic parameters by putting all the microstructure related factors (e.g., G, ρ) on one side and all the experimental parameters (e.g., T, t) on the other side. The term $k(T)t$ on the right hand side of equation (7.16) is called "master variable". The mastering sintering curve states that the sintered density is only dependent on "master variable" which can have different combinations of $k(T)$ and t.

At different holding temperatures, the time needed to reach certain density is varied depending on the holding temperature. The dependence of holding time on temperature is described as following equation:

$$-\ln(t) = -\frac{Q}{R}\left(\frac{1}{T}\right) - \ln\left\{\int\left[\frac{G^n}{A*f(\rho)}\right]d\rho\right\} \tag{7.17}$$

Based on equation (7.17), the activation energy is able to be assessed by plotting $-\ln(t)$ vs. $(1/T)$. In this study, due to the limited experimental data, the time needed to reach the density $\rho = 67\%$ at different temperatures is chosen to evaluate the activation energy of intermediate stage of sintering, and the fitting results is shown in Fig. 7.5. The activation energy is found to be 495 kJ/mol for intermediate stage of sintering, indicating that grain boundary diffusion is the mechanism for intermediate densification. The same conclusion is also obtained from analysis of nonisothermal sintering kinetics.
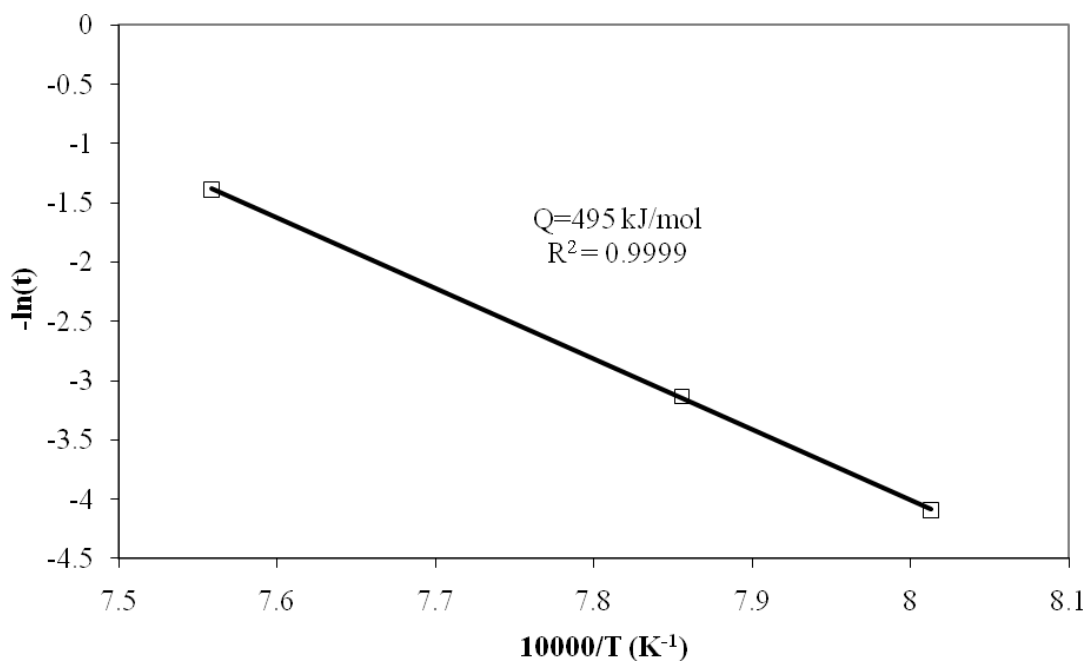
Fig. 7. 5 Calculation of activation energy for intermediate stage of densification using the data at 67% density

7.2.4 Sintering Mechanisms

On the basis of the above discussions for both nonisothermal kinetics and isothermal kinetics, the sintering process and the mechanisms can be summarized here.

The entire sintering process of nanosized tungsten powder in this study experiences three stages: initial, intermediate and final. Due to the characteristics of low green density of nanosized powder, the initial stage of sintering is exceptionally prolonged for sintering of nanosized powders which is an intrinsic difference in comparison with sintering of micron sized powders. The sintering kinetics during initial stage of sintering appears to be linear and the kinetic analysis shows surface diffusion is the mechanism responsible for the densification. These findings do not agree with the traditional sintering theories because linear sintering kinetics is not expected in traditional sintering experiences and surface diffusion does not contribute to densification based on the existing sintering models. Therefore, in order to explain the finding in this study that the surface diffusion contributes to linear densification phenomenon, the role of surface diffusion in sintering needs to be revisited. Actually, in recent years, some researchers have already noticed the effects of surface diffusion on densification of nanosized powders and claimed that surface diffusion can also lead to densification. Shi [22] did an in situ experiment of heating nanosized particles in TEM and observed that particle coarsening and sintering shrinkage occur as a result of surface diffusion. Chen [23] attributed the initial densification upon sintering of nanosized powders to surface diffusion by proposing a mechanism called "coarsening motivated repacking". For this mechanism, Chen claimed whether or not particle coarsening can lead to repacking depends on if the solid frozen sintering skeleton is formed. For micron sized powders, the sintering skeleton is frozen

shortly upon sintering start because of the high compact green density. Once the solid sintering skeleton is formed, surface diffusion only changes the surface morphology of pores and has little effect on densification. However, the green density of nanosized powder is very low and a certain period of time will be required to form a solid sintering skeleton after sintering initiation. In this situation, the densification during this period is believed to be particle rearrangement induced by particle coarsening in the very porous compact state. It is reasonable for nanosized powders that surface diffusion is the predominant mechanism for particle coarsening at low temperature. Therefore surface diffusion is able to indirectly contribute to densification during sintering of nanosized powders. In this study, the finding that surface diffusion is responsible for the initial linear densification can also be rationalized using the mechanism of particle rearrangement by coarsening.

For intermediate and final stages of sintering, the analysis of sintering kinetics shows grain boundary diffusion is the dominant mechanism for densification of sintering of nanosized tungsten powders. According to literature, grain boundary diffusion was also found to be responsible for the densification of micron sized tungsten powder [15, 24-26]. Therefore, there are no substantial differences in densification mechanisms between nanosized powder and micron sized powder during intermediate and final stages of sintering. If the controlling mechanisms for densification are the same for both micron sized powder and nanosized powder, then the benefits in sintering behavior for nanosized powder can be explained by the Herring Scaling Law, which has been mentioned in Chapter 5. For example, nanosized powder has a lower onset of sintering temperature than micron sized powder, or nanosized powder can achieve full densification at lower

temperature comparing with micron sized powder. The advantage of using nanosized powder can be understood using the following scaling law equation:

$$\frac{d\rho}{dt} \propto \frac{k(T)}{G^n} \tag{7.18}$$

where n is the scaling exponent depending on mechanism, usually n = 3 for lattice diffusion and n = 4 for grain boundary diffusion. It can be seen that, for same densification rate, the smaller the particle sizes are, the lower the sintering temperatures are.

Overall, the sintering mechanisms of nanosized tungsten powder in this study are surface diffusion for the linear densification during initial stage of sintering, and grain boundary diffusion for normal densification during intermediate and final stages of sintering with the benefits from fine grain size according to scaling law.

7.3 Kinetic Analysis of Grain Growth

It is well known that the goal of sintering of nanosized powder is not only to obtain full densification but also to remain nanosized crystallites. In order to achieve this goal, both densification and grain growth should be profoundly understood. The densification behavior and mechanisms have been analyzed and discussed in section 7.2, so the following context will be focusing on evaluating and analyzing the kinetics and mechanisms of grain growth process, starting with a brief review on classical grain growth theories.

7.3.1 Brief Review of Grain Growth Theories

Classical grain growth in a single phase bulk material has been theoretically studied since the middle of last century. The thermodynamic driving force for grain growth in single phase bulk materials is the reduction of total grain boundary areas by grain boundary migration. As discussed in a very famous classic paper of the early 1950s by Burke and Turnbull [27], the kinetics of grain growth was firstly deduced from analyzing the movement of grain boundaries with assumption that the velocity of grain boundary movement (v) is proportional to the product of grain boundary mobility (M) and driving force (F):

$$v \propto MF \tag{7.19}$$

where v is velocity of grain boundary movement which is taken to be proportional to instantaneous rate of grain growth dG/dt (G is grain size, t is time); M is grain boundary mobility, $M=D/(kT)$ (D is diffusion coefficient, k is Boltzman constant, T is absolute temperature); F represents driving force for boundary migration which is proportional to curvature of grain boundary $\sim 1/G$ in a single phase bulk material, then

$$\frac{dG}{dt} \propto MF \propto \frac{D}{kT}\frac{1}{G} \tag{7.20}$$

$$\frac{dG}{dt} = A\frac{D}{kT}\frac{1}{2G} = \frac{k_G(T)}{T\,2G} \tag{7.21}$$

where A is a constant, and $k_G(T)=AD/k$.

Equation (7.21) is the typical rate equation of grain growth for normal grain growth in a single phase bulk material. For isothermal holding, equation (7.21) can be integrated into the common parabolic grain growth law:

$$G^2 - G_0^2 = Kt \qquad (7.22)$$

where $K=k_G(T)/T$, G_0 is initial grain size at $t=0$. Equation (7.22) is usually followed in the case of pure single phase bulk materials. However, equation (7.22) is not omnipotent to describe all experimental grain growth data due to the fact that grain growth behavior in reality is determined not only by curvature of grain boundary but also by many other factors such as impurity, second phase, vacancy, porosity etc. For example, the effects of remaining porosity on grain growth during **final stage** of sintering had been studied extensively in literature [28-32]. The interaction between pores and grain boundaries results in two situations: one is that boundary and pore attach together and move forward at the same time; the other is boundary can break away from pore and migrate as in single phase bulk materials. Obviously, the latter case has the same grain growth behavior as equation (7.22) for a bulk material, but in the first case, grain growth kinetics is chiefly dependent on pore migration kinetics. The mechanisms for pore migration could be surface diffusion, vapor transport or lattice diffusion which are different from that of boundary migration. Accordingly the grain growth kinetics is changed to be controlled by the mechanisms of pore migration. Interestingly, no matter whether the grain growth is pore control or boundary control, the kinetics of grain growth is found to follow a generalized power law grain growth equation which, by using different n values, can fit

all the situations and describe the grain size data successfully in almost all the isothermal experiments, i.e.,

$$G^n - G_0^n = Kt \qquad (7.23)$$

where n varies depending on several factors such as material systems, temperature, impurity, second phase, porosity and so on. Table 7.2 summarizes the exponent n for the various mechanisms [32]. For instance, the exponent n was reported to be either n = 3 or 4 in literature [30, 31, 33, 34] for the final stage of sintering. Recently, it was also revealed that grain growth kinetics needs to be described by noninteger exponents, somewhere between 3 and 4 [35].

It should be noticed from the above contents that the grain growth has been intensively studied in bulk materials or in final stage of sintering. According to grain size vs. density trajectory, it has been always shown that grain growth in the final stage of sintering is significant and accounts for the majority of grain growth during sintering. So it is reasonable that grain growth in the final stage of sintering has been focused on in the literature in order to control final grain size in the sintered components. This is especially true in the case of sintering coarse sized particles where grain growth in initial and intermediate stages might be neglected. Nevertheless, for sintering of nanosized powder, although grain growth in final stage of sintering is still dominant during the entire grain growth process, the amount of grain growth in initial and intermediated stages is not negligible but sufficient in many cases to cause the material to lose its nanocrystalline characteristics.

Table 7. 2 Grain growth exponent n in the equation $G^n - G_0^n = Kt$ for various mechanisms

Mechanism	Exponent m
Pore control	
Surface diffusion	4
Lattice diffusion	3
Vapor transport (vapor pressure p = constant)	3
Vapor transport (p = 2γsv/r)	2
Boundary control	
Pure system	2
System containing second-phase particles	
Coalescence of second phase by lattice diffusion	3
Coalescence of second phase by grain boundary diffusion	4
Solution of second phase	1
Diffusion through continuous second phase	3
Doped system	
Solute drag (low solubility)	3
Solute drag (high solubility)	2

In contrast to grain growth in the final stage of sintering, the grain growth in the initial and intermediate stages of sintering has seldom been studied and is not of course well understood. Because the characteristics of microstructure in initial and intermediate stages of sintering are interconnected open pores instead of isolated close pores in final stage of sintering, grain growth process in initial and intermediate stages of sintering could be different from that in the late stage. Greskovitch and Lay [36] and Lange and Kellett [37] proposed a two step grain growth mechanism qualitatively describing the grain growth process in very porous compact during initial and intermediate stages of sintering. In very porous compacts, grain boundary is pinned by the neck groove and its motion induces an increase in its area and is not energetically favorable. The first step in the coarsening is to fill the neck and increase the size ratio between the adjacent particles by interparticle mass transport, and the second step will start until the size ratio reaches a critical value which enables grain boundary migration without increasing its area. This model did not provide quantitative kinetics of grain growth for initial and intermediate stages of sintering. To the best knowledge of the author, there have so far been no specific models that are designed to quantitatively describe grain growth kinetics during initial and intermediate stages of sintering, as a result, the general power law grain growth equation (7.13) has been still commonly employed to fit any stage of grain growth for simplicity.

Greskovitch and Lay [36] showed that the classical power law grain growth equation was still applicable to fit the experimental Al_2O_3 data using exponent n values from 2 to 3, but Shi [38] reported that grain size data in TZP and YSZ compacts cannot be fitted with the powder law grain growth equation, but with a linear relation between grain size

and logarithm of time. This discrepancy indicates the complexity of the grain growth during initial and intermediate stages of sintering.

In this study, we will put emphasis on evaluating grain growth during initial and intermediate stages of sintering and try to explore the mechanisms for this period of grain growth. Grain growth in the final stage of sintering is not the focus of this study since it had been studied well in literature. Both nonisothermal grain growth and isothermal grain growth will be examined during initial and intermediate stages of sintering using generalized grain growth equation (7.23). Based on equation (7.23), the generalized grain growth rate equation can be written as:

$$\frac{dG}{dt} = \frac{K}{nG^{n-1}} = \frac{k_G(T)}{TnG^{n-1}} \tag{7.24}$$

For isothermal condition, integration of equation (7.24) returns to equation (7.23). However, for nonisothermal grain growth, e.g., constant-rate-heating experiment, the integration of equation (7.24) is more complicated than that in the case of isothermal kinetics. Therefore, the following discussion focuses on developing mathematical methods for kinetic analysis of nonisothermal grain growth with constant heating rate.

7.3.2 Analysis of Nonisothermal Grain Growth

Using the generalized grain growth rate equation (7.24) and substituting $\beta = dT/dt$ to the equation, where β is the constant heating rate, a universal expression of grain growth rate as a function of temperature is shown as equation (7.25)

$$\frac{dG}{dT} = \frac{k_G}{\beta T n G^{n-1}} = \frac{k_{G0}\exp\left(-\dfrac{Q_G}{RT}\right)}{\beta T n G^{n-1}} \qquad (7.25)$$

where Q_G is the activation energy for grain growth. Equation (7.25) will be used for following discussion of kinetic analysis of nonisothermal grain growth. By collecting grain size data at different temperatures from nonisothermal grain growth experiments, the kinetic parameters (e.g., n and Q_G) for grain growth can be simply determined using the following two mathematical methods – differential method and integral method.

Differential method. Differential method is referred to using differential equation, i.e., rate equation, e.g., equation (7.25), directly to obtain kinetic parameters n and Q_G. In this method, equation (7.25) needs to be rearranged to form equations as following:

$$\ln T \frac{dG}{dT} = \ln\left(\frac{k_{G0}}{\beta n}\right) - \frac{Q_G}{RT} + (1-n)\ln G \qquad (7.26)$$

$$\left(\ln T \frac{dG}{dT} - (1-n)\ln G\right) = -\frac{Q_G}{R}\left(\frac{1}{T}\right) + \ln\left(\frac{k_{G0}}{\beta n}\right) \qquad (7.27)$$

By plotting $\left(\ln T \dfrac{dG}{dT} - (1-n)\ln G\right)$ $vs.\left(\dfrac{1}{T}\right)$ based on equation (7.27) using different n values, the best linear fitting regression identifies the value of n, and the activation energy Q_G is determined from the slope of linear line.

Integral methods. Integral method indicates that an analytical equation deduced from integration of a differential equation is used to evaluate kinetic parameters. The traditional isothermal grain growth kinetics is typically analyzed using this method. In

case of isothermal kinetics of grain growth, the analytical equation (7.23) is commonly applied to obtain the values of *n* and *K* at different temperatures, and then the activation energy is determined by utilizing the linear relationship between ln(K) and 1/T. However, in the case of nonisothermal kinetics of grain growth, to obtain an analytical equation similar to equation (7.23) is a challenge since the temperature integral on the right side of below equation (7.28) is unable to be analytically solved.

$$G^n - G_0^n = \frac{k_{G0}}{\beta} \int_{T_0}^{T} \frac{1}{T} \exp\left(-\frac{Q_G}{RT}\right) dT \tag{7.28}$$

In order to use this method for nonisothermal kinetics of grain growth, the integration of temperature integral has to be provided. Actually, the temperature integral has been studied in many literatures on phase transformation, chemical reaction analysis, thermal decomposition etc. [39-44], and various approximation forms were deduced in order to precisely represent the temperature integral. According to literature [45], in case of the activation energy $Q_G \gg RT$ and $T \gg T_0$, the temperature integral can be expressed in the following term without sacrificing precision.

$$\int_{T_0}^{T} \frac{1}{T} \exp\left(-\frac{Q_G}{RT}\right) dT \approx \frac{R}{Q_G} \times T \times \exp\left(-\frac{Q_G}{RT}\right) \tag{7.29}$$

Then an analytical equation (7.30) can be obtained and this equation acts as description of grain growth behavior as a function of temperature in a constant heating experiment.

$$G^n - G_0^n \approx \frac{Rk_{G0}}{\beta Q_G} \times T \times \exp\left(-\frac{Q_G}{RT}\right) \tag{7.30}$$

$$\ln\left(\frac{G^n - G_0^n}{T}\right) = -\frac{Q_G}{R}\left(\frac{1}{T}\right) + \ln\left(\frac{Rk_{G0}}{\beta Q_G}\right) \tag{7.31}$$

After rearrangement of equation (7.30), the value of n and Q_G can be easily determined

by plotting $\ln\left(\frac{G^n - G_0^n}{T}\right) vs.\left(\frac{1}{T}\right)$ according to equation (7.31). Similar to the discussion in

the section of differential method, n is evaluated based on the best linear regression

coefficient, and Q_G is calculated from the slope of the linear line.

In this investigation, both differential method and integral method will be applied to

examine the nonisothermal kinetics of grain growth during heating up of nanocrystalline

tungsten powders at 10 ℃/min.

The kinetics of nonisothermal grain growth during initial and intermediate stages of

sintering is evaluated using the grain size data from 800 ℃ to 1100 ℃ in Fig. 6.9. Both

differential method and integral method described above are applied by plotting

"$ln(TdG/dT)-(1-n)lnG$ v.s $1/T$" and "$ln[(G^n-G_0^n)/T]$ v.s $1/T$" respectively using different

grain growth exponent "n" values. The linear regression fitting results for "n" ranging

from 1 to 5 are summarized in Table 7.3. It can be seen that both methods yield the same

conclusion: the best fitting is gained when n = 1. This conclusion means linear grain

growth behavior in the initial and intermediated stages of sintering process. The fitting

results for both methods with n = 1 are demonstrated in Fig. 7.6. The activation energies

are calculated to be 186 kJ/mol using differential method and 226 kJ/mol using integral

method. Both values are close to but lower than the activation energy of surface diffusion

Table 7. 3 Regression fitting coefficient $<R^2>$ using different grain growth exponent values for both differential method and integral method

Grain growth exponent	n=1	n=2	n=3	n=4	n=5
Differential method	0.9997	0.9813	0.9642	0.9523	0.9439
Integral method	0.9850	0.9843	0.9673	0.9517	0.9399
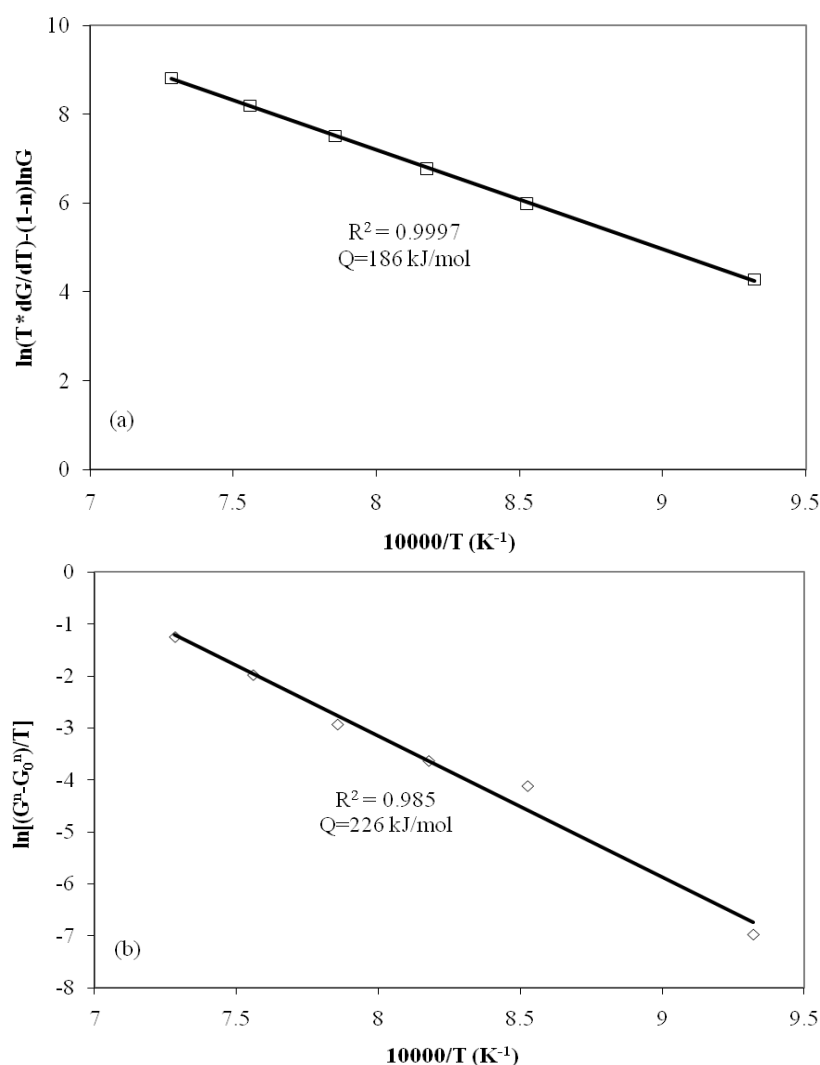
Fig. 7. 6 Analysis of the kinetics of nonisothermal grain growth during initial and intermediate stages of sintering by using both (a) differential method and (b) integral method

in pure tungsten, the latter being reported in literature to be 268-327 kJ/mol [10-13]. The low activation energy in this study may be attributed to nonequilibrium microstructures arising from high energy mechanical milling. Overall, surface diffusion can be regarded as responsible for the grain growth process during initial and intermediate stages of sintering.

7.3.3 Analysis of Isothermal Grain Growth

In order to further understand grain growth behavior of nanosized tungsten powders during sintering, kinetics of isothermal grain growth are analyzed for comparison with nonisothermal grain growth results. The grain size data have been given in Fig. 6.10. According to the fitting results using "$(G^n-G_0^n)$ vs. t" with different n values, it turns out that n = 1 is the best fit for grain growth at 950 ℃, 1000 ℃ and 1050 ℃, and n = 2 becomes the best fit at 1100 ℃. These results indicate that grain growth is linear during initial and intermediate stages of sintering and then transforms to parabolic grain growth law during final stage of sintering at high temperatures. It is in accordance with the analysis of nonisothermal grain growth results showing a linear grain growth behavior in the very porous compacts before 90% relative density.

It should be noted that isothermal grain growth kinetics is usually analyzed using the initial grain size at room temperature as the starting data point G_0 for all the holding temperatures in most studies without taking into account the grain growth during heating up process to the preset isothermal holding temperature. This approximation may stand for when grain growth during heating up is negligible, but in the case of nanosized grain/particles, it is not holding because sufficient grain growth will occur during the heating up process. For example, if the initial grain size at room temperature is used as G_0

in this study, the grain growth curves with a constant starting point are shown in Fig. 7.7. For comparison, grain growth curves with consideration of grain growth during heating up are also displayed in the same figure. Obviously the grain growth curves exhibit nonlinear growth behavior at 950 ℃ and 1000 ℃ when constant G_0 is used, and analyzing results show the best fit goes to n = 2 (dot line) instead of n = 1 if grain growth during heating up is considered (solid line). The comparison in Fig. 7.7 shows that neglecting grain growth during heating up could yield misleading information regarding
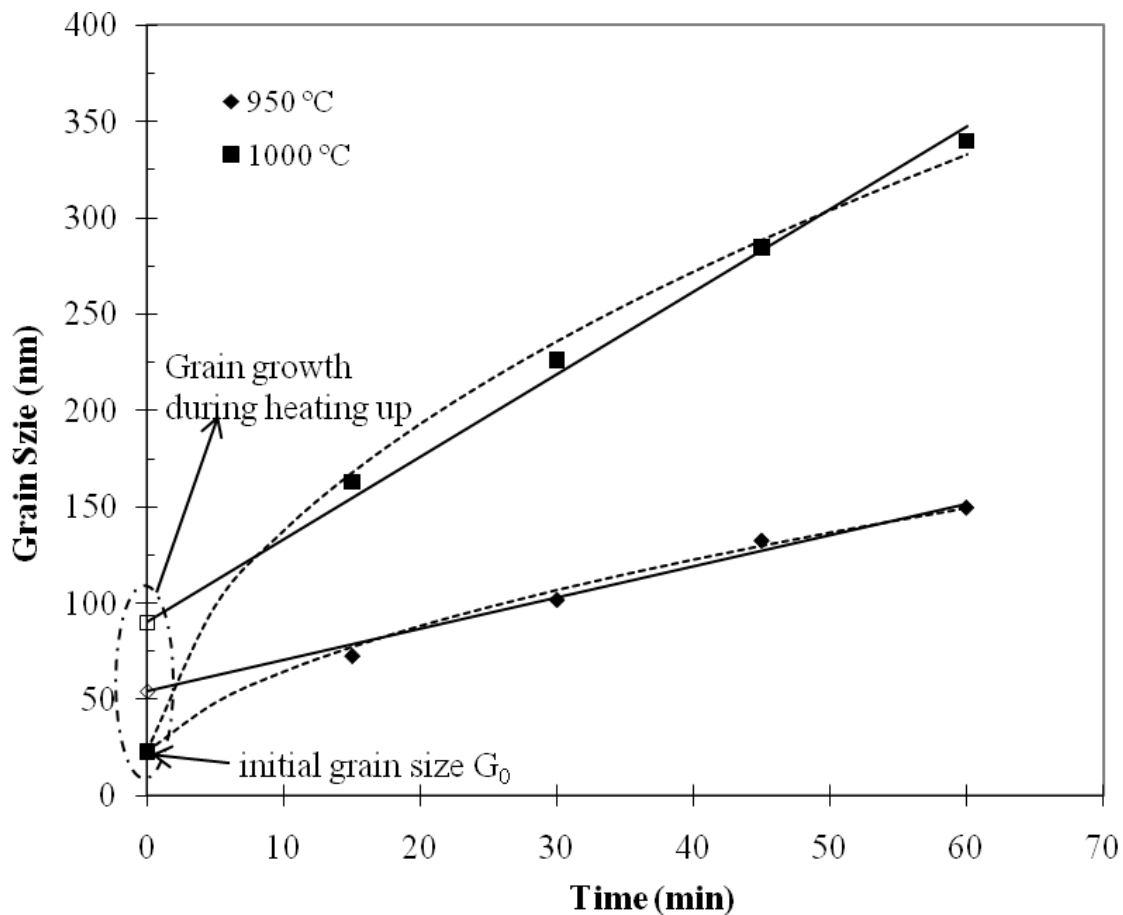
Fig. 7. 7 Comparison of the fitting results for isothermal grain growth at low temperatures with or without consideration of grain growth during heating up

the grain growth during initial and intermediate stages of sintering. Therefore, it is important for nanosize grains to consider the grain growth during heat up and incorporate them into isothermal kinetic analysis in order to acquire correct information for better understanding the process.

In order to explore the mechanisms for the linear grain growth during initial and intermediate stages of sintering, the isothermal grain growth data are evaluated using the following equation:

$$G = G_0 + Kt \tag{7.32}$$

where G is grain size at time t, G_0 is initial grain size at $t = 0$, $K = K_0 \exp[-Q/(RT)]$ is dependent on temperature T. Equation (7.32) is used to fit grain size data at temperature 950 °C, 1000 °C and 1050 °C, then the value of K for each temperature can be obtained. Based on the dependence of K on temperature T, the activation energy Q is able to be derived by plotting $\ln(K)$ vs. $(1/T)$, see Fig. 7.8. The result shows that the activation energy is about 299 kJ/mol and surface diffusion should be accordingly the dominant mechanism for the linear grain growth during initial and intermediate stages of sintering.

7.3.4 Grain Growth Mechanism

Since grain growth in final stage of sintering has been considerably studied in literature, the current study set focus on exploring mechanisms for grain growth during initial and intermediate stages of sintering. Using nanosized tungsten powders, the grain growth during initial and intermediate stages of sintering has been investigated using both nonisothermal heating approach and isothermal holding approach. Based on the above
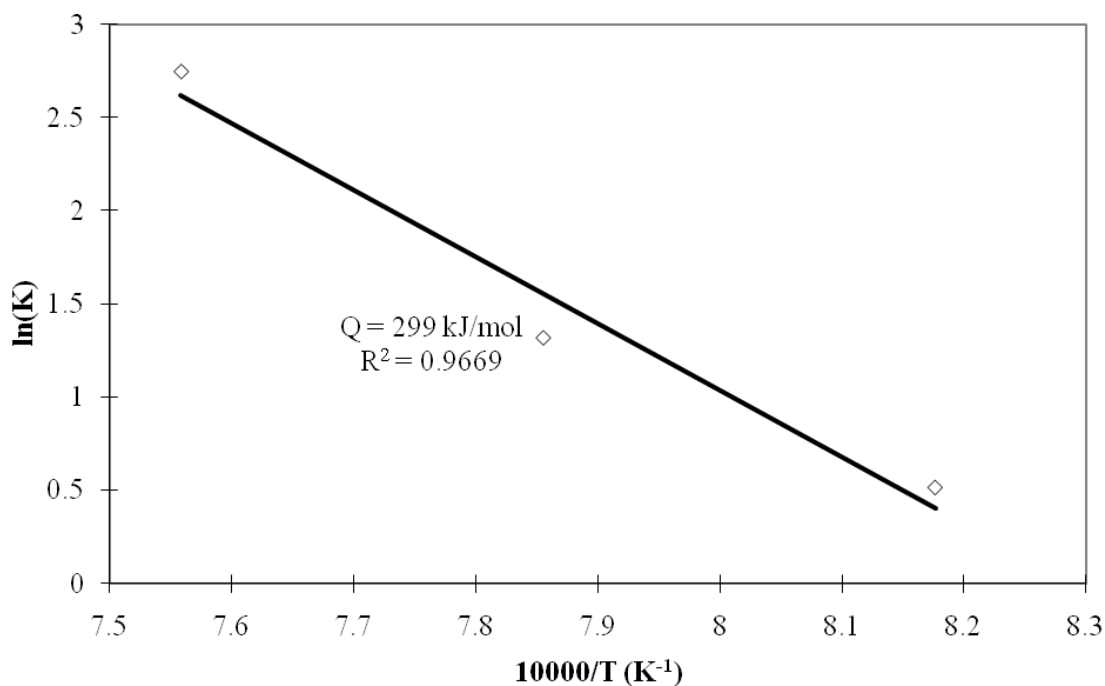
Fig. 7. 8 Evaluation result of the kinetics of initial grain growth using linear grain growth law

kinetic analysis, the evaluation results from both nonisothermal and isothermal grain growth confirm a fact that grain growth is linear and surface diffusion is responsible for this linear grain growth during initial and intermediate stages of sintering. This finding can not be explained by the traditional grain growth theories described in section 7.3.1. For example, in Table 7.2, only "solution of second phase" predicts linear grain growth, which obviously does not fit the situation for this study; further, if surface diffusion is the controlling mechanism, the grain growth exponent should be 4 instead of 1 according to Table 7.2. Therefore, the surface diffusion controlled linear grain growth in the very porous compact is still an unanswered question in the field of grain growth and a new grain growth model may be necessary to describe it in future.

7.4 Microstructure Evolution During Sintering

In general, microstructure of a material defines its properties, consequently microstructure evolution during materials processing and manufacturing processes is extremely important and should be substantially understood in order to tailor or optimize the materials properties. With respect to the sintering process, microstructure evolution involves densification and grain growth which are two intertwined processes taking place concurrently. In the current study, microstructure evolution during sintering of nanosized tungsten powders can be described by viewing it as three stages i.e., initial stage, intermediate stage, and final stage.

Based on density vs. temperature curve during heating up Fig. 6.3, initial stage is the slow densification at low temperatures (<1000 ℃) and then accelerated densification occurs in intermediate stage between 1000 ℃ and 1100 ℃, followed by final stage after 1100 ℃. The microstructure evolution during initial and intermediate stages of sintering is exhibited in Fig. 7.9. At low temperatures between 800 ℃ and 950 ℃, microstructures are extremely fine, but not uniform. Especially at 800 ℃ and 900 ℃, extremely small grains can be seen in the powder compact. With increasing temperatures, the microstructure experienced slow coarsening and a gradual change to becoming more uniform, as shown in (Fig 7.9 c) at 950 ℃. After that, a "chain-like" microstructure was developed at 1000 ℃ with clear outlines of each individual grain which is a result of progressive coarsening. Much more significant coarsening was observed at 1050 ℃ before the microstructure became faceted at 1100 ℃.
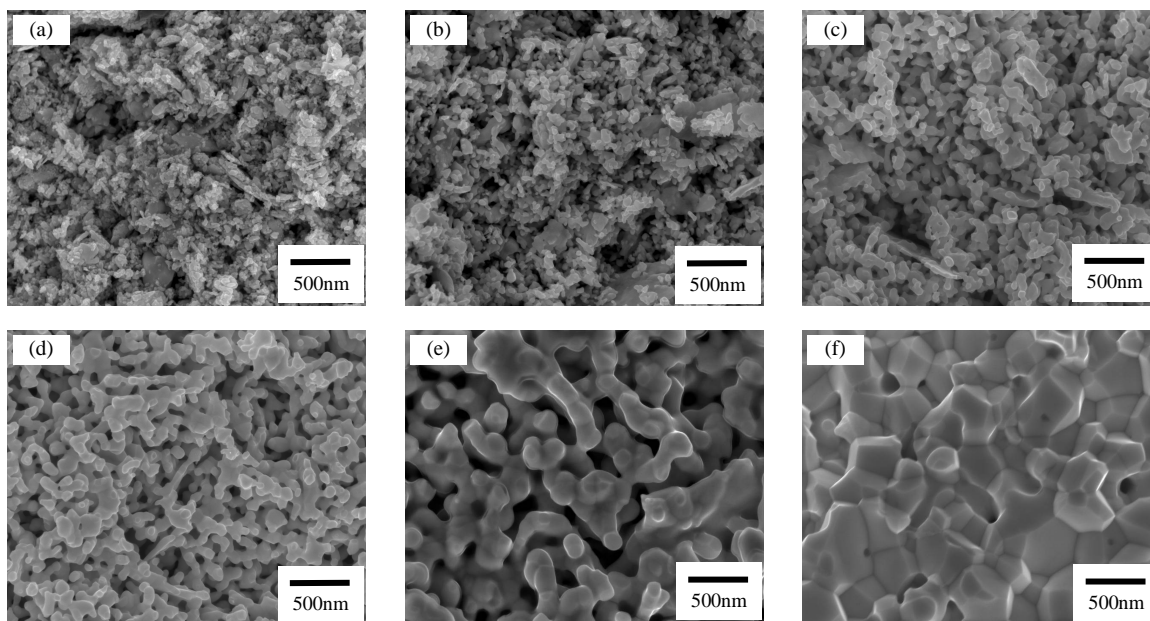
Fig. 7. 9 Microstructure evolution during heating up to different temperatures: (a) 800 °C; (b) 900 °C; (c) 950 °C; (d) 1000 °C; (e) 1050 °C; (f) 1100 °C

It is important to note that the morphology of grains at 1050 ℃ is considerably more rounded. Each grain seemed to be coated with a smooth and round surface layer. This phenomenon is called "surface rounding" hereafter in this study. We believe this is an indication of surface transporting phenomenon. Surface diffusions are extremely active during this period leading to dramatic reductions of total surface energy. The surface rounding process is followed by grain faceting and rapid densification at high temperatures, all contributing to decreasing the system's total energy.

After 1100 ℃, the grains remain faceted in shape, but grain size grows rapidly with temperature, see Fig. 7.10.

The more details on microstructure evolution can be found in Fig. 7.11 for isothermal holding experiments. It shows the same characteristics as described above for each stage of sintering. For example, slow coarsening during the initial stage of sintering is clearly
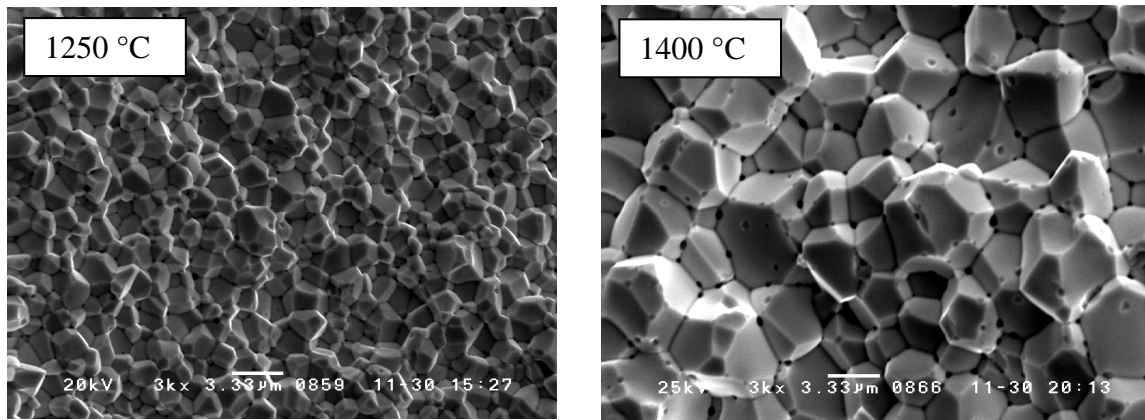
Fig. 7. 10 Microstructure during final stage of sintering after 1100 °C

(a)   950 °C

(b)   1000 °C
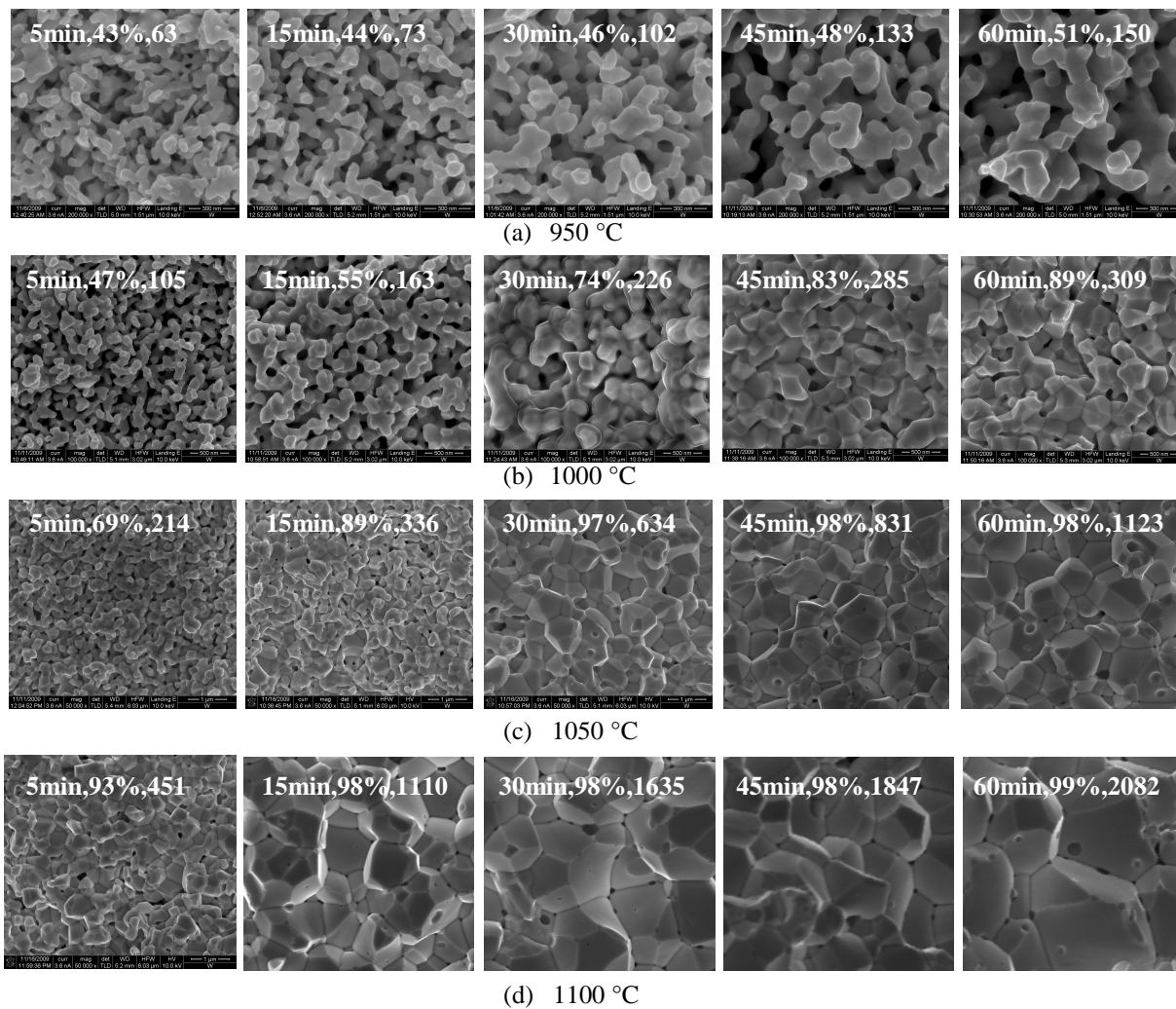
(c)   1050 °C

(d)   1100 °C

Fig. 7. 11 Microstructure evolution during isothermal holding nanosized tungsten powder at different temperatures – (a) 950 ºC, (b) 1000 ºC, (c) 1050 ºC and (d) 1100 ºC, with holding time, relative sintered density and grain size (nm) labeled on each picture

observed at 950 ℃ holding; the faceted grains and fast grain growth are seen at final stage of sintering, e.g., at 1100 ℃ holding; rapid densification and surface rounding phenomena are shown during intermediate stage of sintering at 1000 ℃. But it is necessary to discuss more on the microstructure evolution at 1000 ℃ because the transition from linear densification to normal densification takes place at this temperature according to Fig. 6.4. By comparing the two figures (Fig. 6.4 and Fig. 7.11), it is found that the transition from linear densification to normal densification accompanies "surface rounding" phenomenon, so this phenomenon signifies the densification mechanism is changed and the system starts rapid densification after initial stage of sintering. The reason for this phenomenon will be discussed later.

In order to study the characteristics of microstructure during the initial grain growth process further, the evolution of grain size distribution as a function of temperature is illustrated in Fig 7.12. It shows that the grain size distribution is initially wide at low temperatures, becoming narrower with increasing temperature, finally reaching a steady state distribution after 1000 ℃. These results reflect the observations in Fig. 7.9. The wide grain size distribution indicates the initial inhomogeneous microstructures at low temperatures, which is common for powders produced by high energy ball milling. The steady state size distribution was reached at 1000 ℃ corresponding to a more uniform microstructure as shown by the micrographs of high temperatures in Fig. 7.9. The changes of grain size distribution are consistent with the general theory of the effects of particle size distribution on sintering [46, 47]. Based on Fig. 6.9, Fig. 7.9 and Fig. 7.12, it can be concluded that the initial stage of sintering is a homogenizing process of microstructure by coarsening which sharpens size distribution until reaching a steady
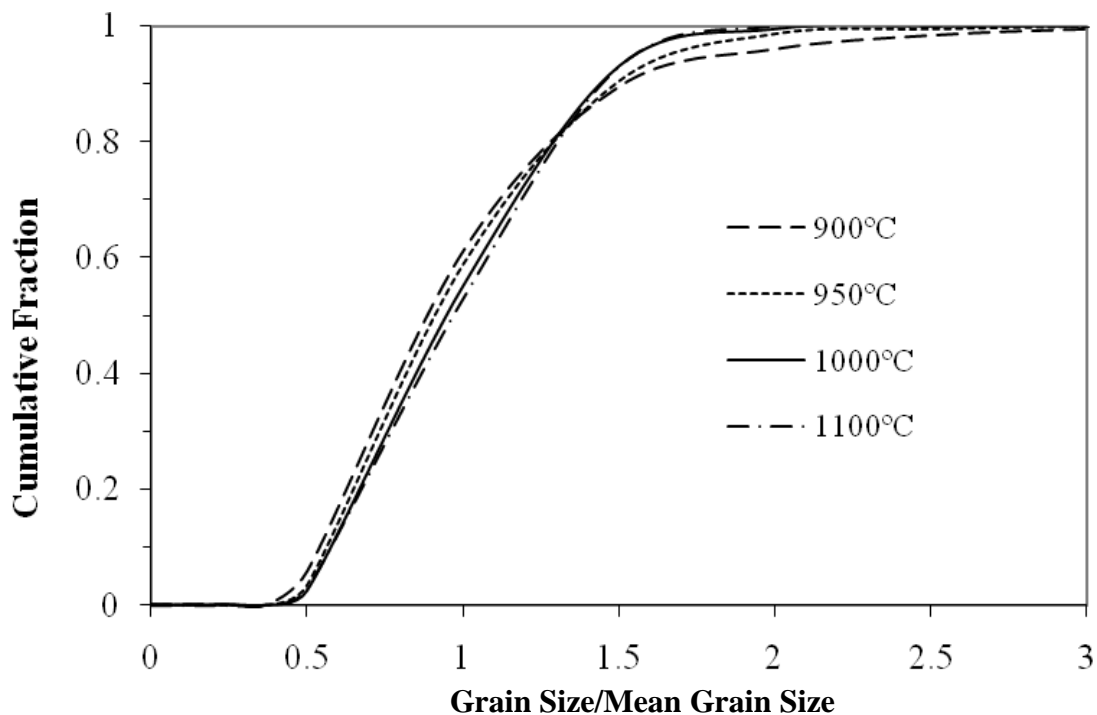
Fig. 7. 10 Evolution of grain size distribution as a function of temperature during heating up process

state as a result of the extremely small particles in the as produced powders consumed by large particles. At the same time, densification is slowly proceeding by "coarsening-induced particle rearrangement" mechanism as described in section 7.2.4, so we assume that the densification kinetics is dependent on coarsening kinetics i.e., $\dfrac{d\rho}{dt} \propto \dfrac{dG}{dt}$. As a result, the linear coarsening kinetics results in the linear densification kinetics at the initial stage of sintering.

After the initial stage of sintering, homogeneous grain size distribution and certain density are achieved. With further sintering, grain size and density keep on increasing and then very rapid densification takes place under some conditions usually between

50%-70% relative densities, indicating the transition from the initial stage to the intermediate stage of sintering. The most prominent feature during intermediate stage of sintering is the rapid and significant densification along with surface rounding phenomenon. Based on kinetic analysis for this stage of densification, grain boundary diffusion is the dominant mechanism, see section 7.2. Therefore, surface rounding phenomenon may indicate that grain boundary diffusion starts playing distinguished role in the system.

The occurrence of "surface rounding" can be explained by the following discussion. With increased density after the initial stage of sintering, connectivity among particles increases accordingly and more and more grain boundary areas are formed in the compact. As a result, the contribution of grain boundary diffusion to the system becomes competitively outstanding. Meanwhile, surface diffusion is still very active to induce coarsening. So the system is at a very activated state where a large number of atoms are transported by surface diffusion and boundary diffusion simultaneously during this stage. The plenty of transported atoms are kinetically unable to be accommodated into the lowest energy's positions on particle surfaces, so instead they form smooth and round layer on the particle surfaces in order to minimize the system's total free energy. Consequently, the surface rounding layer is observed during sintering of nanosized tungsten powders in this study, see Fig.7.9 (e) and Fig. 7.11 (b).

After the surface rounding process, the density of the compact is greatly increased, and then a grain faceting process is followed at the end of intermediate stage of sintering. This is because most surface areas have been consumed during the rapid densification process, and at the end of intermediate stage of sintering, boundary energy becomes the

dominant component for the total system energy instead of surface energy. Thus grain faceting happened in order to reduce the boundary energy. And with further sintering, the system is approaching the final stage of sintering.

During the final stage of sintering, the pores are closed and sitting at grain boundaries and triple junctions of the faceted grains. Densification dramatically slows down as a consequence of high density, but grain growth accelerates rapidly by grain boundary migration in order to reduce the total boundary energies.

Overall, microstructure evolution during sintering of nanosized tungsten powders in this study starts with a homogenizing process in which slow densification and slow grain growth via surface diffusion occur at the beginning of sintering. Then the compact goes through a very rapid densification process via both surface diffusion and boundary diffusion during intermediate stage of sintering. And finally following the grain faceting process, the system experiences very rapid grain growth by boundary migration and slow densification in final stage of sintering. Eventually nearly full densification is obtained after sintering.

7.5 Possible Mechanism for Linear Grain Growth

Based on the above kinetic analysis, the interesting finding in this study is that the initial grain growth of nanosized tungsten powder follows linear kinetic behavior and surface diffusion is responsible for this linear grain growth. The traditional grain growth theory states that the grain growth exponent n should be 4 if the grain growth mechanism is surface diffusion controlled pore migration. In this classical grain growth model, the grain boundaries are pinned by spherical and isolated pores, and grain growth rate is controlled by pore migration rate. There are several mechanisms for pore migration such

as surface diffusion, lattice diffusion and vapor transport. If surface diffusion is responsible for pore migration, the resultant gain growth exponent is derived to be 4 according to this model. So the linear grain growth behavior found in this study cannot be explained by the traditional pore-controlled grain growth models.

Recent developments on grain growth either by experimental test or by simulation have also found the linear grain growth behavior in nanocrystalline materials [48-56]. Some theoretical explanations have been proposed. For example, Krill et al. [51] and Estrin et al. [48-50] found linear grain growth behavior in fully dense Fe materials and attributed this linear grain growth to excessive vacancies dragging effects on grain boundary migration; Zhou et al. [54] and Farkas et al. [55] simulated grain growth in thin film and bulk nanocrystalline Ni, respectively, using molecular dynamics method, and the results also showed a linear grain growth behavior which was explained by the authors considering size effects on the grain boundary mobility; Gottstein et al. [52, 53] proposed a grain growth model in bulk nanocrystalline materials based on the consideration that the motion of a grain boundary is driven by grain boundary curvature with triple and quadruple junctions, and if the grain boundary motion is controlled by the mobility of triple junctions, a linear grain growth results. Another study by Klinger et al. [56] also provided a model for grain growth in porous nanocrystalline materials and showed that for a polycrystal with subcritical pores the average grain size increases linearly with time during initial stage of growth. It should be noted that all of the above studies focused on fully dense nanocrystalline materials or near fully dense nanocrystalline materials, while with respect to grain growth of nanosized particles in the very porous state, i.e., initial grain growth, the linear grain growth has been seldom reported in literature.

Nevertheless, according to the above reported linear grain growth in nanocrystalline materials, a general principle is able to be extracted from these studies, i.e., there exist huge dragging forces for the grain growth in nanocrystalline materials from either vacancies, triple junctions, porosities or free surface grooves, which slow the boundary migration leading to a linear grain growth behavior. This principle is believed to be also shared in the case of grain growth in the very porous compact during initial and intermediate stages of sintering considering the fact that there exists substantial inhibition force for grain boundary migration by extensive porosities and neck grooves in the very porous microstructure. But the detailed process regarding the initial grain growth during sintering is still a scientific issue that needs to be explored further by proposing certain specific models so that the linear grain growth behavior can be explained.

7.6 References

[1]   Kingery WD, Berg M. J Appl Phys 1955;26:1205.

[2]   Majumdar S, Raveendra S, Samajdar I, Bhargava P, Sharma IG. Acta Mater 2009;57:4158.

[3]   Coble RL. J Appl Phys 1961;32:787.

[4]   Zhao J, Harmer MP. J Am Ceram Soc 1988;71:530.

[5]   Chu M-Y, Jonghe L, C. , Lin M, K. F. , Lin F, J. T. . J Am Ceram Soc 1991;74:2902.

[6]   Hansen JD, Rusin RP, Mao-Hua T, Johnson DL. J Am Ceram Soc 1992;75:1129.

[7]   Slamovich EB, Lange FF. J Am Ceram Soc 1993;76:1584.

[8]   Wang J, Raj R. J Am Ceram Soc 1990;73:1172.

[9]   Young WS, Cutler IB. J Am Ceram Soc 1970;53:659.

[10]   Allen BC. Trans AIME 1963;227:1175.

[11]   Allen BC. Trans AIME 1966;236:903.

[12]   Barbour JP, Charbonnier FM, Dolan WW, Dyke WP, Martin EE, Trolan JK. Phys Rev 1960;117:1452.

[13]   Moon D, Koo R. Metall Mater Trans B 1971;2:2115.

[14]   Kreider KG, Bruggeman G. Trans AIME 1967;239:1222.

[15]   Vasilos T, Smith JT. J Appl Phys 1964;35:215.

[16]   Vasil'ev VP, Chernomorchenko SG. Zavodsk. Lab. 1956;22:688.

[17]   Danneberg W. Metallurgy 1961;15:977.

[18]   Andelin RL, Knight JD, Kahn M. Trans AIME 1965;233:19.

[19]   Lassner E, Schubert W-D. TUNGSTEN - Properties, Chemistry, Technology of the Element, Alloys, and Chemical Compounds. New York, Boston, Dordrecht, London, Moscow: Kluwer Academic / Plenum Publishers, 1999.

[20]   Su H, Johnson DL. J Am Ceram Soc 1996;79:3211.

[21]   Gupta TK. J Am Ceram Soc 1972;55:276.

[22]   Shi J-L, Deguchi Y, Sakabe Y. J Mater Sci 2005;40:5711.

[23]   Chen P-L, Chen IW. J Am Ceram Soc 1997;80:637.

[24]   Kothari NC. J Less Common Met 1963;5:140.

[25]   German RM, Munir ZA. Metall Trans A 1976;7A:1873.

[26]   Chen LC. Int J Refract Met Hard Mater 1993;12:41.

[27]   Burke JE, Turnbull D. Progr Met Phys 1952;3:220.

[28]   Kingery WD, Francois B. J Am Ceram Soc 1965;48:546.

[29]   Nichols FA. J Appl Phys 1966;37:4599.

[30]   Nichols FA. J Am Ceram Soc 1968;51:468.

[31]   Brook RJ. J Am Ceram Soc 1969;52:56.

[32]   Brook RJ. Controlled grain growth. In: Wang FFY, editor. Ceramic Fabrication Processes. New York: Academic Press; 1976.

[33]   MacEWAN JR. J Am Ceram Soc 1962;45:37.

[34]   Coble RL. J Appl Phys 1961;32:793.

[35]   Bourgeois L, Dehaudt P, Lemaignan C, Fredric JP. J Nucl Mater 2001;295:73.

[36]   Greskovich C, Lay KW. J Am Ceram Soc 1972;55:142.

[37]   Lange FF, Kellett BJ. J Am Ceram Soc 1989;72:735.

[38]   Shi JL, Yen TS. J Eur Ceram Soc 1994;14:505.

[39]   Cai J, Liu R. J Therm Anal Calorim 2008;94:313.

[40]   Farjas J, Roura P. AIChE J 2008;54:2145.

[41]   Flynn JH. Thermochim Acta 1997;300:83.

[42]   Cai J, Yao F, Yi W, He F. AIChE J 2006;52:1554.

[43]   Popescu C, Segal E. Int J Chem Kinet 1998;30:313.

[44]   Orfao JJM. AIChE J 2007;53:2905.

[45]   Mittemeijer EJ. J Mater Sci 1992;27:3977.

[46]   Fang Z, Patterson BR, Turner ME. Acta Metall Mater 1992;40:713.

[47]   Fang Z, Patterson BR. Acta Metall Mater 1993;41:2017.

[48]   Estrin Y, Gottstein G, Rabkin E, Shvindlerman LS. Scr Mater 2000;43:141.

[49]   Estrin Y, Gottstein G, Shvindlerman LS. Scr Mater 1999;41:385.

[50]   Estrin Y, Gottstein G, Shvindlerman LS. Acta Mater 1999;47:3541.

[51]   Krill III CE, Helfen L, Michels D, Natter H, Fitch A, Masson O, Birringer R. Phys Rev Lett 2001;86:842.

[52]   Gottstein G, Ma Y, Shvindlerman LS. Acta Mater 2005;53:1535.

[53]   Gottstein G, Shvindlerman LS. Scr Mater 2006;54:1065.

[54]   Zhou L, Zhang H, Srolovitz DJ. Acta Mater 2005;53:5273.

[55]   Farkas D, Mohanty S, Monk J. Phys Rev Lett 2007;98:165502.

[56]   Klinger L, Rabkin E, Shvindlerman LS, Gottstein G. J Mater Sci 2008;43:5068.

CHAPTER 8

CONCLUSIONS

Sintering of nanosized powders is one of the primary approaches to manufacturing bulk nanocrystalline materials. Because of their small size and large surface to volume ratio, which distinguish them from micron sized powders, nanosized powders exhibit some different behaviors during sintering. In this study, the characteristics during sintering of nanosized powder were studied by using nanosized tungsten powders with respect to effects of particle size on sintering, densification and grain growth of nanosized powders, and the relationship between densification and grain growth. Based on the experimental results, the following conclusions can be drawn:

1. Particle size has evident effects on sinterability. Fine particles show enhanced sinterability at low sintering temperature. The dependence of sinterability on particle size can be quantitatively described by the Herring Scaling Law.

2. Densification of nanosized tungsten powder can be divided into three stages in this study: initial stage (from green density to ~50% relative density), intermediate stage (~50% to ~90% relative density) and final stage (~90% to 100% relative density).

3. The initial stage, due to the low green density (30%~40% relative density), shows unusual linear densification behavior which can be attributed to the particle repacking process induced by coarsening. The mechanism for initial stage of sintering is evaluated to be surface diffusion. Further, the initial stage sintering is

also a process during which grain size distribution becomes narrower with sintering and reaches a steady state at the end of this stage, resulting in uniform microstructure.

4. The intermediate and final stages have similar densification behavior to those of micron sized powder but with rapid sintering rate due to small particle size. The mechanism for intermediate and final stages of sintering is calculated to be grain boundary diffusion.

5. Grain growth during sintering of nanosized tungsten powder can be viewed as consisting of two parts based on grain size vs. density trajectory: initial grain growth before 90% relative density and normal grain growth after 90% relative density. The normal grain growth is faster compared with the initial grain growth, and accounts for majority of entire grain growth. But the initial grain growth is not negligible because it can usually increase grain size beyond nanoscale (e.g., from 20nm to 400 nm in this study).

6. In contrast to the parabolic grain growth behavior of normal grain growth, the kinetics of initial grain growth shows unusual linear grain growth behavior. The mechanism for the linear grain growth is evaluated to be surface diffusion. The linear grain growth cannot be explained by traditional grain growth model, and a new model is necessary in the future for analyzing detailed process.

In order to achieve the goal of sintering nanosized powder, i.e., full densification and nanoscale grain size, the following strategies are proposed based on the present study for pressureless sintering:

- Powder: the starting powder should have sharp particle size distribution, i.e.,

uniform particle size, to reduce the initial coarsening activities due to size differences.

- Powder processing: some processing methods such as colloidal processing, slip/tape casting are necessary to deagglomerate powders and obtain uniform pore size distribution.

- Compaction: new techniques are needed for compacting nanosized powders in order to gain high green density. It can be seen in this study that the characteristics of nanosized powder during sintering is related primarily to the low green density, e.g., linear densification and/or linear grain growth. Ultrasonic compaction may be a candidate in this case.

- Sintering design: optimized sintering cycles should be designed to enhance densification and inhibit grain growth. One example is the two step sintering, which achieved full densification without final grain growth. New sintering design is necessary to inhibit both initial and final grain growth.

In summary, the sintering of nanosized powder is a challenge with respect to retaining nanoscale grain size. There is no simple answer to this difficulty, but it is possible that the bulk nanocrystalline materials can be successfully produced by careful treatments with powders, compaction and sintering process.